Experimental Investigation of Oscillatory Flow around circular cylinders at low β numbers

by

Silvana Kühtz

Department of Aeronautics
Imperial College of Science, Technology and Medicine



A thesis submitted for the degree of
Doctor of Philosophy of the University of London and the Diploma of Imperial College

July 1996

BIBL. LONDIN. DELT

To the memory of

Maria Luisa Erspamer, Yasmin Saudi and Angela Cuonzo

who left this world before their time

in different tragic circumstances.

Abstract

Experiments have been conducted on circular cylinders in oscillatory flow at low β (or Stokes') parameter (= $D^2/\nu T$). Forces on fixed cylinders and responses of flexible cylinders have been investigated. The aims of the study were to examine the flow phenomena and make comparisons with low β computations carried out by other researchers. Experimental results at similar conditions to those of the numerical solutions have been gathered to validate computational results.

A study of the available literature on the problem showed that apparently the smallest β value reached previously in experiments is around 100.

The oscillatory flow was produced in a U-tube with period T, situated in the Aeronautics Department at Imperial College. Having to measure forces, it was preferable to reduce β by an increase of the kinematic viscosity ν rather than decreasing the cylinder diameter D which would reduce the magnitude of the forces and lower their accuracy. Tests with both pure water and a more viscous solution of water and polyethylene glycol were conducted.

For the fixed cylinder in-line and transverse forces were measured, force coefficients C_D, C_M and C_{Lrms} calculated and compared with other researchers' numerical and experimental results at β of 308, 75, 53 and 35.

In-line displacements were measured for the flexible cylinder in specific ranges of the ratio of the cylinder frequency to the flow frequency, at β of 750, 270 and 60.

In general varying β did not produce large changes in the force coefficients.

The study of the transverse force suggested a 3-D shedding for particular values of KC (= UT/D). This was found to occur notwithstanding the value of β .

For the flexible cylinder in-line displacements were measured in resonant conditions (natural frequency of the cylinder $\sim$ 3 times the fluid oscillation frequency).

All the resonant test cases examined showed that a peak occurred in a critical region of KC, between 8 and 25, for all the β values studied. The physical causes of such peaks are discussed.

Using Morison's equation to reconstruct the cylinder displacement showed that Morison's equation is not adequate to model these resonant conditions.

Acknowledgements

I wish to thank Professor Peter Bearman and Professor Mike Graham for their fairness and supervision throughout the last challenging three and a half years and Mrs Roslee Fairhurst for the encouragement woman-to-woman she gave me during the numerous difficult times I went through.

All the technical staff of the Department of Aeronautics proved efficient and well prepared to meet the needs that this experimental study required. On a personal basis I would like to thank Miss Tilly Hill, Dr Letty Allen, Dr Xhon W. Lin, Mr John O'Leary MBE and Mr John Wye.

Many thanks to my parents Umberto e Francesca for trying to understand and for their love and support.

Special thanks to Annalisa Losacco & Caterina Losacco, I am the only only child who can boast two sisters.

I would like to thank my precious friends Marcello D'Agostino and his sparkling philosophy of life, Maria Bufano Schofield, her witty "vis polemica" and her invaluable deep affection, Oliver Flanagan and his patience and wisdom, Mohammed Basharat and his optimism, Chao Zhou and her reassuring smile.

This research was funded by a European Community project.

Contents

List of Figures 7

List of Symbols 14

1 Flow around smooth cylinders: general review of the subject 18
1.1 Introduction 18
1.2 Objectives and relevance of this work 19
1.3 State of the Art on the subject 22
1.4 Unidirectional flow past a fixed circular cylinder 22
1.4.1 Formation of a vortex in unidirectional flow 24
1.5 Oscillatory flow past a fixed circular cylinder 25
1.5.1 Introduction 25
1.5.2 The time-dependent forces 28
1.5.3 Flow regimes 36
1.6 Flexible cylinders in an oscillating fluid flow 44
1.6.1 Introduction 44
1.6.2 Relevant parameters and Forces 44

2 Oscillatory flow past fixed cylinders: experimental apparatus 52
2.1 Introduction 52
2.2 The U-tube tank 53
2.3 How to get the required parameters? 56
2.4 Damping coefficient 60
2.5 Force measuring system 65
2.5.1 Load cells 65
2.5.2 Moistureproofing the strain gauged load cells 68
2.5.3 The successful methods 71
2.6 Force prediction and load cells' calibration 72
2.7 The data acquisition system 76

3 Force Measurement Analysis for fixed cylinders 77
3.1 In-line Force at various β parameters 78
3.2 Transverse Force at various β parameters 87
3.3 Discussion of the Results 90

3.3.1 Blockage effects 90
3.3.2 Force coefficients 91
3.3.3 Drag and Inertia coefficients 91
3.3.4 Transverse-force coefficients 96
3.3.5 Morison's equation 99
3.3.6 Comparison with Numerical Results 100

4 Oscillatory flow past flexibly mounted cylinders 111
4.1 Introduction 111
4.2 Experimental apparatus and procedure 112
4.3 Measurement of the relevant parameters 117
4.4 The data acquisition system 119

5 Response analysis for flexible cylinders 121
5.1 Introduction 121
5.2 Test Cases Results 122
5.2.1 First set-up, non-resonant case, $\beta = 750$ 122
5.2.2 Second set-up, $\beta = 750$ 124
5.2.3 Third set-up, $\beta = 270$ 125
5.2.4 Fourth set-up, $\beta = 60$ 127
5.3 Discussion of the Results 130
5.3.1 Qualitative Observations 130
5.3.2 Flow visualisation 133
5.3.3 Prediction of Forces and cylinder Displacements with Morison's equation 134
5.3.4 Prediction method applied to the non-resonant case . . . 135
5.3.5 Prediction method applied to a resonant case at β =750 139
5.3.6 Prediction method applied to a resonant case at β =270 143
5.3.7 Prediction method applied to a resonant case at β =60 . 147
5.3.8 Remarks on the prediction method 148

6 Conclusions 152
6.1 Achievements 152

Bibliography 156

List of Figures

1.1 Drag coefficient for circular cylinders as a function of Reynolds number, (from Schlichting, 1968) 23
1.2 Schematic diagram showing Gerrard's entrainment flows, (from Gerrard, 1966) 24
1.3 Drag and Inertia coefficients versus KC for various values of β (from Sarpkaya, 1976b) 32
1.4 (a) Drag coefficient versus KC. (b) Inertia coefficient versus KC (from Obasaju et al. 1988) 33
1.5 Vortex shedding at KC $\langle$ 4 (from Walker, 1990) 38
1.6 Vortex shedding pattern (a) in the asymmetric regime at KC $\sim$ 7; (b) in the transverse regime at KC $\sim$ 10; (c) in the diagonal regime at KC $\sim$ 18 (from Obasaju et al., 1988) 41
1.7 Three pairs wake regime, vortices C+D, B+E and F+G are for example the three vortex pairings occurring in a cycle (from Williamson 1985) 42
1.8 In-line response versus KC for 4 frequency ratios. □, measured; +, predicted. (from Bearman et al., 1992) 50

2.1 Sketch of the U-tube tank 55
2.2 KC-Re values for different cylinder diameter and fluid viscosities; □, water; o, 4 times more viscous than water; △, 10 times more viscous than water 58

2.3 Viscosity tests for the polyethylene glycol solutions 59
2.4 Damping Coefficient versus Maximum Amplitude of oscillation of water in different conditions 64
2.5 Load cell 65
2.6 The housing of the load cell (from Singh, 1979) 67
2.7 Schematic Set-up of the Calibration procedure using load cell type RS-2Kg, not in scale 74
2.8 Calibration lines 75

3.1 Drag coefficient and Inertia coefficient versus KC; ×, $\beta = 301$, Obasaju et al.; o, $\beta = 308$, present results; —, Wang's Theory. . 83
3.2 Drag coefficient and Inertia coefficient versus KC; ▼, $\beta = 75$, present results; —, Wang's Theory. 84
3.3 Drag coefficient and Inertia coefficient versus KC, □, $\beta = 53$, present results; •, $\beta = 35$, present results; —, Wang's Theory (upper line $\beta = 35$) 85
3.4 Root mean square coefficient for the in-line force versus KC . . 86
3.5 Total force coefficient $C_{F_{tot}}$ for the in-line force versus KC 86
3.6 $C_{L_{rms}}$ and correlation factor versus KC, $\beta = 308$ 88
3.7 $C_{L_{rms}}$ and correlation factor versus KC, $\beta = 70$ 89
3.8 Drag coefficient and Inertia coefficient versus KC for all the test cases: o, $\beta = 308$; ▼, $\beta = 75$; □, $\beta = 53$; •, $\beta = 35$; —, Wang theory lines ($\beta = 308$, lower line) 91
3.9 Drag and Inertia coefficients versus KC (from Sarpkaya 1976b) . 95
3.10 $C_{L_{rms}}$ and correlation factor versus KC, o, $\beta = 308$; △, $\beta = 70$. 97
3.11 Competition of subsequent shedding modes at KC regime boundaries as sketched may result in lack of spanwise correlation between each of the signals from the two cylinder ends . . 98

3.12 $C_{L_{rms}}$ versus KC to outline 3-D effects as evidenced in this research 98

3.13 Comparison between the measured in-line force time history — –, and the one predicted using Morison's equation – · – · –; KC = 3.16, β =308 101

3.14 Comparison between the measured in-line force time history — –, and the one predicted using Morison's equation – · – · –; KC= 30.45, β =308 101

3.15 Comparison between the measured in-line force time history— –, and the one predicted using Morison's equation – · – · –; KC = 5.18, β = 75 102

3.16 Comparison between the measured in-line force time history — –, and the one predicted using Morison's equation – · – · –; KC = 11.18, β = 75 102

3.17 Comparison between the measured in-line force time history— –, and the one predicted using Morison's equation – · – · –; KC = 15.30, β = 75 103

3.18 Comparison between the measured in-line force time history — –, and the one predicted using Morison's equation – · – · –; KC = 29.28, β = 75 103

3.19 Comparison between the measured in-line force time history— –, and the one predicted using Morison's equation – · – · –; KC = 4.64, β = 53 104

3.20 Comparison between the measured in-line force time history — –, and the one predicted using Morison's equation – · – · –; KC = 12.67, β = 53 104

3.21 Drag coefficient and Inertia coefficient versus KC, Experimental and Numerical results: □, $\beta = 53$, •, $\beta = 35$, present results; Numerical results: ⋆, $\beta = 34$, ∗, $\beta = 53$, Iliadis (1995). 106

3.22 Root mean square coefficient for the in-line force versus KC, Experimental and Numerical results: △, $\beta = 53$, •, $\beta = 35$, present results; Numerical results: ⋆, $\beta = 34$, ∗, $\beta = 53$, Iliadis (1995). 107

3.23 Drag coefficient and Inertia coefficient versus KC, Experimental results: ▼, $\beta = 75$, present results; Numerical results: $\beta = 76$: ∗, Sherwin (1995). 108

3.24 Drag coefficient and Inertia coefficient versus KC, Experimental results: ▼, $\beta = 75$, present results; Numerical results: $\beta = 76$: —, Wu's method, Lin et al.(1996); — · — · - pressure integration method, Lin et al. (1996); dotted line, Wang theory 109

3.25 Root mean square coefficient for the in-line force versus KC, Experimental and Numerical results: o, $\beta = 75$, present results; Numerical results: $\beta = 76$: ⋆, linear momentum method, Lin et al. (1996), □, pressure integration method, Lin et al.(1996); . . 110

4.1 U-tube, cylinder and suspension system 114

4.2 View of the cylinder and the pendulum suspension system . . . 115

4.3 Sketch of the cylinder motion 116

5.1 In-line measured response (r.m.s./D) versus KC for $F_r = 4.376$ and $\beta = 750$ 123

5.2 Power spectrum of the in-line measured response signal for KC $= 30.83$, $F_r = 4.376$ and $\beta = 750$ 123

5.3 In-line measured response (r.m.s./D) versus KC for 6 frequency ratios and β = 750 126
5.4 Power spectrum of the in-line measured response signal for KC = 12.06, F_r = 2.840 and β = 750 128
5.5 In-line measured response (r.m.s./D) versus KC for 3 frequency ratios and β = 270 128
5.6 In-line measured response (r.m.s./D) versus KC for 4 frequency ratios and β = 60 129
5.7 Drag and Inertia coefficients versus KC (from Sarpkaya 1976b) . 131
5.8 Test cylinder with wool tufts during flow visualisation 133
5.9 Drag coefficient and Inertia coefficient versus KC for the flexible cylinder, First set-up, x, β = 750, F_r = 4.376; and for the fixed cylinder, —, Sarpkaya, β = 784 136
5.10 Comparison between in-line force trace — from measured cylinder displ. and the predicted one — · — · —; non-resonant case First Set-up, at KC = 16.60 137
5.11 Comparison between in-line force trace — from measured cylinder displ. and the predicted one — · — · —; non-resonant case First Set-up, at KC = 22. 137
5.12 Comparison between measured cylinder displ. —, and the reconstructed one — · — · —; non-resonant case First Set-up, at KC = 16.60. 138
5.13 Comparison between measured cylinder displ. —, and the reconstructed one — · — · —; non-resonant case First Set-up, at KC = 22. 138
5.14 In-line response (r.m.s./D) versus KC for the First Set-up case; o measured; — predicted 139

5.15 Drag coefficient and Inertia coefficient versus KC for the flexible cylinder, Second set-up, x, β = 750, F_r = 2.808; and for the fixed cylinder, —, Sarpkaya, β = 784 140

5.16 Comparison between measured cylinder displ. —, and the reconstructed one − · − · −; resonant case Second Set-up, at KC = 8.50. 141

5.17 Comparison between measured cylinder displ. —, and the reconstructed one − · − · −; resonant case Second Set-up, at KC = 14.81 141

5.18 Comparison between measured cylinder displ. —, and the reconstructed one − · − · −; resonant case Second Set-up, at KC = 29.81 142

5.19 In-line response (r.m.s./D) versus KC for the Second Set-up case; o measured; — predicted 142

5.20 Comparison between in-line force trace — from measured cylinder displ. and the predicted one with flexible cylinder coefficients and fixed cylinder ones; resonant case Second Set-up, at KC = 10.0 144

5.21 Drag coefficient and Inertia coefficient versus KC for the flexible cylinder, Third set-up, o, β = 270, F_r = 2.990; and for the fixed cylinder, • , present research, β = 308 145

5.22 Comparison between measured cylinder displ. —, and the reconstructed one − · − · −; resonant case Third Set-up, at KC = 10.50 146

5.23 Comparison between measured cylinder displ. —, and the reconstructed one − · − · −; resonant case Third Set-up, at KC = 19.23 146

5.24 In-line response (r.m.s./D) versus KC for the Third Set-up case; o measured; • predicted 147

5.25 Drag coefficient and Inertia coefficient versus KC for the flexible cylinder, Fourth set-up, · $\beta = 270$, $F_r = 2.961$; and for the fixed cylinder, present research, $\beta = 75$ and $\beta = 53$ 148

5.26 In-line response (r.m.s./D) versus KC for the Fourth Set-up case; o measured; • predicted 149

5.27 In-line response (r.m.s./D) versus KC for the Fourth Set-up case; o, measured; •, predicted with flexible cylinder coefficients; x, predicted with fixed cylinder coefficients 149

List of Symbols

A amplitude of the oscillatory motion

A_r ratio of the amplitude of two successive peaks

A_w wetted area

b_r blockage ratio

c damping coefficient

C_A added mass coefficient

C_D drag coefficient

C_{F_x} in-line force coefficient

$C_{F_{rms}}$ root mean square in-line force coefficient, defined in section 3.1

$C_{F_{tot}}$ total force in-line force coefficient, defined in section 3.1

$C_{L_{rms}}$ root mean square transverse force coefficient, defined in section 3.2

C_M inertia coefficient

D cylinder diameter

f frequency

f_o cylinder natural frequency in air

f_{of} frequency of oscillation of the cylinder in oscillatory flow

f_{ow} cylinder natural frequency in still fluid

f_w fluid oscillation frequency

f_v vortex-shedding frequency

F force

$\overline{F}$ time mean of F

F_{xmax} maximum of the force

F_r frequency ratio

F_{rms} root mean square of transverse force signal

k stiffness

k_s structural stiffness

KC Keulegan Carpenter number, defined in section 1.4

KC_{cr} critical Keulegan Carpenter number value, boundary between attached and symmetric shedding regimes

KC_{crH} critical Keulegan Carpenter number value proposed by Hall, [17]

KC_s Keulegan Carpenter number corresponding to the onset of separation according to Bearman et al., [3]

l length of the arms of the pendulum

L cylinder length

L_w wetted length of the tank

m mass

m_d displaced mass

m_r mass ratio

m_s structural or effective mass

Re Reynolds number, defined in section 1.4

S Strouhal number

SKC surface Keulegan Carpenter number

t instantaneous time

T period of the fluid motion

U velocity of the flow

U_m maximum velocity of the flow

V volume occupied by the body

V_R velocity ratio

x in-line direction

x(t) cylinder response in the in-line direction (sometimes it is indicated as x only)

$\dot{x}$ time derivative of x(t)

$\overline{x}$ time mean of x

X_{rms} root mean square of the cylinder response

y transverse direction

W tank width

β viscous, or Stokes' parameter, defined in section 1.5

δ boundary layer thickness

δ_d logarithmic decrement

ΔE loss of energy in one cycle

ζ_s structural damping

$\theta = \omega$ t

μ dynamic viscosity

ν kinematic viscosity

ρ fluid density

ω_o angular frequency of the cylinder measured in air

Chapter 1

Flow around smooth cylinders: general review of the subject

1.1 Introduction

Prevailing trends in modern engineering require closer attention to the dynamic loading and response of structures either under aerodynamic or hydrodynamic excitation. Not only are the flows around ocean pipelines and off-shore platforms of practical importance, but they are also interesting as physical phenomena. An off-shore or coastal engineering structure sited in the ocean suffers from the effects of waves, currents and winds, and sometimes their complex combinations. For example, slender structural members such as riser pipes respond under the action of hydrodynamic forces and interactions may occur between the motion and the loading. These elements are particularly sensitive to resonant vibrations therefore both the in-line and transverse oscillations can be greatly magnified and if not appropriately predicted the effects on the structures can be dangerous and cause structural collapse.

Therefore it is fundamental to develop methods for designing coastal and off-shore structures which are able to resist the very hostile real environments (like open seas) and satisfy health and safety criteria to prevent catastrophic events from happening.

The ability to predict the hydrodynamic loads which these structures must suffer from, arises from the study of the flow around bluff bodies [1], from

[1] A bluff body is defined as a body which generates separated flow over a large portion of

the view of understanding the mechanisms of separation, recirculation, vortex shedding and vortex-induced oscillation of a body. The research on bluff body flows has recently experienced an intensive growth. The attention of engineers and fluid mechanicists has been drawn in particular to circular cylinders, because they are fundamental structural components. In the last fifty years a great deal of experimental and computational work has been done to understand this complex unsteady flow. Work with numerical models requires validation by basic hydrodynamic data which may be found from experiments.

The conventional procedure is to carry out laboratory experiments that deal firstly with the simplified situation (e.g. using idealised conditions we can obtain a reliable model of the loading and response of the structures) and then to consider additional parameters. Finally, it is possible to improve the model itself by trying to extend the results towards full scale. The laboratory study can be extended by research in the field, but the acquisition of reliable data in the ocean has proved problematical and difficult to interpret because of the large number of parameters involved and of the difficulty of making measurements.

1.2 Objectives and relevance of this work

The main aim of the present work was to investigate experimentally the flow field around a smooth circular cylinder in oscillating flow and to study some characteristic behaviour of both rigidly and flexibly mounted cylinders. The investigation was carried out mainly at low Reynolds number, [2] (all the parameters involved are defined in the next sections), where the flow around the cylinder is assumed two-dimensional and laminar. This is much lower than

its surface, when placed in a fluid stream if certain conditions either of the flow or of body geometry are fulfilled.

[2] $Re = UD/\nu$, expression (1.1) section 1.4, this parameter is often termed Re number

one may expect on a real off-shore structure, but the object of the investigation was to study the physics of the phenomenon rather than to provide design data, and to enable the validation of low Reynolds number, 2-D computations.

Because of the development of computers, considerable advances in the area of numerical simulations of flows around bluff bodies have been made over the last fifteen years. Most studies of flow passing a cylinder deal with the problem at low Reynolds number, Re, for which the flow is assumed two dimensional and laminar, because they require significantly less computer resources. In fact they do exhibit many important intrinsic features which are found in similar 3-D flows, but when 3-D effects are important to the flow, two-dimensional calculations cannot be expected to give reliable results.

On the other hand it is easier to get experimental results at somewhat higher Re values and therefore β (Stokes' parameter) values [3] (i.e. in cases where forces have to be measured because their magnitude is reasonably big to be recorded and analysed easily), but difficult to get full scale values.

In general it is known that at Reynolds number greater than 150 the wake behind a circular cylinder in steady incident flow develops spanwise motions through a process of secondary instability and becomes 3-D; this onset of three-dimensionality can be delayed up to Reynolds number $\sim$ 200 by using an appropriate form of control (end plates) as shown by Williamson, [51].

For oscillatory flows around cylinders three dimensionalities have been detected experimentally around the body surface at very small β values by Honji, [18], and by Tatsuno and Bearman, [47] as will be described in the course of this chapter.

Nevertheless three-dimensional simulations are currently being modelled only by a few research groups, because they require considerable computer

[3] $\beta = \frac{D^2}{\nu T}$, expression (1.3) section 1.5

resources.

Hence the attempt to compare computation with experiment has faced so far two major difficulties which can be summarised as follows: lack of detailed experimental measurements at low β , and restrictions in computer resources.

A study of the available literature on the problem was undertaken and apparently the smallest β value reached previously in experiments dealing with force measurements is around 100, [33]. Therefore the present experiments, carried out for the first time at β values as low as 35, stand out for their originality and usefulness, casting new light on a better understanding of the phenomenon.

The ultimate goals of the present research were in fact to study the effects of decreasing β on the flow features and to gather experimental results at similar conditions to those of a two-dimensional numerical solution (i.e. where the flow is still laminar), in order to confirm and validate the computational results by a direct comparison. In this way 2-D simulations can play a more practical role in the 'real engineering' applications. In the next sections of this chapter the development of the present understanding of the problems arising in oscillatory flow past immersed cylinders will be discussed with reference to the relevant literature.

1.3 State of the Art on the subject

1.4 Unidirectional flow past a fixed circular cylinder

This work describes research concerning the behaviour of both rigidly and flexibly mounted circular cylinders in oscillatory flow, but it is believed that for the comprehension of its mechanics, some features of the unidirectional steady flow case can be briefly highlighted.

The principal parameter in the description of the flow of an incompressible, viscous fluid is only the Reynolds number:

$$Re = \frac{UD}{\nu}, \tag{1.1}$$

where U is a characteristic velocity of the flow, D is a characteristic length scale (e.g. cylinder diameter) and ν is the kinematic viscosity, which represents the ratio of the inertial force to the viscous force.

This means that the general behaviour of a mean flow can be predicted when the Re number is known. For a circular cylinder over the range of Reynolds numbers it is usually possible in fact to distinguish different flow patterns that characterise the 2D flow. Nevertheless the regimes are not always well defined so the statement that a regime is found between two given Re numbers can only be approximate. As yet there is no universal agreement about the number or names of the various regimes, see for example Basu, [1], Gerrard, [14], Roshko, [34].

The different regimes can cause pronounced changes in the drag coefficient with varying Re. Figure 1.1 where C_D is shown versus Re, clearly displays that the state of the flow can exert a significant influence on the forces acting on a body in a fluid and that the value of the Reynolds number alone may describe the flow conditions in a uni-directional flow.

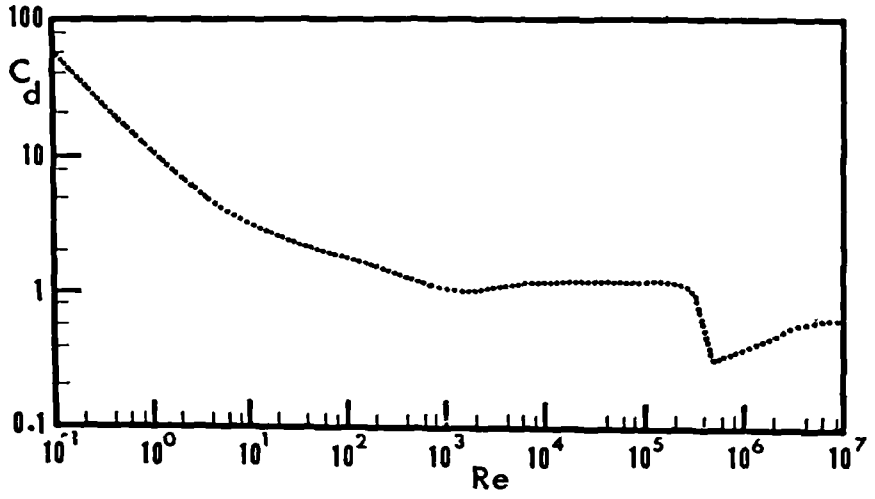


Figure 1.1: Drag coefficient for circular cylinders as a function of Reynolds number, (from Schlichting, 1968)

A brief description of the flow patterns occurring at different Re numbers follows, with particular attention to the laminar flow state as it is often defined when Re varies between 0 and 200.

For very small Reynolds number (less than about 1) the viscous force dominates over the inertial forces in the flow. The boundary layer remains attached all around the circumference of the cylinder. The flow pattern is almost symmetrical about the diameter of the body, parallel and normal to the undisturbed stream. As the Reynolds number increases the so-called separation region is formed (at around Re = 5, Batchelor, [2]). The separation region is composed in the first place of two standing eddies, rotating in opposition to one another, forming a recirculation bubble, and then, at higher Reynolds number (about 50), the separation bubbles become more and more elongated in the direction of the main stream and asymmetric instability sets in. As the Reynolds number rises above this critical value the flow is still laminar but the

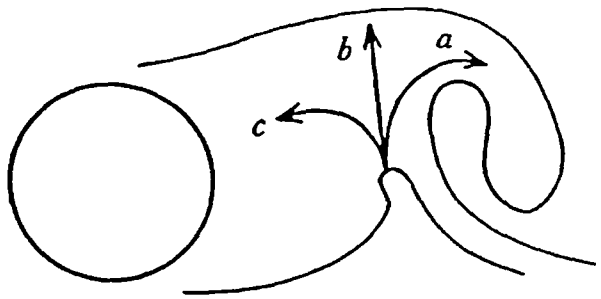


Figure 1.2: Schematic diagram showing Gerrard's entrainment flows, (from Gerrard, 1966)

near wake becomes unstable and oscillates periodically, vortices become asymmetrical, leave the cylinder and move downstream. Moving downstream they form a regular pattern consisting of two rows of alternating vortices known as a von Karman vortex street (1911). It is this alternating shedding of vortices that produces a transverse force, the lift, normal to the direction of the free stream. The relationship that links vortex-shedding frequency, cylinder diameter and the velocity of the ambient flow is denoted as $S = f_v D/U$, where S is known as Strouhal number.

For larger Re numbers the processes become more irregular and complicated: instabilities of the shear layer move upstream until they cause transition to turbulence prior to vortex roll-up. The appearance of large scale three-dimensionality also occurs, see also [1], [34], [51].

1.4.1 Formation of a vortex in unidirectional flow

The mechanics of the interaction between the two layers formed in the rear region of the body due to the separation can be seen in figure 1.2, (from

Gerrard [14]). Part of the generated vorticity is cancelled by mixing of the two layers which are characterised by opposite circulation, reducing the strength of each growing vortex which is shed and carried downstream.

The figure is a schematic diagram of the various entrainment flows which play an important role in the formation region. Here we see a vortex growing as it is being fed with vorticity from the upper shear layer. At one stage it becomes strong enough to draw the opposing shear layer across the wake.The vorticity carried by the opposing shear layer is then entrained in three possible directions. Most of it (a) gets drawn into the forming vortex and thus reduces its strength, but there is also entrainment into the shear layer (b). The remainder finds its way into the near wake and is cancelled a half period later by vorticity of the opposite layer.

The size of the formation region is determined by the balance between entrainment into the shear layer and the growing vortex and the replenishing of fluid by the induced reversed flow. The approach of oppositely signed vorticity in sufficient concentration cuts off further supply of circulation to the vortex. We may speak of the vortex as being shed at this stage.

1.5 Oscillatory flow past a fixed circular cylinder

1.5.1 Introduction

In harmonically oscillating flow, the onset of different flow conditions are considerably complicated by the effects of flow reversal or wake re-encounter and the Re number is not sufficient any more to describe them. Since the fluid changes direction, some or all of the vortices shed in one half cycle are swept past the body during a subsequent half cycle and this has an effect on the shedding in the next half cycle, on the magnitude of the fluid-induced forces

and on the frequency of the lift force. In this case it is not possible to describe the formation of a vortex as in the section above for unidirectional flow. In fact, in harmonically oscillating flow the vortices may form in different places around the cylinder in an extremely complex manner and moreover it is not always appropriate to talk about an 'opposite shear layer'. Nevertheless, as is illustrated in section 1.5.3, for certain values of the parameters involved (i.e. at high KC, see below) a regime where the wake from the cylinder resembles a von Karman vortex street is estabilished and section 1.4.1 description may be qualitatively applied as well.

The patterns of the flow field and the associated hydrodynamic forces are governed in this case by two dimensionless numbers (see Chapter 3 for dimensional analysis): (i) the Keulegan-Carpenter number KC, [22]:

$$KC = \frac{U_m T}{D} = \frac{2\pi A}{D} \tag{1.2}$$

where U_m is the maximum fluid velocity , T is the period of the flow, D is a characteristic length scale (e.g.the diameter of the cylinder), A is the amplitude of the motion, and (ii) the Reynolds number Re, (expression 1.1) with U_m as the characteristic velocity of the flow. Alternatively, a parameter combining Re and KC is expressed by their ratio, the parameter:

$$\beta = \frac{Re}{KC} = \frac{D^2}{\nu T} \tag{1.3}$$

called the viscous or Stokes parameter. Their physical relevance is underlined in this section.

The study of the literature that deals with wave loading on off-shore structures shows that when measuring velocities and conducting flow visualisations in planar flow experiments the flow past a body in incompressible fluid of constant density is kinematically the same regardless of whether the body accelerates through the fluid or the fluid accelerates past the body.

Garrison [13] showed the equivalence between the two cases and therefore results from either type can be directly compared.

The only difference arises when measuring forces or pressures. In fact, in the moving fluid case, an additional force acts on the cylinder due to the pressure gradient that would exist in the absence of the body. This gradient is proportional to the acceleration and produces an increment in the inertial part of the force. This additional term is a buoyancy-like force in-line with the flow, generally known as the Froude-Krylov force $\rho V\dot{U}$ where V is the volume occupied by the body, ρ is the fluid density and $\dot{U}$ is the fluid acceleration.

The practical differences between the actual realization of the two methods are delineated in Chapter 2 where the experimental apparatus is described.

Planar oscillatory flows are inherently different from the more complex wave induced flows. For example, they cannot reproduce the free surface effects, neither the orbital motion of particles found in waves, nor the attenuation of wave motion with depth. For this reason a traditional approach of investigation consists of separating the effects brought about by the wave induced nature of the flow from the periodic reversal of flow in simply harmonic rectilinear motion. Such simplifications of the flow have been crucial in enabling greater understanding of wave flows to be reached. All in all force measured on sections of cylinders in regular waves appear to correlate well with measurements made in planar oscillatory flow.

The starting point for all off-shore structural analysis is the estimation of the forces generated by the fluid loading. In terms of components relative to the direction of the incident wave it is usual to consider the total force divided into **in-line** and **transverse** components.

1.5.2 The time-dependent forces

Over the years harmonic flow has been investigated by a number of researchers who faced serious difficulties when trying to describe the time-dependent forces acting on an immersed body.

Stokes [46], in 1851 showed that the force acting on a sphere oscillating in a liquid could be resolved in two main components, an inertial force linearly dependent on acceleration and a drag force linearly dependent on velocity. As a continuation of Stokes equation, which was applicable only to attached flow conditions as both components of the force depended upon the fluid viscosity, Iversen and Balent [20], Keim [21], and Bugliarello [11], embarked on an analysis of the separated flow condition. It proved very unsatisfactory revealing that much of the desired information needed to be obtained experimentally.

In this respect the semi-empirical method proposed by Morison et al. in 1950, [32], to estimate wave forces on piles proved to be invaluable. Again they assumed that the in-line force acting on a section of the pile due to wave motion was made up of two components: a drag force, F_d, and an inertial force, F_i. The former is all the force in phase with the velocity, it has the same form as the force on a cylinder in steady flow, the absolute value of the water particle velocity is inserted in the case of oscillatory flow to insure that the drag force is in the same direction as the velocity. The latter is all the force that is in phase with the fluid acceleration and has the same form as the force in unsteady inviscid flow. The force expression therefore became:

$$F = F_d + F_i = \frac{1}{2}\rho D C_D U \mid U \mid + \frac{1}{4}\pi\rho D^2 C_M \frac{dU}{dt} \tag{1.4}$$

where F is the force per unit length, U and $\frac{dU}{dt}$ are respectively the incident flow velocity and acceleration, ρ is the density of the fluid, D is the diameter of the circular cylinder. C_D and C_M are the drag and the inertia coefficients

which are usually determined experimentally (their calculation is described in Chapter 3).

Morison's equation is based on the assumption that the kinematics of the undisturbed flow can be taken as constant over the region of the cylinder. This implies that the body size is small relative to the wave length so that the incident flow is virtually uniform in the vicinity of the body. Bodies of diameter much smaller than the wavelength will be considered in this research.

A great deal of investigations began then into understanding how the force components varied and upon what they depended.

Keulegan and Carpenter [22] in 1958 studied the oscillatory flow around both flat plates and circular cylinders, they suggested that the force acting on a cylinder in oscillatory flow was dependent upon Re and t/T and also upon the non-dimensional parameter $\frac{UT}{D}$ which was referred by the authors as the 'period parameter' but has since become known as the Keulegan-Carpenter number.

They showed that the drag and inertia coefficients in Morison's equation were a function of the KC number, but were unable to find any significant effect of Reynolds number on these coefficients. However, when they related the coefficients to the period parameter a definite and regular dependence was discovered.

On the basis of flow visualisation Keulegan and Carpenter observed that for low values of the KC parameter flow separation was suppressed and as the KC value increased, vortex formation and shedding of vortices began to appear. This led to the concept of a critical value of KC below which flow separation was suppressed and also clarified much about the physical significance of the period parameter. KC can be viewed as a parameter which compares the distance a fluid particle moves during the passage of a wave with the structure (cylinder)

diameter. When KC is small the inertial forces dominate, the vorticity does not have enough time to diffuse thus the flow is essentially attached (see also the section regarding the different flow regimes 1.5.3).

As KC increases the boundary layers separate, vortex formation and shedding occurs and drag forces become increasingly important. The transport of vorticity by convection in addition to that by diffusion plays a fundamental role on the flow.

Even periodic time-dependent flows are difficult to deal with analytically, and so to simplify further the analytical approach Sarpkaya [36] suggested to eliminate time as an independent variable in the evaluation of the force coefficients (Chapter 3) and also to use the frequency parameter $\beta = \frac{Re}{KC} = \frac{D^2}{\nu T}$ instead of the Reynolds number. In the particular case of a U-tube where the oscillation period T is fixed it is in fact more convenient to replace the Reynolds number by β .

For a series of experiments conducted with a cylinder of a given diameter D in a fluid of uniform and constant temperature, β is constant while KC may be varied. Then the variation of a force coefficient with KC may be plotted for constant values of β . Nevertheless the Reynolds number can easily be found from $Re = \beta \times KC$.

From a physical standpoint the parameter β can be seen as the ratio of the time that the vorticity takes to diffuse a distance equal to the cylinder diameter to the flow oscillation period or, that is the same, the ratio of the rate of diffusion through a distance δ [4] (i.e. ν/δ^2) to the rate of diffusion through a distance D (i.e. ν/D^2). Large β means that the boundary layer is thin compared to the cylinder diameter.

Sarpkaya in 1976, [36], showed in fact that a representation of the force

[4] $\delta \propto \sqrt{\frac{\nu T}{2\pi}}$ is the boundary layer thickness

coefficients for a fixed cylinder irrespective of the β values (as was done by Keulegan and Carpenter [22]) may obscure their dependence on β and hence Re. He re-examined the work of Keulegan and Carpenter and carried out a series of new experiments in a U-shaped vertical water tunnel. In this way he showed the importance of β as one of the controlling parameters. Some of Sarpkaya's results are presented in figure 1.3 for a β range between 5260 and 497.

The force experienced by a cylinder can roughly be divided in to three KC regions: when KC is small the force induced on the cylinder is mainly inertial, as KC increases the drag force becomes also important as a direct force, for KC more than 25, the flow approaches a quasi-steady situation and inertial effects are less important (Graham [15]).

Considering the trend with β the picture that emerges from figure 1.3 is that for decreasing β C_D increases for all KC and C_M is fairly constant for KC up to 7 and then decreases. Experimental data taken at β values between 1665 and 109 were carried out by Obasaju et al. [33], (as mentioned in section 1.2), figure 1.4. They found indications that at around $\beta = 1000$ the C_D is not so sensitive to β and sometimes, due to variations in the spanwise correlation of the vortex shedding C_D can take 2 values for the same KC values, especially in the regimes named as transverse and diagonal, see section 1.5.3. Their observations suggested that the higher value of C_D occurs in runs where the spanwise coherence of vortex shedding is high. Obasaju et al.'s C_D coefficient, [33], exhibits a trend similar to the one depicted by Sarpkaya for β between 1665 and 301, i.e. it increases with decreasing β , but it reverses than between 301 and 109. C_M instead appears to drop with β up to KC = 6, but then it increases with decreasing β . These trends are interesting especially in the light of the present research, conducted for β between 308 and 35, see section

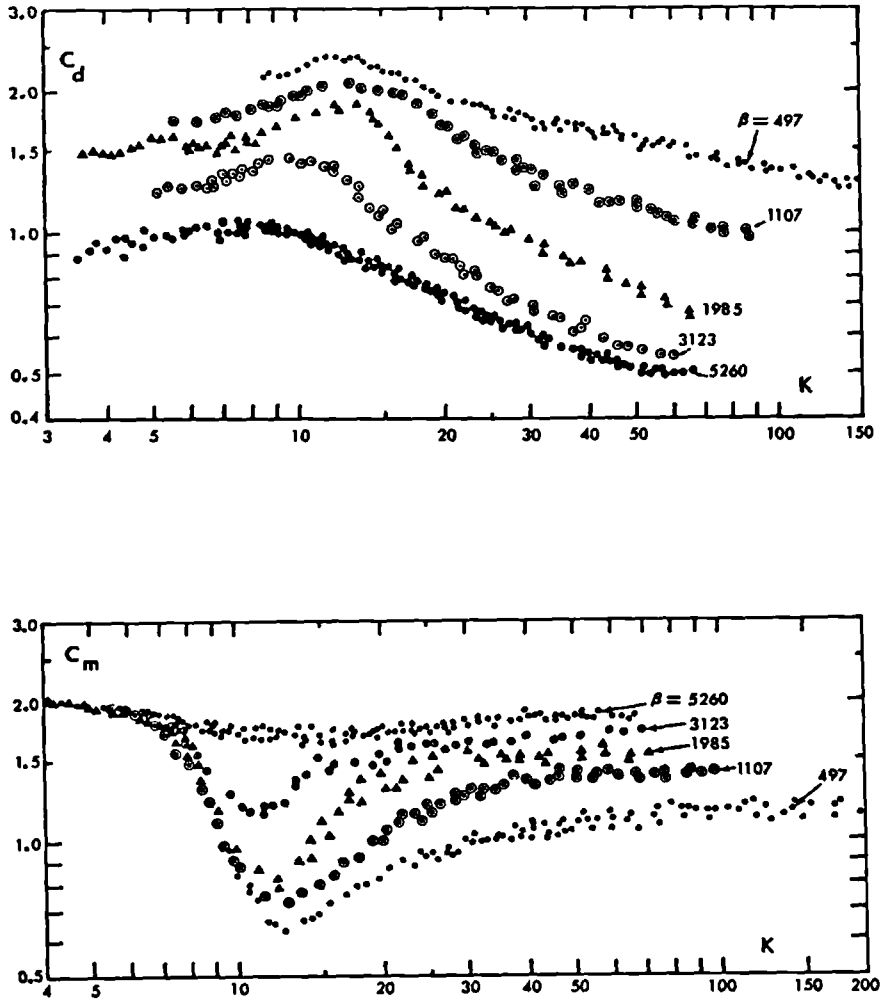


Figure 1.3: Drag and Inertia coefficients versus KC for various values of β (from Sarpkaya, 1976b)

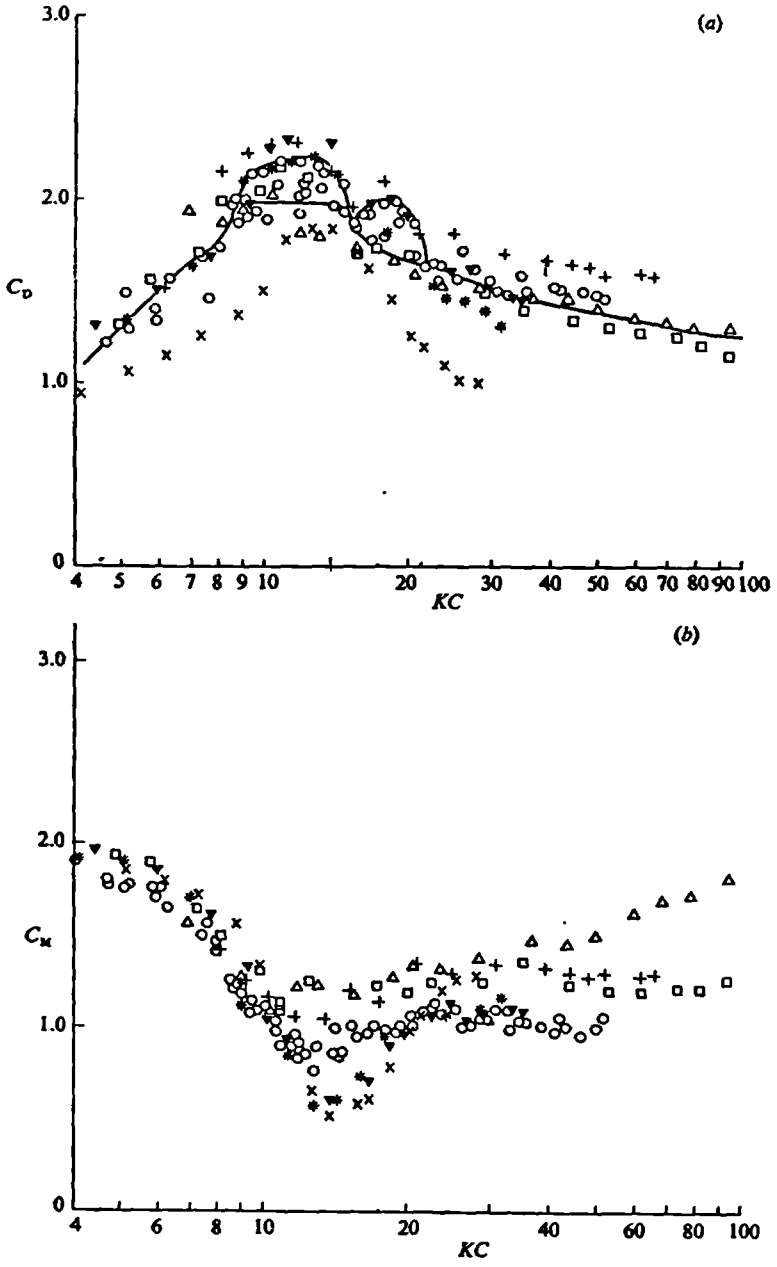


Figure 1.4: (a) Drag coefficient versus KC. (b) Inertia coefficient versus KC (from Obasaju et al. 1988)

3.3.

Although no one has suggested a better alternative, the use of Morison's equation gives rise to a great deal of discussion on what values of the coefficients should be used. In fact it does not indicate the way in which the coefficients may be expected to vary, and it doesn't always predict time history correctly.

Numerous attempts have been made either to improve Morison's equation or to devise new equations. Sarpkaya and Isaacson [40], for example, have described methods to improve the Morison's equation in terms of matching the measured data by adding higher odd harmonic terms. Several authors (Sarpkaya [35], Maull and Milliner [28] and Graham [16]), have proposed the use of an equation due to Blasius, to calculate both in-line and transverse forces, but its application requires detailed information on vortex strengths and motion which is difficult to obtain experimentally.

So it appears that it would be rather difficult to abandon the linear-quadratic sum and the reason for this is the very complicated flow picture that occurs for flows around marine structures.

All in all in fact, Morison's equation has proved reliable in accurately predicting wave forces on small members in simple flows or for predicting the magnitude of the in-line maximum force. The small discrepancies experienced may be regarded as unimportant in the presence of many other uncertainties in a design. Moreover, a vast library of data on C_D and C_M is available from numerous laboratory and field experiments. Except in a narrow range of KC values, between about 8 and 25 circa, where the motion of the vortices is more complex, the simulation of the forces is good (see section 3.3.5 for a direct comparison between the measured forces and the ones predicted via Morison's equation at different KC values), however more research is needed in a systematic and controlled way both in the laboratory and in the field to develop

reliable design curves for these coefficients.

As for the aforementioned **transverse** force it has been shown, [28], [4], [6], that cylinders immersed in oscillatory flow can experience side forces due to formation and shedding of vortices. They are more difficult to analyse than in-line ones since they are more sensitive to the ways in which vortices are shed and move. Not only can their magnitude be of the same order as the in-line ones, [5], [36], but being characterised by higher frequency they may have a major influence on the fatigue life of some structural members.

Moreover, [44], these forces do not repeat but vary from cycle to cycle and have periods of very little lift followed by sudden high amplitude sequences, in an apparently random way. This was also noticed in the present research. For this reason they are generally studied with reference to a C_{Lrms} lift coefficient (section 3.2). Several authors have proposed ranges of KC for particular types of vortex-shedding behaviour (see Singh, [44], Sarpkaya and Isaacson, [40], Bearman et al., [5], they are described in next section) and even when KC and β are fixed, more than one mode of shedding is possible, and the flow may switch between the possible modes (Bearman et al., [5]).

For large KCs the flow about circular cylinders tends to a quasi-steady state (see section 1.5.3). This has led to a method of describing the form of the lift force known as the quasi-steady theory, Bearman et al., [6], Obasaju et al., [33]. Because of the apparent randomness from cycle to cycle, they developed a mode-averaging technique sorting and averaging together the force and the velocity for those cycles with the same mode of vortex formation. This avoided the problem of a zero resultant. The fit was good for high KC, when comparing the predictions with experimental results. At lower KC the accuracy of the method deteriorated, because the wake from the cylinder is no longer similar to shedding in steady incident flow.

1.5.3 Flow regimes

The use of flow visualisation has improved the understanding of the role of vortices in fluid loading. It was observed that within particular ranges of flow amplitudes certain repeatable vortex-shedding patterns occur around a circular cylinder subjected to oscillatory flow. Several authors have studied each of these patterns through flow visualisations (for a more detailed discussion and visual description of flow regimes see Williamson, [50], Bearman et al., [3], Obasaju et al.[33], Tatsuno and Bearman, [47]) and proposed ranges of KC corresponding to each of the flow regimes with corresponding force traces. Moreover not only did they find that the process of development and shedding of vortices depends on the values of KC but also that it depends on the β parameter, (Bearman et al., [5]).

The flow regimes can then be listed with reference to the KC ranges of occurrence, considering that regime boundaries do not always occur at exactly the same value of KC and, as mentioned, they depend on β too (for a detailed description of flow regimes for $KC < 15$ and $\beta < 160$, see Tatsuno and Bearman, [47]) so the values of KC given below have to be considered as a mere indication.

- The flow remains **attached** throughout the motion regardless of β, as long as KC is small enough (as said in section 1.5.2 when KC physical meaning was highlighted). Many researchers ([3],[18], [39], [47]) have investigated what happens at low KC for different β . Generally for $0 < KC < KC_{cr}$, where KC_{cr} equals 1 or 2 depending on β , the laminar flow is thought to be symmetrical, attached, stable and two-dimensional. In this case it is possible to compute the two force coefficients analytically with a high degree of accuracy. The analysis for oscillatory viscous flow was first given by Stokes, (1851) [46], for the case of spherical and

cylindrical pendulum bobs. Wang (1968) [49], studied the problem of a fixed circular cylinder in oscillatory incompressible viscous flow and derived the drag and inertia coefficients as:

$$C_D = \frac{3\pi^3}{2KC}[(\pi\beta)^{-\frac{1}{2}} + (\pi\beta)^{-1} - \frac{1}{4}(\pi\beta)^{-\frac{3}{2}} + ...]; \qquad (1.5)$$

$$C_M = 2 + 4(\pi\beta)^{-\frac{1}{2}} + (\pi\beta)^{-\frac{3}{2}} + ... \qquad (1.6)$$

that are valid for small KC, small ReKC and large β .

These force coefficients are found to agree well with experiments at sufficiently small KC values ([3], [39], and present results, see section 3.3). This agreement holds if the flow is two-dimensional. For a critical combination of KC and β a small scale three-dimensionality in the boundary layer was at first reported by Honji, in 1981, [18], who found that the attached boundary layer on a circular cylinder may exhibit a three-dimensional instability leading to the generation of axially periodic vortices running around the cylinder. These results were confirmed by many researchers and in particular Hall [17] proposed an equation relating the critical Keulegan-Carpenter number, at which these instabilities may ap pear, to β :

$$KC_{crH} = 5.778\beta^{-\frac{1}{4}}(1 + 0.205\beta^{-\frac{1}{4}})$$

which was in excellent agreement with Honji's observations over a wide range of β .

Experiments at low KC values were conducted by Bearman et al., [3],for KC between 0.1 and 1, and for β ranging between 196 and 1665. They concluded that the experimental values are in approximate agreement with Wang's predictions below a given value of KC, termed KC_s, and

attributed the increase in C_D for $KC > KC_s$ to the onset of flow separation and vortex shedding. Sarpkaya, [39], extended the research and found that the appearance of Honji instability is accompanied by a rise in C_D above the prediction of Wang. This may be explained considering that this is a local three-dimensionality which takes place in the boundary layer and as it were increases its thickness and the skin friction drag.

- For KC between KC_s and about 4, depending on the value of β , the flow separates and remains symmetrical. In this **symmetric** shedding regime two vortices with rotations of opposite signs, are formed symmetrically behind the cylinder and as the flow reverses they are convected towards the cylinder but do not survive into the next half cycle and depending on β , they may be cancelled by mixing with vorticity of opposite sign in the cylinder boundary layer, figure 1.5 [48].

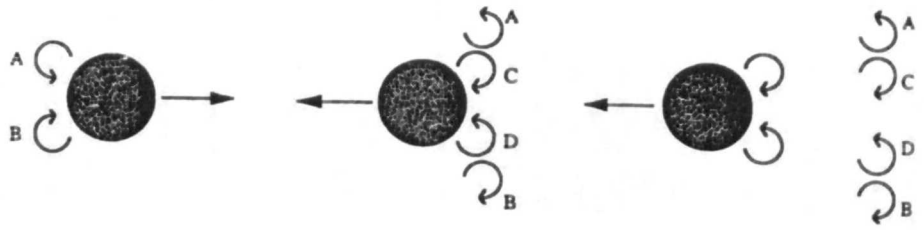


Figure 1.5: Vortex shedding at KC ⟨ 4 (from Walker, 1990)

For $\beta = 730$ and KC around 4 Williamson, [50], found via flow visualizations that two symmetric pairs of vortices are formed in each half

cycle, as the cylinder reverses it pushes through the second pair causing one vortex to move past one side and the other vortex to move past the other side of the cylinder, these vortices then form two pairs with the new vortices formed in the next half cycle. Both these pairs are shed and move away from the cylinder along the axis of oscillation. Two more vortices form then and the process is repeated.

In the symmetric regime there is very little change in the inertial coefficient, which is slightly larger than the potential flow value of 2, while the drag coefficient decreases. The dominant forces are inertial as mentioned also above.

As KC increases, an asymmetry is noticed in the process of vortices formation which corresponds to the **asymmetrical** regime described hereafter [3], [38], [50].

- For KC between 4 and 8 the two initial vortices become stronger but one of the two vortices grows more rapidly than the other, figure 1.6 (a). As they are swept back over the cylinder the larger vortex cancels out the greater amount of vorticity in the boundary layer on that side of the cylinder so the vortex formed on that side in the next half cycle is the weaker of the two, with the result that the larger vortex forms on the other side of the cylinder. This asymmetry causes a lift force to be generated. The presence of the vortices causes an increase in the drag and a decrease in the inertia coefficient, see figure 1.3. The two terms in the Morison's equation start being of comparable importance, their values depending on the changes in the vortex shedding patterns as described herein and below.

- For $8 < KC < 15$ one large vortex is shed during each half cycle and

the most of the vortex shedding takes place on one side of the cylinder. A vortex from one half cycle is swept back over the cylinder causing an increase in velocity and therefore initiating shedding on that side of the cylinder, this vortex grows until, as the flow reverses, it draws the opposite vortex over to that side, in doing so cancelling a lot of the vorticity. What remains of this vortex has vorticity of the same sign as the first formed, in the next half cycle shedding on the same side of the cylinder initiates as the flow reverses. The shed vortices convect away roughly normally to the main flow direction in the form of a street. This flow regime is therefore termed **transverse street** or single pair, figure 1.6 (b). The role played by vortices becomes most pronounced if the duration of flow in one direction is not too long (e.g. if the amplitude-to-diameter ratio is about two). In this range in fact drastic changes in the drag and inertia and lift coefficients are observed, section 3.3.

- At $15 < KC < 24$ an additional vortex is shed per half cycle, and the vortex pair in the one half cycle is shed diametrically opposite to the pair in the previous half cycle. The two vortices convect away at an angle of about 45 degrees. This flow regime is termed **diagonal shedding mode** or double pair, figure 1.6 (c).

- For $24 < KC < 32$ three full vortices are formed during each half cycle and three vortex pairs convect away from the cylinder during a complete cycle, this is the **three pairs** regime, figure 1.7. Progressively increasing KC, additional vortices form during a half cycle. The wake tends to a vortex street-like structure on each side of the cylinder, similar to that formed in uni-directional flow.

Williamson, [50], noted that for flow regimes above KC = 7 the flow

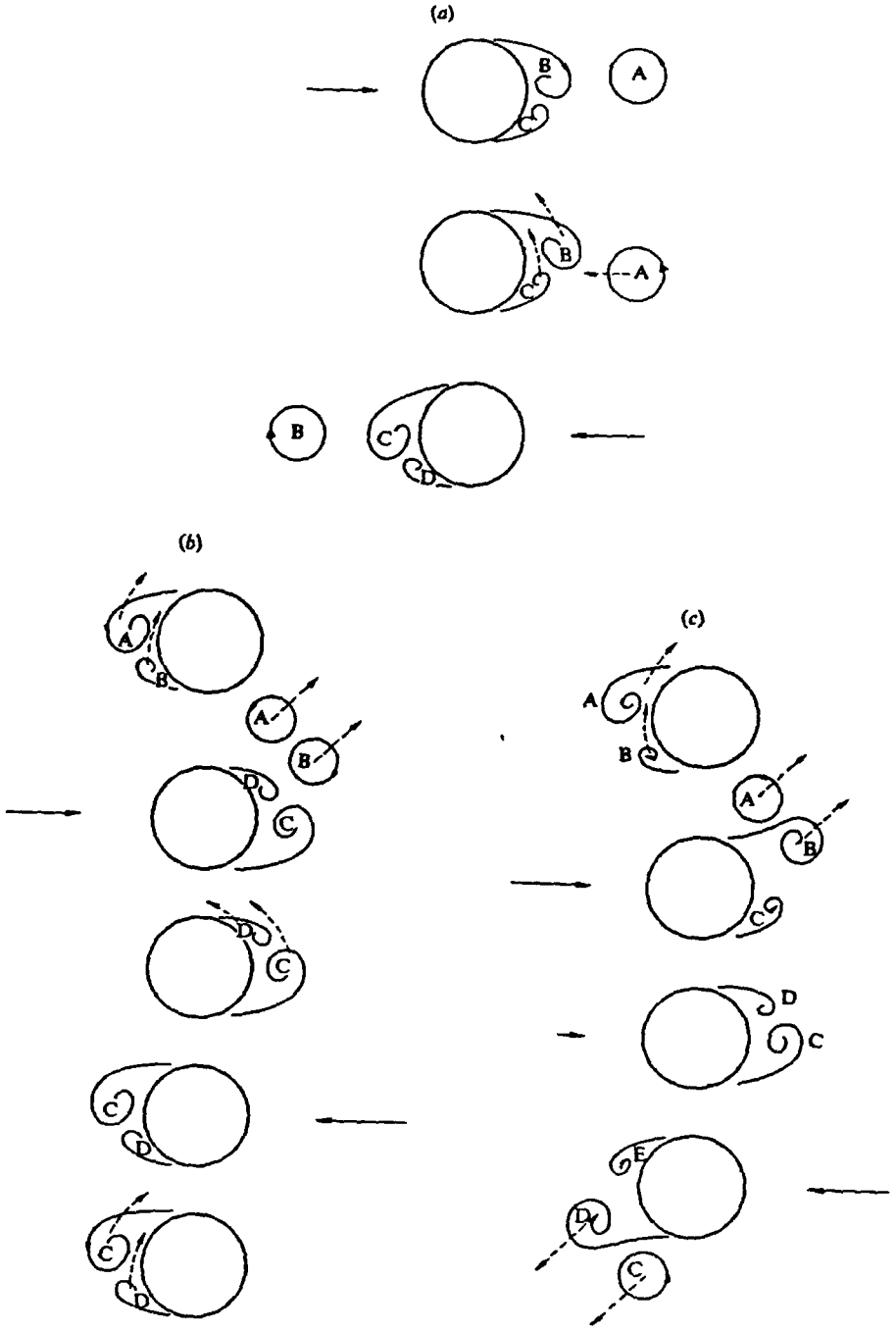


Figure 1.6: Vortex shedding pattern (a) in the asymmetric regime at KC $\sim$ 7; (b) in the transverse regime at KC $\sim$ 10; (c) in the diagonal regime at KC $\sim$ 18 (from Obasaju et al., 1988)

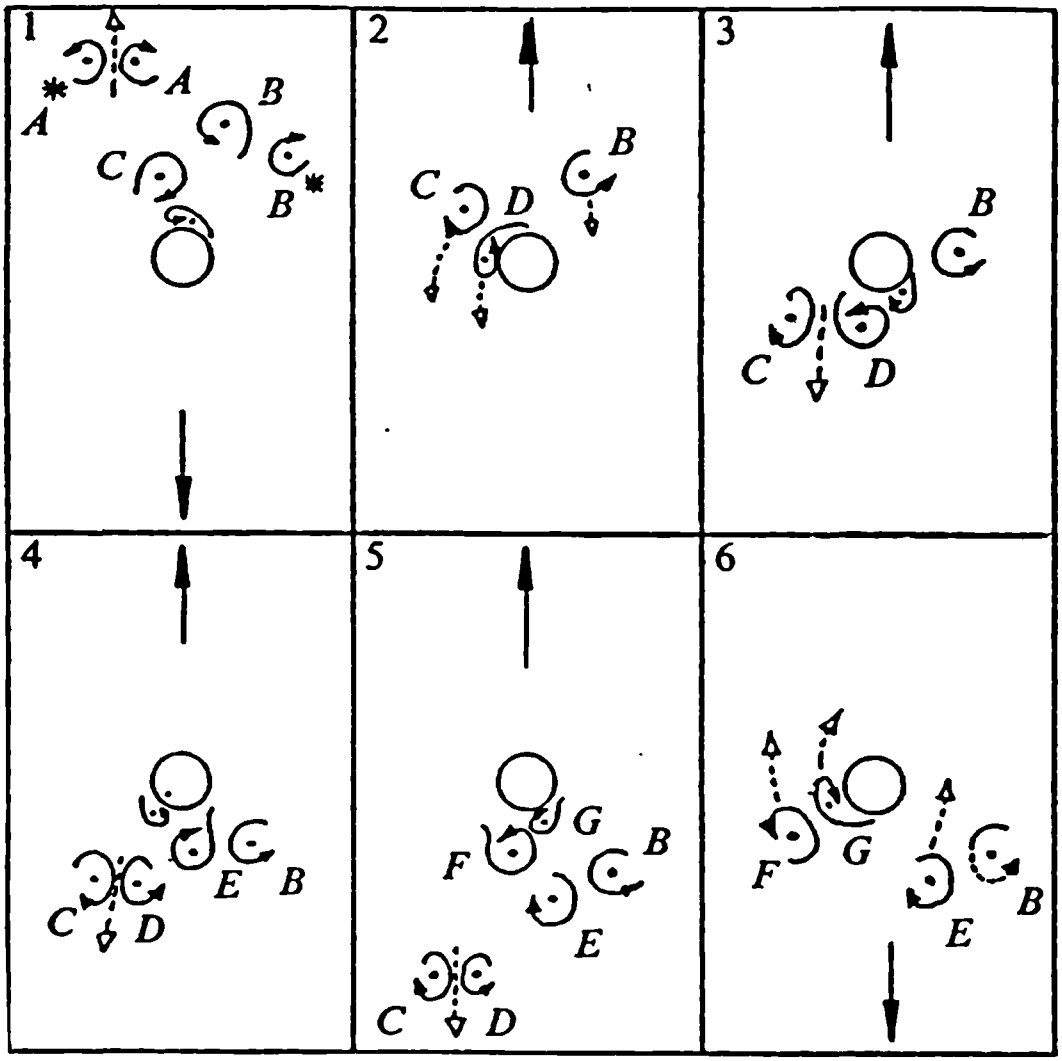


Figure 1.7: Three pairs wake regime, vortices C+D, B+E and F+G are for example the three vortex pairings occurring in a cycle (from Williamson 1985)

regime changes as KC is increased in steps of about 8. He reported in fact that an increment of about 8 generates one more vortex per half cycle.

For large KC values the drag term dominates the force equation. A change in KC does not produce a large change in the in-line force, the drag and inertia coefficients vary very little, as can be seen in figure 1.3, and section 3.3.

As mentioned in section 1.2, strictly two-dimensional flows can only exist in computer simulations and in fact large-scale three dimensionality has been found via flow visualisations by for example, Tatsuno and Bearman, [47]. They used the electrolytic precipitation method and illuminated through slits several cross-sectional planes around the cylinder. They were able to establish the three-dimensional nature of the induced flow structure for different β and KC pairs and showed that the flow can be three-dimensional along the cylinder axis at β numbers as small as 30 and KC = 6.

1.6 Flexible cylinders in an oscillating fluid flow

1.6.1 Introduction

Wave loading on flexibly mounted vertical cylinders is of particular interest to off-shore engineers. Some elements of off-shore structures and associated systems, for example fixed steel jacket platform structures and marine risers which consist of small-diameter circular cylinders, may have natural periods in the same range as wave periods. In these cases, depending on their orientation and the nature of their mounting system, they may be prone to vortex-induced transverse vibrations at frequencies which are integer multiples of the wave frequency, and in-line vibrations at frequencies which are odd multiples of the wave frequency. These may be important as regards the fatigue life of the structure, if the system is not heavily damped, and can result in an amplification of fluid loading and oscillation amplitudes in excess of those predicted using loading estimated from fixed structures.

Although there are several detailed summaries of the dynamic behaviour of flexible structures in oscillating flow such as given by Sarpkaya and Isaacson [40], the subject has not received as much attention as that of fixed structures in waves, and in particular there are very few investigations of in-line responses of compliant cylinders in oscillatory flow at low β numbers. Therefore there is plenty of scope for further research.

1.6.2 Relevant parameters and Forces

As seen so far in harmonic oscillatory flow the fluid forces are governed both by the Keulegan-Carpenter number, and the Reynolds number or the viscous parameter β.

In the case of an elastically mounted cylinder three additional variables

affect the response characteristics: mass, damping and stiffness (m,c,k). They are defined per unit length of the cylinder and relate to the structure, (therefore sometimes the subscript s is used). If the cylinder is allowed one degree of freedom say in the in-line direction x, the equation of motion governing the response of the cylinder can be written as:

$$m\ddot{x} + c\dot{x} + kx = F(t) \tag{1.7}$$

where F(t) is the total fluid force acting on the cylinder. The damping is generally expressed as ζ_s, that is the structural damping measured in air where $\zeta_s = c/2m\omega_o$, and the cylinder natural frequency in air for small amplitude oscillation $f_o = \omega_o/2\pi = \frac{1}{2\pi}\sqrt{\frac{k}{m}}$. Through the dimensional analysis the response x can be expressed as a function of several non-dimensional parameters:

$$x/D = f(KC, \beta, m_s/\frac{1}{4}\rho\pi D^2, \zeta_s, f_{ow}/f_w), \tag{1.8}$$

where ρ is the density of the fluid, f_w is the fluid oscillation frequency, m_s is the effective mass, including the contribution from the support system. The ratio $m_r = m_s/\frac{1}{4}\rho\pi D^2$ is called the mass ratio and $F_r = f_{ow}/f_w$ the frequency ratio.

Further remarks on the frequency ratio are pointed out in Chapter 4. At this point it must be underlined that it is debatable whether the cylinder natural frequency in air f_o, or in still water f_{ow}, should be used, for none of them represents the natural frequency of oscillation in oscillatory flow, since the added mass does not remain unchanged for all types of flows (Sarpkaya and Isaacson, [40]). Generally the one with f_{ow} is used.

Strictly, all the parameters mentioned whose measurements are taken in air should be carried out in vacuo.

The foregoing indicates the increased complex nature of wave loading and structural response in this case, when compared to uni-directional and planar

oscillatory flow past fixed cylinders, nevertheless the general characteristic features of vortex formation and shedding described in previous sections apply herein.

Using flow visualisations Sawaragi et al., [41], examined the response motions of a vertical cantilevered pile in waves for $2 \leq SKC \leq 20$.[5] They found separation for SKC below 3 and observed two symmetric attached vortices for $3 < SKC < 8$. Between 8 and 13 two vortices were again observed but one of them was shed per half cycle, whereas in the range of SKC between 13 and 20 there were three vortices.

Drag and lift forces over four and a half times the uniform flow values were obtained by Laird, [24], who oscillated a flexibly mounted cylinder in still water.

From U-tube experiments Sarpkaya, [40], suggested that both the in-line and transverse fluid loading may be larger on a flexibly mounted cylinder than on a fixed cylinder.

McConnell and Park, [30], measured the lift forces and responses of a vertical cylinder oscillated in still water. The cylinder was able to be either restrained or else flexibly mounted in the transverse direction. They suggested that, since the response of an elastically mounted cylinder has a feedback on the fluid loading, forces on elastically mounted cylinders in oscillating flows cannot be predicted using data from fixed or flexibly mounted cylinders in steady flow.

A theoretical model was proposed by McConnell and Park and the transverse forcing frequencies predicted. They suggested that the velocity ratio $V_R = KC/F_r$ is a significant parameter for characterising general regions of

[5]SKC is the surface Keulegan-Carpenter number, used in waves, where the vertical distribution of velocities is not constant and the the maximum velocity at wave surface is considered

behaviour. Their theoretical model showed that there were three significant frequency components, at $f_v - 2f_w$, f_v and $f_v + 2f_w$ where f_v is the vortex shedding frequency, and they can be found to occur in three distinct V_R ranges.

In a later experimental investigation McConnell and Park, [31], suggested that the most important dimensionless parameter in determining fluid loading problems involving flexible cylinders in an oscillating flow is the frequency ratio $F_r = f_{ow}/f_w$ where f_{ow} is the natural frequency of the cylinder in still fluid.

McConnell and Jiao, [29], determined the Morison drag and inertia coefficients from the in-line forces measured on a cylinder elastically mounted in the transverse direction, oscillated in still water. For small KC numbers they found that the drag coefficient was more dependent on the ratio of natural frequency to driving frequency than either the Reynolds number or the velocity ratio. At high values of the frequency ratio the drag coefficient became nearly constant. Similar behaviour was observed for the inertia coefficient and transverse response amplitude of the cylinder indicating that the in-line force coefficients are highly coupled with the transverse response.

It should be noted at this point that in neither set of experiments did McConnell and Park, [30], [31], or McConnell and Jiao, [29], allow the cylinder to respond in the in-line direction.

Measurements of transverse response (with the cylinder constraint in the in-line direction) were also presented by Bearman et al., [9], who conducted experiments on a circular cylinder suspended in a U-tube (the same one used in the present research, Chapter 2 and 4). In the first sets of the experiment they kept the structural damping of the system low to determine likely maximum responses for different ranges of the frequency ratio. They confirmed previous research groups' results when they found that the cylinder oscillates predominantly at either $2f_w$, $3f_w$ or $4f_w$ depending upon frequency ratio and

KC, but when tuning the natural frequency of the cylinder to an exact multiple of f_w the response did not exhibit the maximum peak. This result was in agreement with the previously cited McConnell and Park, [30], but not with the work of Maull and Kaye, [27]. The latter in fact found response peaks at integer values of frequency ratios. Their apparatus though was very different. It consisted of a bottom-pivoted-cylinder placed in a wave tank and it could therefore undergo strong three-dimensional effects.

Bearman et al., [9] also increased the structural damping and found the striking result that an increased damping produced an increased response, concluding that vortex induced vibration in harmonic flow is a very complex phenomenon and there may be very subtle interactions between the flow and the motion of the cylinder, involving the structural parameters.

In recent years the use of numerical simulations of response of flexible cylinders has improved the understanding of the phenomena. Bearman et al., [7], for example, carried out numerical simulations of transverse response using a discrete vortex formulation, that predicted amplitude levels in good agreement with experiment over a range of Keulegan-Carpenter numbers.

As for the in-line response it has already been said that it has not received as much attention, and the majority of the research focusses on transverse response only.

Maull and Kaye, [27], in the research quoted above studied also wave direction response and speculated upon the possible interactions between transverse and in-line responses. They showed that transverse oscillations of a vertical circular cylinder is the same irrespective of its constraint in the in-line direction, whilst this seemed not to be the case for in-line oscillations. In fact these amplitudes seemed greater if the cylinder was allowed to move in the x direction only, as opposed to when it was allowed two degrees of freedom (x and y

at the same time). They suggested that this may be due to increased vortex strength and change in the vortex trajectory.

Bearman et al., [8], investigated in-line response of circular cylinders both via predictions and experimental measurements at $\beta = 750$. They used the same U-tube apparatus and pendulum suspension system quoted above (that is also the same used in the present research, see Chapter 4 for a detailed description), that in this case allowed motion of the cylinder in-line with the U tube flow.

Their work showed that the general form of the response in the in-line direction can be fairly well described by using the relative motion form of Morison equation for frequency ratios around 2 and 3 (using the cylinder natural frequency of small amplitude oscillation in still water in the ratio), when the response increased smoothly with KC and the dominant cylinder oscillation frequency is the fluid frequency, but it also showed that Morison's equation gives a poor estimate of the force in a resonant case, for example when the frequency ratio is close to 2.85.

In this case a peak was observed around KC from 8 to 25 and the major component of the response is precisely at three times the flow frequency, that is the second harmonic of the tank, see figure 1.8. This resonance peak was not represented by a Morison's equation prediction carried out as follows. If a mass/spring/damper system is used to describe the response of the cylinder as in expression 1.7, inertia and drag coefficients appropriate for flexible cylinders can be obtained using the measured response x(t), the measurements of the structural parameters m, k and ζ and reconstructing the force time histories F(t). Using then Morison's equation in relative form:

$$F(t) = \frac{1}{2}\rho D C_D (U - \dot{x}) \mid U - \dot{x} \mid + \frac{1}{4}\pi\rho D^2 C_M (\dot{U} - \ddot{x}) \qquad (1.9)$$

with these C_D and C_M coefficients and equation 1.7, the response of the cylin-



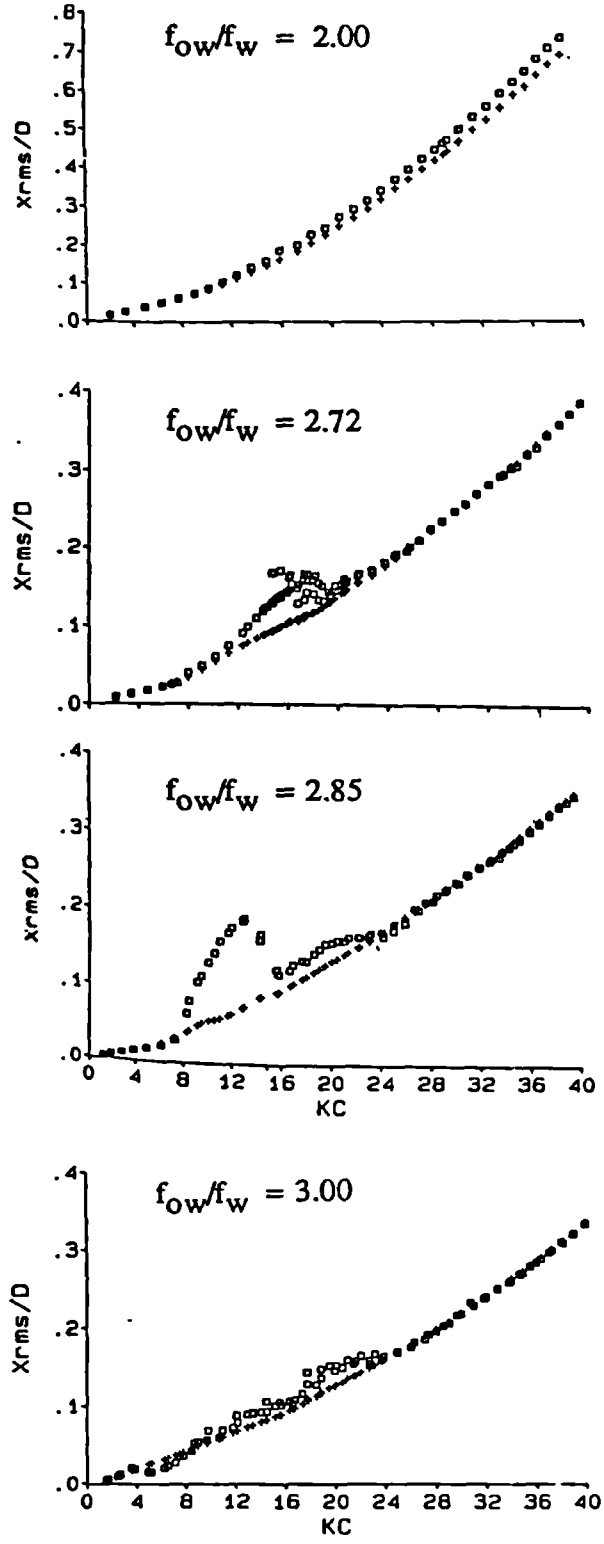


Figure 1.8: In-line response versus KC for 4 frequency ratios. □, measured; +, predicted. (from Bearman et al., 1992)

der can be reconstructed and compared with the measured one [6].

While this procedure showed a good agreement for non-resonant response it underestimated the response by as much as 50% for the resonant frequency ratio 2.85 in the region of KC where the resonant peak occurred.

Moreover Bearman et al., [8], tried force coefficients appropriate for rigid cylinders but this did not improve the agreement.

Tests to allow both in-line and transverse responses at the same time were also undertaken. These responses did not seem to vary a great deal from the one-degree of freedom cases, suggesting that there is no interaction between the two direction responses.

Given the interesting implications of the research aforementioned and the need for more investigation in the field of in-line vortex induced oscillations the present research was directed towards the understanding of the possible changes in the in-line response with decreasing β . Therefore the study described in Chapters 4 and 5 was undertaken for β equal to 750, 270 and 60.

[6]Note that when Morison's equation is written as in 1.9 care must be taken to consider the correct mass m in the equation of motion 1.7, here m is the effective mass in still fluid, which is the sum of the effective mass of the system in air and the added mass of the cylinder: $m_{ef} = m_s + md$

Chapter 2

Oscillatory flow past fixed cylinders: experimental apparatus

2.1 Introduction

Oscillatory flow can be generated either by moving the body in a fluid otherwise at rest (method 1) or by producing an oscillatory movement of the fluid and keeping stationary the body (method 2), as mentioned in section 1.5. Practically there are substantial differences between the two cases and they will be highlighted in the course of this section.

They can be explained in terms of advantages and disadvantages for the experimental measurements.

1. The advantages offered by the first method are that the amplitude and frequency can be varied independently, hence the effect of Reynolds number can be analysed separately once KC is fixed and vice versa. Usually higher Reynolds number may be achieved than when the fluid is oscillated in a U-tube water-tunnel.

   One of the disadvantages of this method occurs for force measurements. This is related to the inertial force due to the mass of the body, which must be subtracted from the total force in order to find the fluid force. This can be achieved by mounting a second identical instrumented cylinder above the test body such that it performs the same motion in air; the aerodynamic forces on this image cylinder however are ignored as the

forces on the test cylinder are about 1000 times greater. Other correction methods have also been used.

Other disadvantages stem from free surface or end effects which are difficult to assess, consisting respectively of surface waves or different kinds of disturbances induced by the oscillating model or support system and of unwanted motions in the area between the cylinder and the floor of the rig.

Another negative element is the noise, particularly caused by vibration of measurement equipment.

2. For the second case, where the body is kept fixed and the fluid moves, oscillatory flow is often carried out in a U shaped tank known as a U-tube.

   The fact that fewer structural moving parts need to be present is probably the most important advantage offered by this method. The main disadvantage that can be pointed out is that the Reynolds number cannot easily be varied independently of KC, the oscillations are in fact usually at the natural frequency of the system, and thus the frequency of oscillation is fixed. Because the frequency of oscillation is inversely proportional to the square root of the wetted length of the tank, L_w, (see expression 2.1 and section 2.3), only increasing L_w, and thus the total tank size could for example decrease the frequency. But only a large increase in the tank length would vary the frequency significantly.

2.2 The U-tube tank

The experiments conducted in this project were based on the second process mentioned in the previous section, by using a U shaped tank, already existing

in the Department's Hydrodynamics laboratory.

Important factors of the design of the U-tube water tank that had been considered for its realization (Singh [44]), were the geometry of the corners, the length of the working section and the height of the upright arms.

If the bends are too tight, separation can occur, introducing disturbance into the flow, and more power will be required to sustain the oscillations. If the corner is too gentle, the tank will be unnecessarily long, thus causing problems of finding sufficient space and of excessive time periods. The final decision about all these parameters had been taken after testing them on a model of a U shaped tank made of perspex. It was then decided to use a corner that had a mean radius of 1.5 times the cross-sectional height. This corner was tight enough to make the tank compact but still gentle enough to avoid any flow separation. The working section was chosen to have a length roughly 2.5 times the cross-sectional height. The height of the arms was based on the mean water level and maximum amplitude, such that when the water levels are at the extreme of the oscillation they are still above the entry to the corners and below the tops. This device has a square cross section of about 0.6 m, vertical limbs of 2.5 m and a horizontal working section of 1.52 m. The natural period is just over three seconds (circa 3.33 sec) with the tank normally filled with fluid to within 0.6 m of the top of the vertical arms. It is shown in the sketch of figure 2.1. The fluid, once set in motion, performs oscillations at a constant frequency which in the absence of excitation would be damped slowly by frictional losses. For this reason it is necessary to impart a small amount of energy via a blower so that constant amplitude oscillations are maintained.The blower is attached to the top of one limb and it is thus used to sustain the flow. It is mounted on a cover plate. The pressure generated by the blower may be varied by switching it on and off. A custom designed controller, triggered by

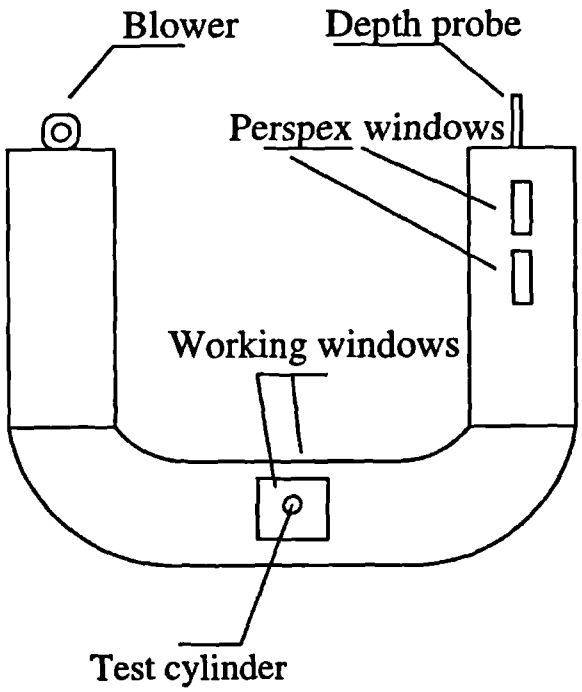


Figure 2.1: Sketch of the U-tube tank

the water level passing through the mean water level and sensed by the depth probe activates the blower after a set interval and for a fixed time in each flow cycle. The amplitude of the water oscillations is controlled by varying the speed of the fan and thus the amount of energy fed into the system. In this way a planar sinusoidal flow can be generated in the working section.

A conductivity probe was used both to measure the instantaneous water level and to control the drive system, as already mentioned above. It is fixed in the upright arm of the tank which has two small perspex windows. It works on the principle of measuring the current flowing in a probe which consists of a pair of parallel stainless steel wires, 1.5 mm in diameter by 1000 mm long and held 12.5 mm apart. The wires dip into water and the current that flows between them is proportional to the depth of immersion. It is claimed to be

accurate to within 0.5 mm. An overall calibration from wave height to output voltage is performed by noting the change in output voltage when the probe is raised and lowered by a known amount in still water. The operation is facilitated by means of the calibrated holder which has a series of holes drilled along its length accurately spaced every 50 mm. The calibration is done by a suitable subroutine in the data logging software. The calibration factor is printed out at the end as a result of a linear regression.

The wave probe calibration was carried out each day at the beginning of the experiment. An estimate of the reliability of the calibration was done by repeating the procedure twice. Each value was typically within $\pm 0.2\%$ of the mean.

In order to enable reliable measurement of the in-line and transverse forces, a complete measuring system is required. This consists of two strain gauged load cells (the same used by Singh [44]) mounted in special windows of the working section, and the test models (see section 2.5).

2.3 How to get the required parameters?

In these investigations low Re numbers were required, over a range of KC up to about 50. Therefore, the first step was to decide how to obtain low values of the parameter $\beta = D^2/\nu T$. Theoretically, three procedures could lead to the same solution. A U-tube normally operates at its resonant frequency which is:

$$f = \frac{1}{2\pi}\sqrt{\frac{2g}{L_w}} \tag{2.1}$$

where L_w is the wetted length of the tank and from the expressions (1.2) and (1.1), it can be seen that increasing L_w and thus the overall tank size, decreases the frequency and hence the velocity, resulting in a lower Reynolds number. However this procedure was considered impractical because it would have led to very slow velocities and requires a very large increase in tube

length to change the Reynolds number significantly. Another possibility is to decrease the characteristic dimension of the model, but it is clearly evident from the formula 1.4 (Morison's eqn.[32]), that reductions in either flow velocity or characteristic dimension would reduce the magnitude of the forces leading to difficulties in obtaining consistent measurements. In order to obtain low values of the parameter β the alteration of the kinematic viscosity of the liquid involved appeared to be the best option.

A study of the KC-Re data pairs for different cylinder diameters (26.5, 32 and 40 mm) suggested the use of a fluid whose dynamic viscosity could be adjusted between 4 and 10 cP [1] keeping almost the same density of water so that β varied between 35 and 75 and Re could vary respectively between circa 90 and 3000 (see figure 2.2).

Therefore, a clear and harmless liquid, able to exhibit such a high viscosity, preferably without great sensitivity to temperature or other variables and independent of shear rate was required. [2]

A survey among different chemical distribution companies was then carried out in order to obtain physical data tables and relative costs of the materials that appeared most convenient, such as glycerin and glycols.

The comparison of these data showed that polyethylene glycols were cheaper. Therefore the features of the different anhydrous glycols (both liquid and in grains) and their aqueous solutions had been studied in detail, focusing on viscosity and density. It is well known that viscosity is a measure of the internal friction of a liquid. As viscosity increases, the tendency to flow decreases. Viscosities of the glycols vary inversely with temperature. Hot glycols flow freely but their viscosities increase as they cool, until they eventually set

[1] $1P = 100cP; 1cP = 0.001\frac{Kg_m}{ms}$

[2] Newtonian fluid: the graph of stress against rate of shear is a straight line through the origin, with slope equal to the dynamic viscosity.

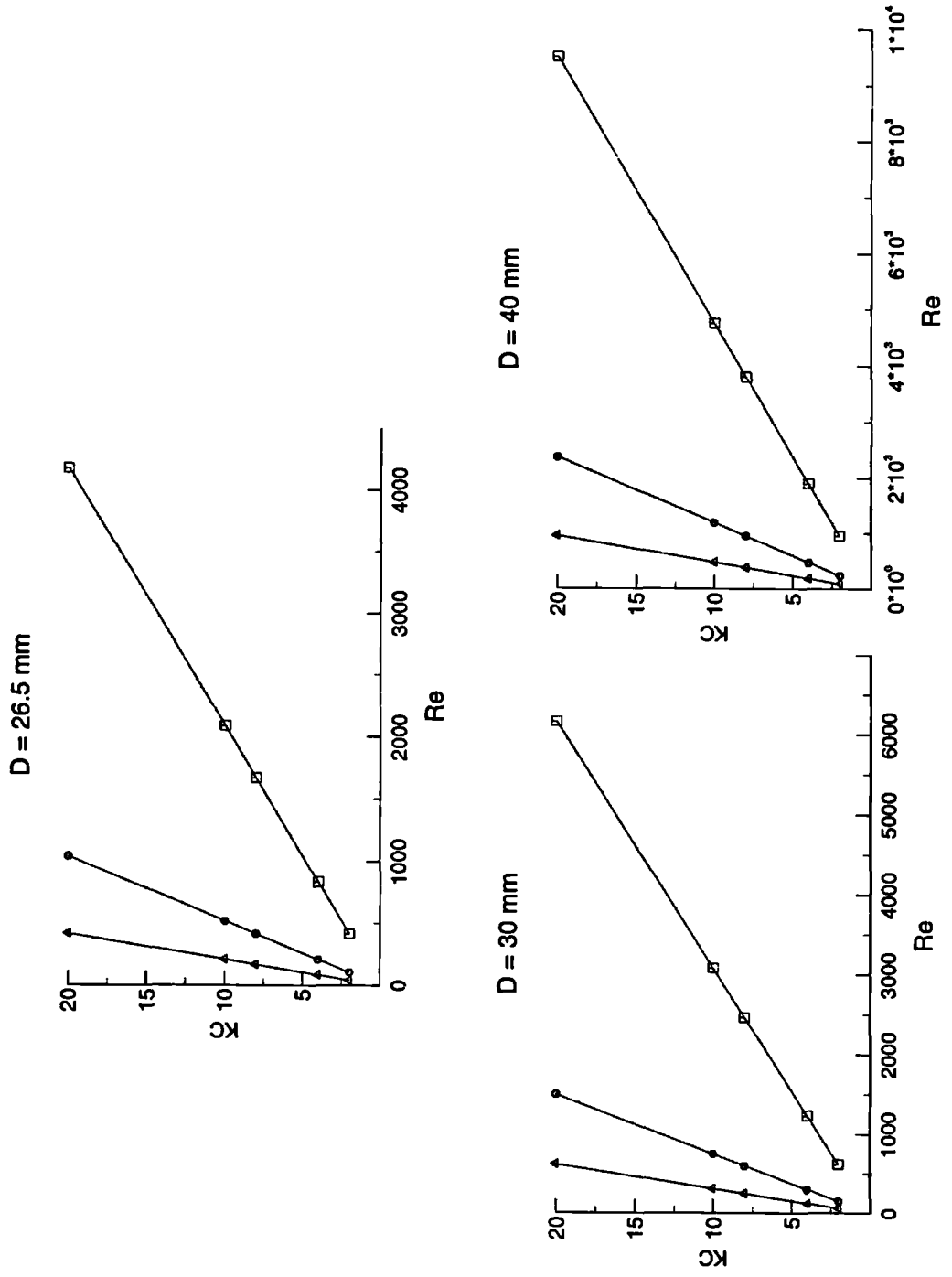


Figure 2.2: KC-Re values for different cylinder diameter and fluid viscosities; □, water; o, 4 times more viscous than water; △, 10 times more viscous than water

and fail to flow.

Direct viscosity measurements have been carried out in the Imperial College Physiological Studies Unit, both using a so-called Oswald viscometer and a programmable rheometer S&M Brookfield, Model DV-111. The materials tested were the glycols 15000, 20000 and 35000 [3] which are a solid substance in grains easily miscible with water. This feature (miscibility) has been experimentally verified by putting the solution in a centrifuge, and by testing then the solutions at the top and the bottom of the container; they showed the same value of the viscosity. Different solutions have been obtained by simply adding water to 20 grams of material. For each mixture the viscosity has been measured. The solution has proved to be Newtonian since for different values of the shear rates a given mixture always exhibited the same value of the viscosity. A solution of 5% was required to give a viscosity of about 8 cP (see

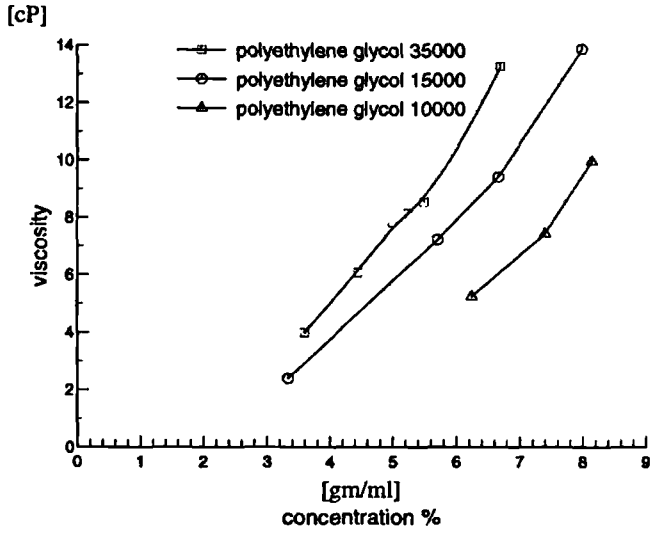


Figure 2.3: Viscosity tests for the polyethylene glycol solutions

figure 2.3). This meant that for the present U-tube with a capacity of circa

[3]This number indicates the molecular weight; for polymers the bigger the molecular chain, the higher the viscosity

2000 litres, only 100 kilograms of glycol were needed to satisfy the present purposes and this turned out to correspond to an affordable price. Once a suitable value of the viscosity was chosen it was necessary to verify how good the performance of the U-tube alone would be with a fluid more viscous than water. The first step of the investigation was to measure the viscous damping with water and then with an increased viscosity fluid. In particular, a first approximation calculation was carried out by estimating the wall skin friction from the (so-called) Stokes boundary layer solution as it is described in the next section.

2.4 Damping coefficient

The flow near an oscillating flat plate: theoretical estimate of the viscous damping on the walls of the U-tube. For free decay oscillations the system fluid-U-tube behaves as an ideal mass-spring-damper system with equation of motion:

$$m\ddot{x} + c\dot{x} + kx = 0 \tag{2.2}$$

and solution

$$x = X_0 e^{-\frac{ct}{2m}} \cos \omega t \tag{2.3}$$

For $\omega t = 2\pi n$, where n=0,1,2..., and put $X_0(t) = X_0 e^{-\frac{ct}{2m}}$ and $U_m = \omega X_0$, the loss of energy over one cycle is:

$$\Delta E = \frac{1}{2} m\omega^2 (X_0^2(t) - X_0^2(t+T))$$

neglecting second order terms:

$$\Delta E = m U_m^2 \frac{cT}{2m} \tag{2.4}$$

The so-called log decrement is the ratio of the amplitude of two successive peaks, that is:

$$\delta_d = \ln \frac{X_0(t)}{X_0(t+T)} = \frac{cT}{2m} \tag{2.5}$$

where c is the so called damping coefficient.

A theoretical estimate of the viscous damping of the fluid motion in the U-tube was carried out in order to verify the results obtained both by Singh [44] and by the present research. The order of magnitude of the viscous damping coefficient was the target of these calculations. Yet, the real conditions like corners and boundary walls of the U-tube had not been forgotten when comparing experimental and theoretical results.

The Stokes' solution is a simple exact solution of the Navier-Stokes equations in the case of the flow generated in a semi-infinite mass of fluid by viscous action at an infinite flat plate oscillating in its own plane. For the analysis see Schlichting, [42].

From the foregoing it is possible to write: Damping force = $c\dot{x}$;
but

$$\mu \frac{\partial u}{\partial y} A_w = \mu A_w \dot{x} \sqrt{\frac{n}{2\nu}}$$

where it can be seen that the damping coefficient is equal to:

$$\mu A_w \sqrt{\frac{n}{2\nu}} \tag{2.6}$$

Now using the wetted area of the U tube (cross section 600 mm) as A_w, $n = \sqrt{\frac{k}{m}} = \sqrt{\frac{2g}{L_w}}$, where L_w is the wetted length (is taken to be approximately 5620 mm as adopted in the experiments carried out by Singh , [44]) and substituting in expression (2.6), the damping coefficient has a value of approximately 13. This was the theoretical estimate, and was found to be of the same order of magnitude as the values found experimentally by Singh

[44] the difference being due to the evident real differences between an equivalent area of an infinite flat plate oscillating in its own plane and the U-tube device where the damping is obviously not constant, but smaller at the lower amplitudes. Corner flows and curved flow as well as air flow into the vertical limbs of the U-tube play an important role in the experimental result.

The second step of the research regarding the damping coefficient consisted of direct measurements of the viscous damping

1. in water to confirm the data from Singh [44] and
2. with a higher viscosity fluid to verify the performances of the U-tube and the blower .

1. A direct measurement of the viscous damping has been provided by getting the oscillation up to a given amplitude, switching the blower off, and letting the oscillations decay due to the frictional losses. In this case there was no model inside the working section. Practically, for an initial amplitude of about 30 cm, a damping coefficient of about 60 was obtained when referred to the successive peak.

2. A fluid which exhibits a viscosity higher than water will give rise to a higher viscous damping. For a fluid n times more viscous than water since Stokes theory is linear it follows that the damping coefficient is incremented n times. It was therefore necessary to check how good the performance of the U-tube would be for a more viscous fluid, and also to understand whether the blower could support the larger resistance. In order to do this a simulation of the higher damping was undertaken retaining water as the fluid, by causing in some way an additional damping in the system. In our case this was done in two ways:
   a) by putting a large bluff body into the flow,

b) by partially closing the top of the limb on the open side of the U-tube with wooden plates generating an air damper.

The energy lost to damping in one cycle is:

$$\Delta E = \int_0^T FUdt \tag{2.7}$$

from expressions (2.4) and (2.5)

$$\Delta E = mU_m^2 \delta_d \tag{2.8}$$

where m is the mass of the fluid.

Suppose we put a cylindrical body in the U-tube as the required additional model, the Fourier averaged value of the drag coefficient (from the Morison's equation (1.4)) for a circular cylinder is:

$$C_D = \frac{3\pi}{2T\rho DU_m^3 L} \int_0^T FUdt \tag{2.9}$$

from (2.7), (2.8) and (2.9) and substituting (2.5) in the latter expression, the damping caused by a cylindrical body is:

$$c_1 = \frac{4\rho D^2 KCC_D L}{3\pi T} \tag{2.10}$$

For a flat plate the drag coefficient is generally assumed to be approximately (Singh[44]):

$$C_D = 7KC^{-1/3}. \tag{2.11}$$

A steel flat plate with a width of 200 mm and spanning the section of the U-tube was then put in the right hand side limb of the U-tube at a depth of 1.5 meters and some measurements of the damping had been taken in the same way described before.

Method (b) was tried also, using two plates which could close the open limb partially or completely according to the way they were juxtaposed.

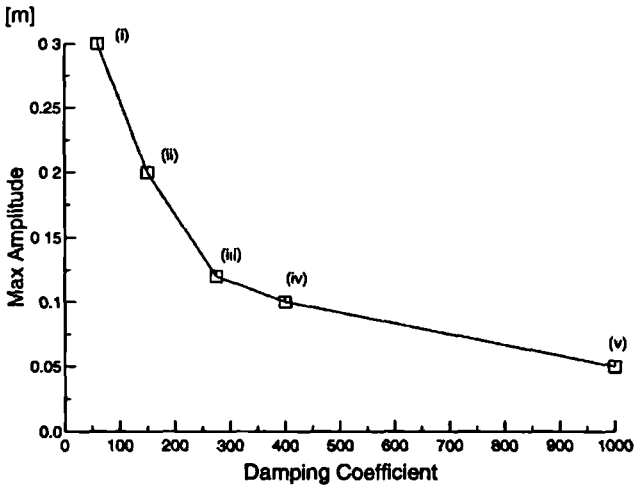


Figure 2.4: Damping Coefficient versus Maximum Amplitude of oscillation of water in different conditions

The limb was considered completely closed when only a small hole of 20 mm diameter was left for the wave probe. Figure (2.4) is a summary-plot which shows the damping coefficient versus the maximum amplitude that it was possible to reach in different cases: (i) for the U-tube as it is, (ii) with the steel flat plate in as described above, (iii) with the wooden plate partially closing the open limb of the U-tube and no model inside, (iv) with both steel flat plate and wooden plate partially closing the right hand side limb and (v) with the wooden plate totally closing the open limb of the U-tube. The values of the coefficient obtained proved that the blower would have worked even in the very prohibitive conditions that yield damping coefficients of about 1000.

2.5 Force measuring system

2.5.1 Load cells

The force measuring system was composed of two stainless steel load cells (with an external diameter of 100 mm), one at either end of the model with the strain measuring elements of dimensions 25.4 x 3.2 x 1.6 mm (see figure 2.5), so that the total force could be measured independently of the point of

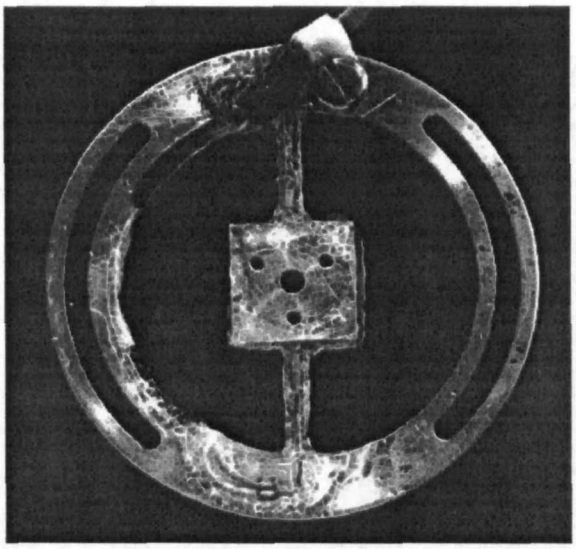


Figure 2.5: Load cell

application, by simply summing the outputs of the two cells. The design of the load cells must incorporate such features as high natural frequency, linearity, imperceptibly small deflections, sensitivity and a mechanical strength for any expected load. The model used in the research was a Perspex circular cylinder (thus very smooth). [4] The two cells making up a pair are slightly different in design, one has a 4.8 mm hole centrally positioned; the other has instead a 7.9 mm clearance hole. This was chosen such that the model would be fixed to one

[4] It has been said that β was changed by varying ν, nevertheless also the cylinder diameter was changed slightly to tune β to the desired values. Cylinders with diameters of 26.5 mm, 32 mm and 40 mm were used.

load cell at one end, but free to move, in the axial direction only, at the other end connected to the other load cell. It is necessary to do this because, had the model been fixed at both ends to the load cells, when filling the tank the effect of the very large static pressure on the windows would set up lateral bending strains in the load cells which could possibly cause damage to them and to the mounted cylinder. Resistance strain gauges (length 6mm, resistance 120 Ω, GF 2.12) were mounted, one on each 3.2 mm wide face of the element, giving a total of four gauges per load cell and connected as a Wheatstone bridge.

A pair of windows made of thick aluminium alloy reinforced with 'T' section stiffeners were used to close the working section. A special housing for the load cells and a 25.4 mm clearance hole, through which the model was connected to the load cells are centrally positioned in these windows.

The gauges were connected to a two channel conditioning unit, one channel per load cell, to form a full bridge. The unit consisted primarily of a pair of amplifiers, one for each channel, and was connected to a power supply, a low pass filter, another amplifier (whose amplification factor it is possible to choose in a range 1-500), an oscilloscope, and a meter. A continuous $\pm$ 10 volts output was available for each channel which was then connected to the computer available in the laboratory (section 2.7). Prior to a set of experiments on a model, the load cells had to be carefully aligned and calibrated with the model connected. As can be seen in figure 2.6, the housing for the cell is outside the working section of the tank, but during operation this housing was completely full of water which totally covered the load cells. When measuring in-line forces, the cells must be positioned such that the axes of the measuring elements are vertical; for measurements of transverse forces the cells are rotated until these axes are horizontal.

The wires for the strain gauges on the load cells passed through a hole with

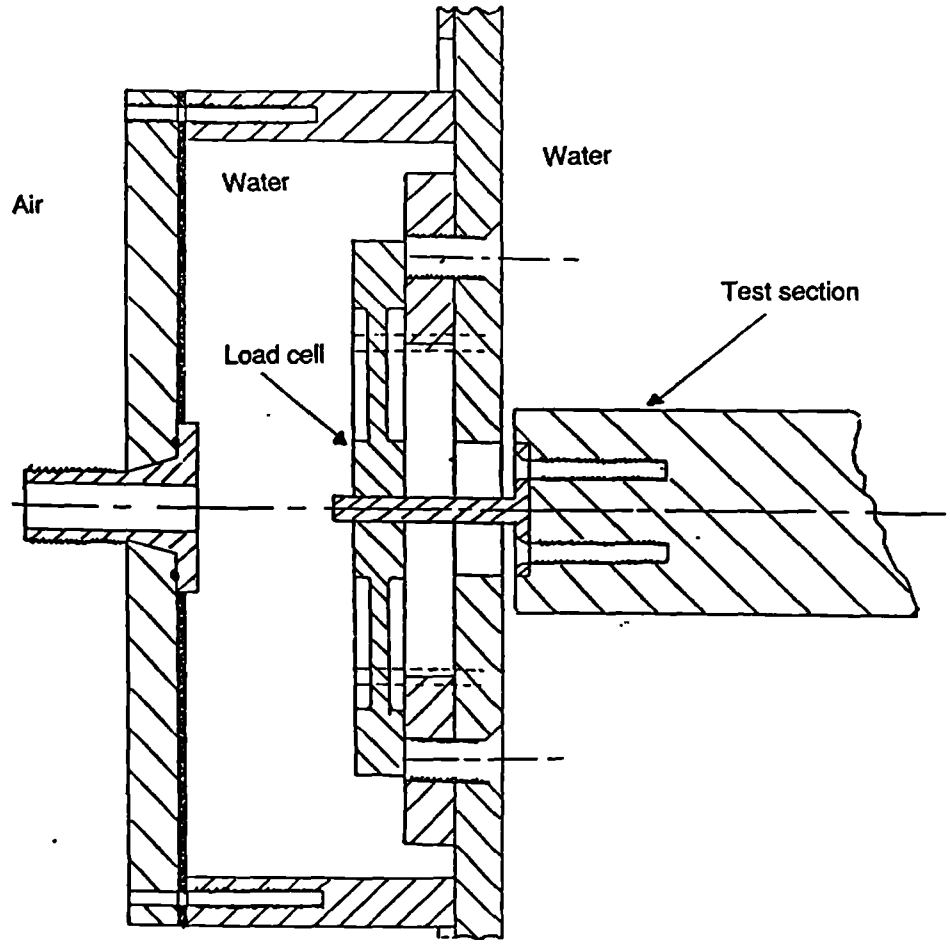


Figure 2.6: The housing of the load cell (from Singh, 1979)

suitable rubber grommets in the cover plate. Every time that the U-tube was filled up with the operating fluid the air was bled out of the load cells housings through the top hole on the cover plate and then tightened with a brass screw to seal in the water.

It is well known that strain gauge performances are easily degraded by the effects of moisture and water immersion.

Great effort was therefore devoted to overcoming the numerous problems encountered related to the waterproofing of the load cells and to obtain con-

sistent response to the applied stress, by searching for a suitable coating protection.

Other arrangements for completely preventing the fluid from filling the cells' housing were also taken into consideration, but were excluded for different reasons. For example, the possibility of mounting a series of strain gauges inside the cylinder was considered, but there were practical difficulties in doing so (the max cylinder diameter used was 4 cm). Also the use of membranes, flanges or bellows was contemplated to isolate the cells' housing (see for example Sarpkaya, 1986 [39], where the system worked but forces higher than the present ones were measured so that the effect of the membranes was minimal). Problems likely to arise using these techniques were (a) the need to find a material to keep the fluid out with virtually no stiffness, so that the small fluid forces would not be attenuated, and (b) the difficulty of calibrating such a system.

2.5.2 Moistureproofing the strain gauged load cells

The task of choosing the most suitable protection proved very complicated. On the one hand it was necessary to cover with protective coatings the load cells' arms (where the strain gauges were mounted) preventing the liquid from reaching the strain gauges. On the other hand it was fundamental to leave flexibility and responsiveness of the measuring elements. Numerous protective coatings and different procedures were tried before finding those that had the required features. Not only had the material to be applied easily as a thin layer over the elements but, once cured, it also had to resist the pressure exerted by the liquid, leaving the strain gauges completely dry, i.e. isolated from the water.

Despite the wide selection of typical methods and protective sealants recommended by several strain gauge suppliers their effectiveness proved to be

inadequate for the case in consideration. Generally the fluid penetration produced a spurious strain by swelling or contraction of the cement and by loss of insulation resistance within the wire grid and between grid and test structure. The imperfect insulation of the gauges often generated signal drifts and noise, not to mention hysteresis and creep of the signal.

The following methods of coating the strain gauges are some of those that have been tried before obtaining the desired results. The problems manifested have been listed so as to help other researchers who might be confronted by a similar problem, [23]:

1. Method one

   a) • one layer of a polystyrene resin adhesive;

   or alternatively

   • two layers of polyurethene coating;

   followed by

   b) Microcrystalline wax with as many layers as necessary to cover all the arms where the strain gauges are mounted.

2. Method two

   Same procedure as above with the addition of another layer of a silicone sealant acetoxy;

   With methods one and two the watertightness turned out to be partially successful. After a few hours in water at a depth of about 2000 mm, one of the two load cells did not work any more. Also the calibration was not repeatable over a few hours.

3. Method three

   a) one layer of a polystyrene resin adhesive;

followed by

b) Silicone sealant acetoxy, several layers;

This method revealed immediate problems: the solvent contained in the silicone modified the strain gauges resistances even before putting the cells in water.

4. Method four

   a) one layer of a polystyrene resin adhesive;

   followed by

   b) one layer of araldite rapid adhesive;

   and by

   c) Silicone sealant acetoxy, several layers;

   This method successfully prevented the water from touching the strain gauges, and in fact both the cells continued to work even after the runs in the tank. A problem however was the creep in the signal which occurred when under a stress. The material responsible for this was the araldite layer which increased the stiffness of the arms.

5. Method five

   a) one layer a polystyrene resin adhesive;

   b) three layers of silicone frame seal-neutral curing.

   This silicone is acid free, but is very difficult to apply and proved not to be watertight.

6. Method six

   a) Araldite rapid adhesive, several layers.

   The application of a thin layer on the arms has proved very difficult and an unwanted drift in the signal was observed.

2.5.3 The successful methods

The first prerequisite for successful moistureproofing is a thorough drying procedure applied to the gauge assembly. All the materials used were characterised by room temperature cure and all the applications suggestions were carefully followed.

- The use of the coating Dow Corning 3140 Rtv (a silicone elastomer) caused a great change in the performance of the load cells. It was applied to the cells very easily after having treated the gauges and the arms with Dow Corning 1204 primer to improve adhesion of the silicone rubber. Being a solventless material, flowable and self-levelling it did not give rise to the problems presented by the other silicons used and moreover, after curing it exhibited a good flexibility. Repeated calibrations in air as well as in water at room temperature have shown that the cells responses are linear and the signals repeatable. The only problem is the difficulty of spreading on the gauges layers with a thickness similar to the arms' thickness.

- All the problems were completely overcome by using the Moistureproof material N-1 supplied by the company Tokyo Sokki Kenkyujo. This is a Neoprene rubber coating material which formed a good elastic coating, proved very convenient to use and complied with its promises of good long term stability.

Thanks to these findings the planned U-tube experiments were able to be carried out with β values of 35, 53, 70, 75 and 308 circa, obtained by using different combinations of model diameter - fluid viscosity, as will be seen in the next sections.

2.6 Force prediction and load cells' calibration

As a consequence of what has been stated so far, it should be quite clear at this point that the prediction of force and flow characteristics of a periodic and separated flow around a circular cylinder can be difficult because of the complex nature of the history of the motion and the effect of vortices. As mentioned in the first Chapter, one way around these difficulties is to assume that the total time-dependent in-line force may be expressed as a sum of a velocity-squared dependent drag and an acceleration-dependent inertial force, and this is the basis for Morison's equation.

Before going forward with the actual calibration of the load cells, a theoretical estimate of the maximum in-line forces that would load the cylinder was conducted through the Morison's equation, (1.4).

The velocity can be assumed to be given by $U = U_m \sin \omega t$, and substituted in expression 1.4. To find the phase of the maximum force the first derivative is imposed to be zero. One solution is given by the expression $\cos \omega t = \frac{\pi^2 C_M}{2C_D KC}$ and the maximum force, for $KC \geq \frac{\pi^2 C_M}{2C_D}$, can be written as:

$$F_{xmax} = \frac{1}{2}\rho D U_m^2 \{[1 - (\frac{\pi^2 C_M}{2KCC_D})^2]C_D + \frac{C_M^2 \pi^4}{2KC^2 C_D}\}$$

$$= \frac{1}{2}\rho D U_m^2 \left(C_D + \frac{\pi^4 C_M^2}{4C_D KC^2}\right)$$

For $KC < \frac{\pi^2 C_M}{2C_D}$ where the regime is inertia-dominated, the solution is given by $\omega t = 0$, which yields to the expression:

$$F_{xmax} = \frac{1}{2T}\rho \pi^2 D^2 U_m C_M \tag{2.12}$$

Assuming a KC = 34, drag and inertia coefficients respectively equal to approximately 2 and 1 [40], given the dimensions of the cylinder D and L (expression 2.12 gives the force per unit length), a first estimate of the maximum

force was obtained, (it can be noted that C_M has very little effect on F_{xmax} in this case of a drag-dominated regime) so as to have an idea of the order of magnitude of the loads to apply to the load cells for their calibration.

Calibration The calibration of the load cells proved to be a very difficult process for all the reasons described in the previous sections, (2.5.2) and (2.5.3). Moreover, a good reliable method of calibrating them was fundamental to guarantee good force measurements, and so different calibration procedures have been tried before finding the ideal one.

The calibration of each load cell when calibrating for the in-line force, was carried out in the first place by directly hanging weights onto the cells themselves, but this system reproduced a loading regime which was very different from the one the cells would have experienced in the tank.

It was then decided to place the model in the tank as described in section 2.5, and to calibrate the cells with the model connected, both with and without fluid in the tank. The first elementary system that was used to apply the in-line load was composed of a simple pulley and weights system, which consisted of a pulley mounted on a small vertical traverse. By adjustment of the traverse a horizontal load was applied to the model and hence the cells. Calibration was carried out in both directions, towards left and towards right. With a sampling frequency of 10 Hz, 200 samples were recorded and averaged for each weight. The final calibration coefficient was calculated through the method of least squares. Several sets of loading and unloading measurements were conducted in order then to average among all the force coefficients found.

This method proved unsatisfactory because, to start with, the pulley was not absolutely friction-less, and also because it was very impractical: it was not easy to check that the wire was horizontal every time that a weight was attached, and when in water these problems amplified even more. So it was

impossible to assure the repeatability.

An enhancement was accomplished by the use of a third load cell type RS - 2Kg, connected to a power supply and an amplifier, that was firstly calibrated on its own and showed linearity, repeatability (less than 2 % difference), and no hysteresis when loading and unloading. To carry out the cells' calibration this cell was then provided with an extension (a metallic bar) rigidly attached to the loading platform, and so that it could still work even when the cylinder and the cells were immersed in fluid, with a metallic L-shaped arm, set on a pivot in order to act as a lever and exert a force on the cylinder (i.e. the cells) every time that a weight was placed on it, figure 2.7. Before starting

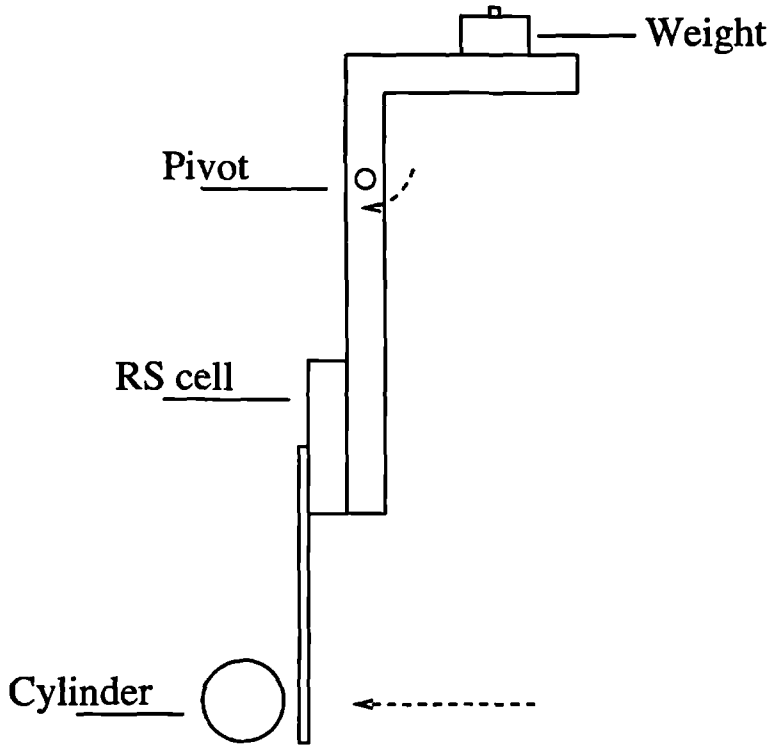


Figure 2.7: Schematic Set-up of the Calibration procedure using load cell type RS-2Kg, not in scale

any set of experiments this device was mounted on the upper window of the working section of the tank and the calibration of the cells was carried out when the cylinder and the cells were immersed in the working fluid, in both

directions, left and right. By changing the position of the RS cell, the force was applied in different positions and precisely, at the middle, one third and two thirds of the cylinder length, in order to check that the sum of the two cells' output signals gave the same values for each position of the loads. The calibration factors were calculated for at least 4 different calibration sequencies every day in the same way described above. Both the cells gave calibration constants typically within 2 % of the mean. When possible the calibration was repeated also after having carried out the experiment to be sure that the actual loadings exerted on the cells had not affected their performances. Yet again, the difference resulted very small, and within 2 %. The calibration lines of one day of experiment are shown in figure 2.8, where both linearity and repeatability can be checked.

For transverse force measurements, calibration was easier: loads acting vertically were applied simply by hanging weights from the model. The accuracy

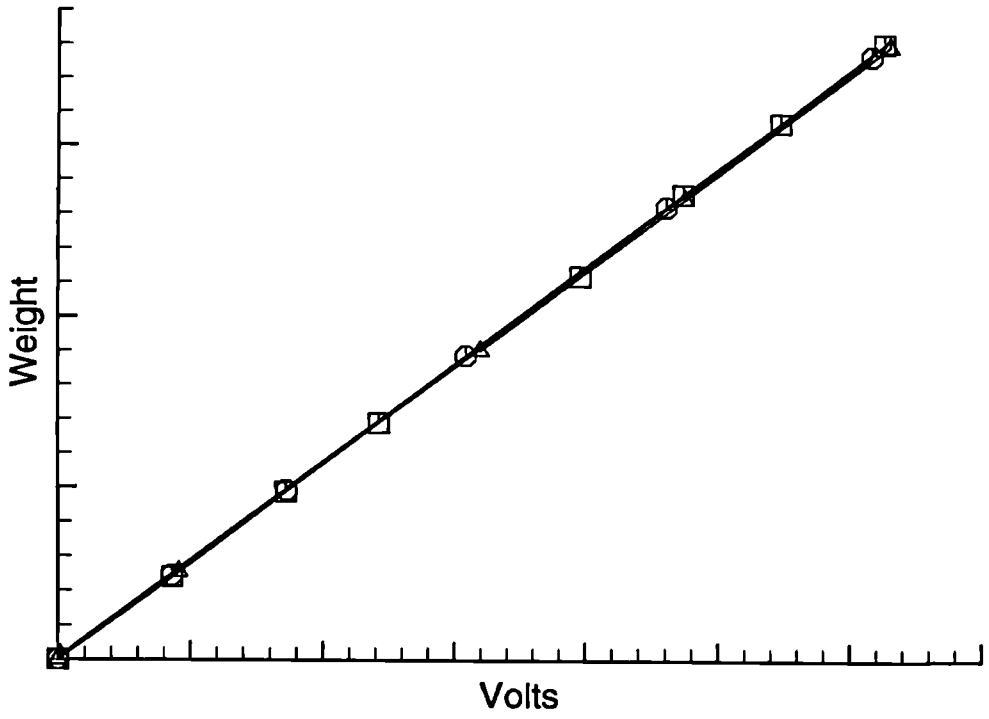


Figure 2.8: Calibration lines

of the cells was estimated via an 'inverse' calibration, that is by applying the calibration factor to the cells' signals for a series of known weights, and it was found to be of ± 0.3 gm.

2.7 The data acquisition system

The force and displacement signals from the force load cells and the wave probe amplifier respectively, in all 3 channels, were connected to the Analog-Digital converter, on a 286 P.C. which was fitted with a Scientific Solutions data acquisition expansion card. The signals are in range -10/+10 Volts. Just before entering the A/D converter the signals were filtered using low pass filters. The use of filters are mainly to take away high frequency electrical noise introduced in the amplifiers and cables. The filters were usually set at low pass 10 Hz for KC greater than about 15 and at low pass 5 Hz for smaller values of KC. From spectral analysis it was observed that these filter settings were adequate in that no significant component that would have been attenuated or cut off was present.

Zero voltage outputs were read by the computer for the three channels before starting the blower. This reading was repeated after the experiments when the fluid was still, so to check that there were no drifts in the amplifiers.

The computer programs for controlling the U-tube oscillating tank, collecting the data and analysing the recorded time series are written in Fortran 77 and run both on the P.C. 286 available in the laboratory and on the Silicon Graphics computer network of the Department.

The plots of displacement signals and forces have been acquired through the Unigraph 2000 facility available as a software package on the Silicon Graphics workstations in the Department. Fortran programs have been written to analyse the data and calculate the force coefficients.

Chapter 3

Force Measurement Analysis for fixed cylinders

Preamble The problem studied was a uniform harmonic flow about a circular cylinder placed with its axis normal to the flow. The features of this flow have already been described in Chapter 1.

The resulting flow field is extremely complex, as has already been stressed throughout this thesis, and is a function of the Keulegan-Carpenter number and the viscous parameter β as can be drawn also via a dimensional analysis.

Consider a sinusoidal fluid motion of maximum velocity U_m and period T, a smooth cylinder characterised by diameter D and length L, a fluid whose properties are its density, ρ, and its kinematic viscosity, ν. The instantaneous force per unit length of cylinder can be expressed as:

$$F = f(t, U_m, T, D, \rho, \nu).$$

As the flow is harmonically varying, the horizontal velocity U can be represented by:

$$U = -U_m \cos \omega t \tag{3.1}$$

where $\omega = \frac{2\pi}{T}$.

The dimensional analysis of the flow under consideration yields that the time-dependent forces acting on the cylinder in oscillating flow may be written in non-dimensional form as:

$$C_F = \frac{2F}{\rho D U_m^2} = f(\frac{U_m T}{D}, \frac{U_m D}{\nu}, \frac{t}{T}) \tag{3.2}$$

in which F represents the in-line or the transverse force per unit length. Therefore any force coefficient that would be calculated could be written as a function of the same parameters:

$$C_F = f_i(KC, Re, \tfrac{t}{T})$$

or, alternatively:

$$C_F = f_j(KC, \beta, \tfrac{t}{T})$$

In the particular case of a U-tube where the oscillation period T is fixed it is more convenient to use the second form which replaces the Reynolds number by β (as suggested by Sarpkaya [36], [40]).

The force measurement system used in this research to measure the forces on a circular cylinder as described in Chapter 2, was capable of measuring in-line and transverse forces, one at a time. In the course of this chapter in line and transverse force coefficients will be defined and calculated and the results of the experiments will be presented and discussed.

3.1 In-line Force at various β parameters

As studied so far (section 1.5) the force in-line with the fluid motion may be considered to be composed of two parts as proposed by Morison et al. (equation 1.4). Substituting for U and $\frac{dU}{dt}$ from (3.1) into Morison's equation results, [22], in:

$$C_{F_x} = \frac{2F_x}{\rho D U_m^2} = \frac{\pi^2}{KC} C_M \sin\omega t - C_D \mid \cos\omega t \mid \cos\omega t. \qquad (3.3)$$

Representing the measured force by a Fourier series and comparing with equation 3.3 yields expressions for C_D and C_M, the drag and inertia coefficients which have been used in this research. In particular the Fourier averages of C_D and C_M are obtained by multiplying both sides of 3.3 once with $\cos\omega t$ and

once with $\sin\omega t$ and integrating between the limits $\omega t = 0$ and $\omega t = 2\pi$. This procedure leads to:

$$C_D = -\frac{3}{8}\int_0^{2\pi} \frac{F_x \cos\omega t}{\frac{1}{2}\rho U_m^2 D} d\theta \tag{3.4}$$

$$C_M = \frac{U_m T}{\pi^3 D}\int_0^{2\pi} \frac{F_x \sin\omega t}{\frac{1}{2}\rho U_m^2 D} d\theta \tag{3.5}$$

where $\theta = \omega t$.

The drag and inertia coefficients can therefore be obtained by direct substitution of the total measured force [1] into equations 3.4 and 3.5 respectively as the other quantities are known. This yields constant values, averaged over a cycle. In this research the coefficients were calculated for each cycle and averaged over a large number of cycles, that was never less than 100. In fact, especially at large values of KC the vortices are shed and subsequently swept back against the body producing a flow which may not be the same for each half cycle nor from cycle to cycle. Consequently, the force is not quite symmetric and the degree of asymmetry is variable. Averaging over a large number of cycles will therefore tend to make the signal symmetric.

Although there are some combinations of KC and Re for which Morison's equation gives worse time accuracy, the use of time-invariant coefficients leads to a good estimate of the in-line force dependent on KC and Re and facilitates the comparison among results obtained from experiments conducted by different research groups. They are therefore very useful in design applications.

Another method of representing the force is in terms of its root mean square value which for the measured total force is given by:

$$C_{Frms} = \frac{\sqrt{\overline{F_x^2}}}{\frac{1}{2}\rho U_m^2 DL} = \frac{\sqrt{\frac{1}{T}\int_0^T F_x^2 dT}}{\frac{1}{2}\rho U_m^2 DL} \tag{3.6}$$

[1] The total measured force is the sum of the signals recorded by each of the two load cells

Through the use of Morison's equation it may be shown [4] that expression 3.6 can be reduced to:

$$C_{Frms} = \frac{\sqrt{\overline{F_x^2}}}{\frac{1}{2}\rho U_m^2 DL} = \left(\frac{3}{8}C_D^2 + \frac{\pi^4 C_M^2}{2KC^2}\right)^{\frac{1}{2}} \tag{3.7}$$

In this way at high KC C_{Frms} tends to 0.61 C_D whereas as KC $\rightarrow$ 0 $C_{Frms} \rightarrow \infty$, so C_{Frms} does not have C_D and C_M as asymptotes at either KC end. Therefore, following an idea conceived by Bishop [10], a new total force coefficient $C_{F_{tot}}$ which has the advantage of converging on the inertia force coefficient in the inertia regime as well as on the drag coefficient in the drag regime, was defined as:

$$C_{F_{tot}} = \left(\frac{\frac{3}{8}C_D^2 + \frac{\pi^4 C_M^2}{2KC^2}}{\frac{3}{8} + \frac{\pi^4}{2KC^2}}\right)^{\frac{1}{2}} \tag{3.8}$$

So, when drag is dominant:

$$C_{F_{tot}} = \left(\frac{C_{Frms}}{\frac{3}{8}}\right)^{\frac{1}{2}} = C_D \tag{3.9}$$

and when inertia is dominant:

$$C_{F_{tot}} = \left(\frac{C_{Frms}}{\frac{\pi^4}{2KC^2}}\right)^{\frac{1}{2}} = C_M \tag{3.10}$$

In the mixed regime formula 3.8 has to be applied. $C_{F_{tot}}$ can be evaluated using equation 3.8 for data which have already been processed to give values of C_D and C_M over a range of Keulegan-Carpenter numbers, or it can be evaluated in the form:

$$C_{F_{tot}} = \left(\frac{\overline{F_x^2}}{(\frac{1}{2}\rho U_m^2 DL)^2(\frac{3}{8} + \frac{\pi^4}{2KC^2})}\right)^{\frac{1}{2}} \tag{3.11}$$

where $\sqrt{\overline{F_x^2}}$ is the root mean square value of the total measured force. The two formulations, 3.8 and 3.11, do not give identical results unless the measured force fits perfectly Morison's equation through the whole flow cycle.

Several test cases have been investigated. For all of them the instantaneous water level and the force signals were recorded on the PC available in the Hydrodynamics laboratory. The water displacement probe was calibrated every day and the calibration of the load cells was performed as often as possible, in order to check the repeatability and the general conditions of the cells themselves, see sections 2.2 and 2.6. The sampling rate for the in-line force was such that one cycle of oscillation was defined by at least 100 points. The program written for the calculation of the force coefficients was tested by inputting a synthetic force trace (generated from Morison's equation) and checking the output values of C_D and C_M. The following table summarises the characteristics of all the test cases investigated in terms of cylinder diameter, kinematic viscosity of the fluid and the resulting parameter β , having calculated the period of oscillation through the water displacement signal (as mentioned in Chapter 2 it was always around 3.3 s):

Diameter [mm]	ν $[mm^2/s]$	β	Test cases
32.00	1.01	308	Case 1
32.00	4.00	75	Case 2a
32.00	5.70	53	Case 3
26.50	6.00	35	Case 4
40.00	6.30	78	Case 2b
32.00	4.40	70	Case 2c

It has to be noted that the value of the viscosity used to obtain a certain β is slightly different from one case to another because runs with different values of the parameters were tested (from 308 downwards) in the first place. Wanting to repeat some of them it was difficult to mix water and polyethylene glycol in such an exact percentage to reproduce what had already been done. Moreover it was interesting to note that the repeatability of the results is good no matter how a specific β was obtained (e.g. whether varying the diameter of the model or the viscosity of the fluid). This observation raises the question of

blockage effects and blockage corrections for force coefficients, but in this case they proved to be negligible (see section 3.3.1).

The repeatability of the results obtained in cases 2a, 2b and 2c leads also to the conclusion that the effect of small variations of β (of the order of 10 %) on the force coefficients is unimportant. From now on, therefore, slight variations in β will be neglected. The test cases analysed will hence be four, for values of β respectively equal to 308, 75, 53 and 35 approximately.

Test Case 1 The complete set of in-line force data is shown in figure 3.1 for the test case under consideration. Also some test points for $\beta = 301$, by Obasaju et al. ([33], using the same U-tube) are plotted for a comparison. In fact the tests with such a β value have been carried out to assess the achievement of the complete control of the rig, and this could be done collecting data at values of β already available. The agreement was extremely good. This agreement showed that the apparatus and the data analysis techniques used worked well and that, if the necessary care is taken in setting the whole instrumentation, experimental conditions in the U-tube can be reproduced confidently and the results of experiments conducted years apart are comparable.

Test Case 2 The values of C_D and C_M presented in figure 3.2 are the result of several different days of measurements and refer to the Case 2, whose characteristics are listed in the table above, where $\beta = 75$.

Test Case 3 In figure 3.3 C_D and C_M are presented for $\beta = 53$.

Test Case 4 Also the case where the lowest β was reached is presented in figure 3.3, β in this case is equal to 35.

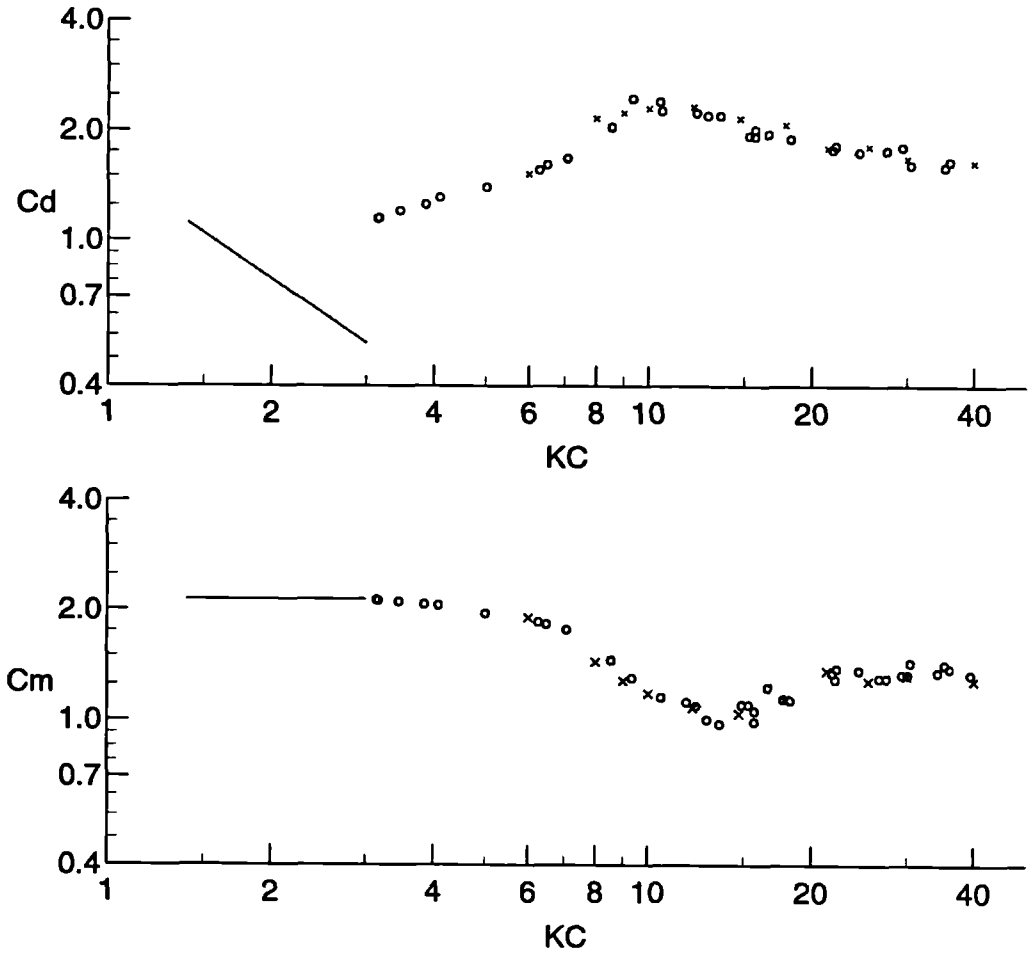


Figure 3.1: Drag coefficient and Inertia coefficient versus KC; $\times$, $\beta = 301$, Obasaju et al.; o, $\beta = 308$, present results; —, Wang's Theory.

The good agreement with the Wang theory values at low KC numbers can be observed in all the cases. The discussion of the results of all the test cases is left to the last section of this chapter. For all the four test cases investigated the C_{Frms} coefficient is presented in figure 3.4, while the $C_{F_{tot}}$ coefficient, (given in 3.8) is then shown in figure 3.5.

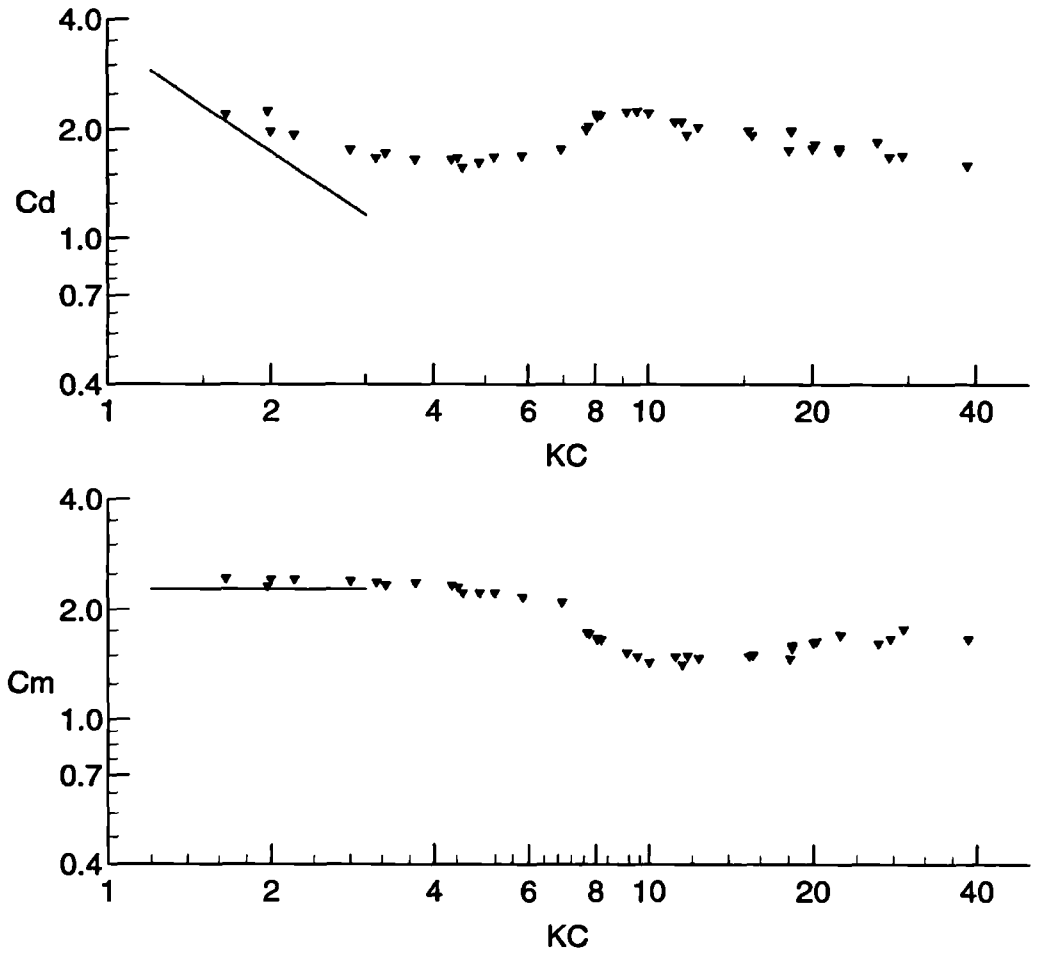


Figure 3.2: Drag coefficient and Inertia coefficient versus KC; ▼, β = 75, present results; —, Wang's Theory.

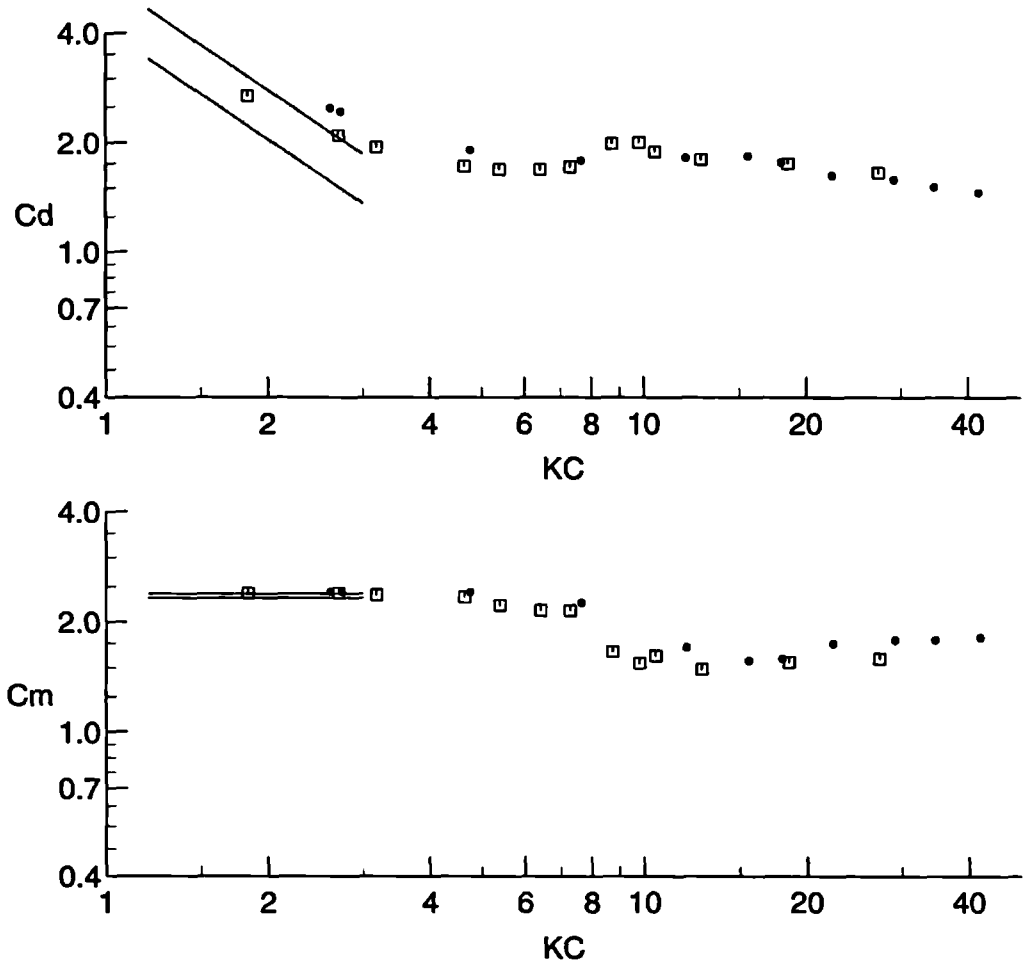


Figure 3.3: Drag coefficient and Inertia coefficient versus KC, □, $\beta = 53$, present results; •, $\beta = 35$, present results; —, Wang's Theory (upper line $\beta = 35$)

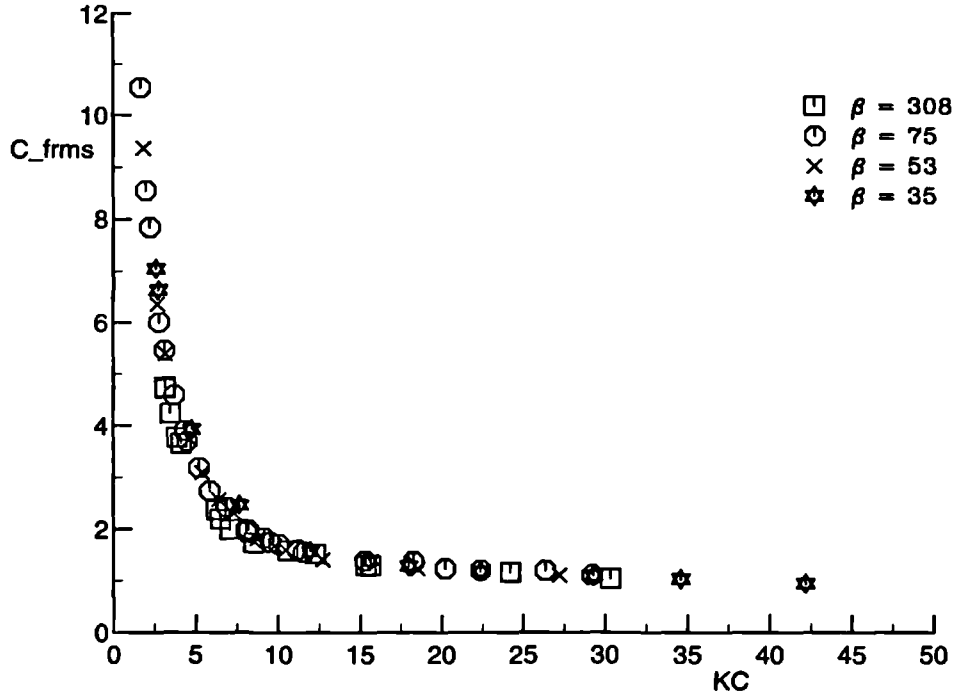


Figure 3.4: Root mean square coefficient for the in-line force versus KC

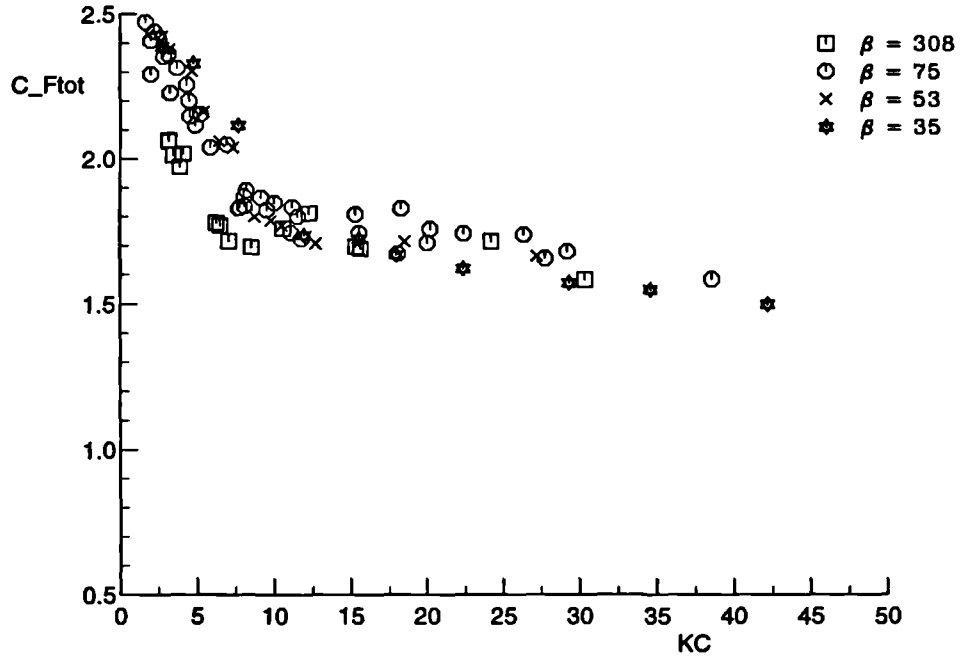


Figure 3.5: Total force coefficient $C_{F_{tot}}$ for the in-line force versus KC

3.2 Transverse Force at various β parameters

As a result of the formation and shedding of vortices, circular cylinders in an oscillatory flow can experience transverse forces. These are more difficult to analyse than the in-line ones because of their sensitiveness to the ways in which vortices are formed and move. They are important not only for their magnitude which can be of the same order of the in-line ones, but being characterised by higher frequency and an alternating nature, they may have a major influence on the fatigue life of some structural members. Moreover, it is known [44] (and was also noticed in the present research) that these forces do not repeat but vary from cycle to cycle with periods of very little lift followed by sudden high amplitude sequences, in an apparently random way. For this reason they are generally studied with reference to a C_{Lrms} lift coefficient. Several authors have proposed ranges of KC for particular types of vortex-shedding behaviour (see Singh, [44], Sarpkaya and Isaacson, [40], Bearman et al., [5]) and even when KC and β are fixed, more than one mode of shedding is possible, and the flow may switch between the possible modes (Bearman et al., [5]).

To measure the transverse force the load cells were rotated through 90 degrees from the position used for the in-line measurements (i.e. the axes had to be horizontal, see section 2.5). The test cases examined were two: $\beta = 308$ and $\beta = 70$.

The root-mean-square coefficient of the lift force was calculated simply through the equation:

$$C_{Lrms} = \frac{\sqrt{\overline{F_y^2}}}{\frac{1}{2}\rho U_m^2 DL} = \frac{\sqrt{\frac{1}{T}\int_0^T F_y^2 dT}}{\frac{1}{2}\rho U_m^2 DL} \tag{3.12}$$

Its values are presented in figures 3.6 and 3.7. Similar trends have been found elsewhere, for example by Obasaju et al. [33], and Williamson, [50].

Departures from the vortex shedding two-dimensional conditions (as other

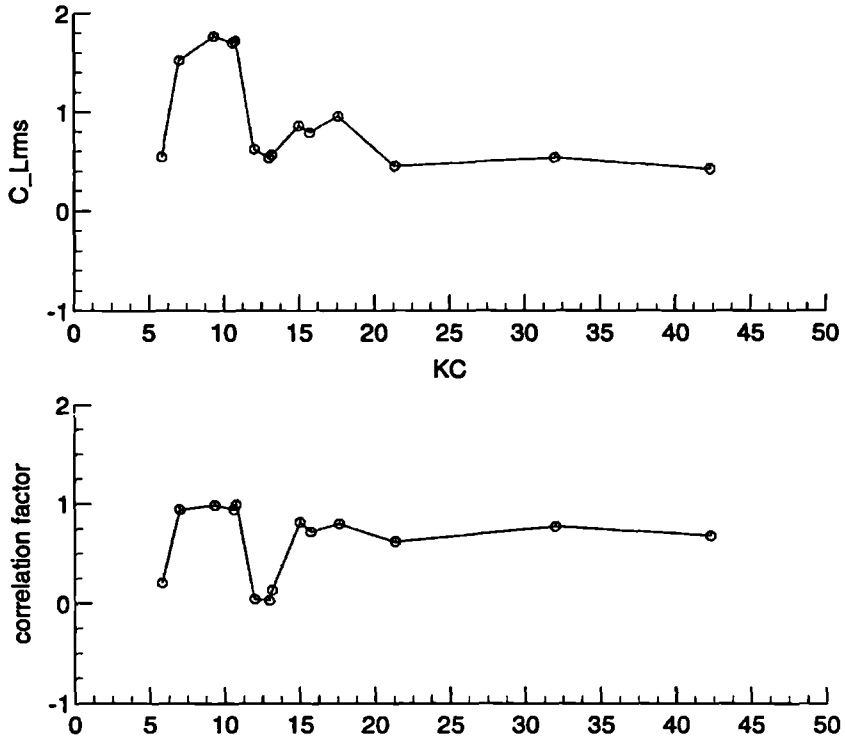


Figure 3.6: $C_{L_{rms}}$ and correlation factor versus KC, $\beta = 308$

studies suggested occur even at small β values, [47]), were investigated when examining the transverse force time histories. It was found in both cases ($\beta = 308$ and $\beta = 70$) that the two signals from the load cells at either ends of the cylinder may at times be in anti-phase which confirmed previous results [5].

A correlation coefficient between the forces signals measured at the two cylinder ends where the load cells are placed was in fact calculated as follows:

$$correlation12 = \frac{\overline{F_{y1}F_{y2}}}{F_{rms1}F_{rms2}} \tag{3.13}$$

where F_{y1} and F_{y2} are the force signals recorded at the two ends of the cylinder and F_{rms1} and F_{rms2} are the root-mean-square values of F_{y1} and F_{y2}. It is plotted against KC in figures 3.6 and 3.7. The peaks and the troughs correspond to the ones in $C_{L_{rms}}$. It can be noted that the lift is correlated strongly in

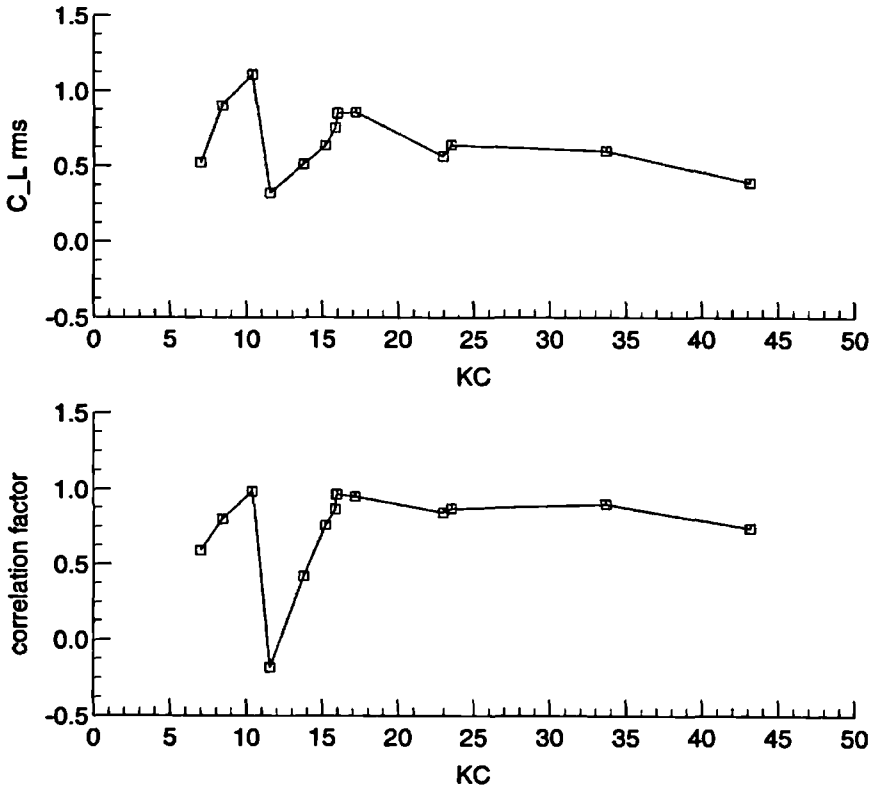


Figure 3.7: $C_{L_{rms}}$ and correlation factor versus KC, $\beta = 70$

the range $7 < KC < 10.8$ and between 15 and 18. The interpretation of the results is left to section 3.3.4.

3.3 Discussion of the Results

3.3.1 Blockage effects

One of the test cases under consideration, $\beta = 75$, was repeated to obtain the same β by using different diameter sizes (for example 32 mm and 40mm) and different viscosity values (4.00 mm^2/s and 6.30 mm^2/s), as in cases 2a, 2b and 2c (see section 3.1 and related comments). When there is a change in the model dimensions in a fixed size of working section, blockage effects may show up. By measuring for the same β and KC using different diameters these effects could be assessed.

Sarpkaya [37] has made a set of experiments to determine the role of blockage in oscillating flow. From pressure measurements around a circular cylinder in a U-tube he concluded that the blockage effect in harmonic flow is negligible for D/W ratios less than 0.18, where D is the diameter of the cylinder and W is the width of the test section. Not only does the largest cylinder tested in this study, with a diameter of 40 mm, have a blockage ratio of 0.066, well below Sarpkaya's limit, but the experiments named 2a, 2b and 2c cited above, produced the same results showing that blockage effects were in fact negligible as expected.

Coates, [12], conducted some experiments to study drag and inertia coefficients oscillating fluid flow past a cylinder at 4 different blockage ratios (0.067, 0.089, 0.13 and 0.222). The results agreed with theoretical conclusions in that these coefficients increased according to blockage effects as shown:

$$C_D = C_{D0}(1 + \frac{\pi^2 b_r^2}{6}) \tag{3.14}$$

$$C_M = C_{M0}(1 + \frac{\pi^2 b_r^2}{12}) \tag{3.15}$$

where the 0 subscript indicates the coefficients before correction. According to

these formulae the correction that should be applied to the coefficients in the present study is therefore at the most 0.7 %, and can therefore be neglected.

3.3.2 Force coefficients

3.3.3 Drag and Inertia coefficients

The present results will be discussed with reference to the main regimes

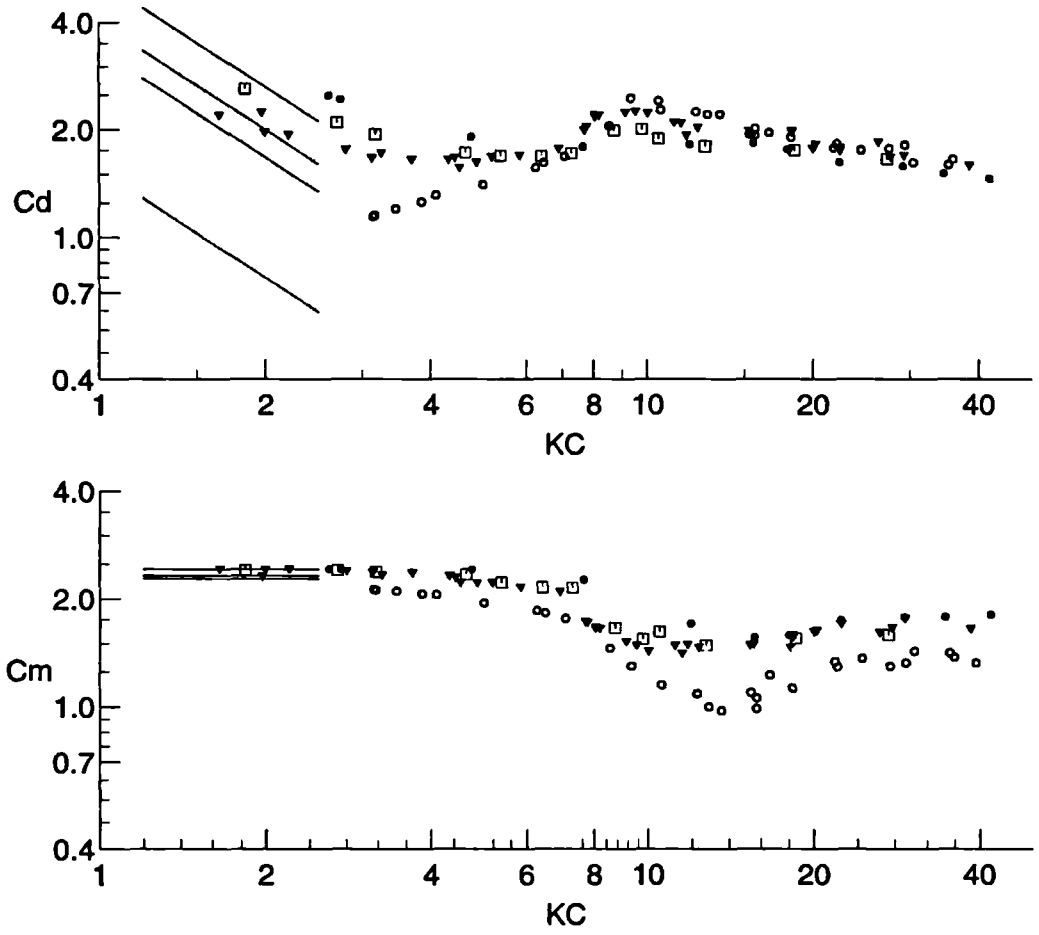


Figure 3.8: Drag coefficient and Inertia coefficient versus KC for all the test cases: o, $\beta = 308$; ▼, $\beta = 75$; □, $\beta = 53$; •, $\beta = 35$; —, Wang theory lines ($\beta = 308$, lower line)

observed bearing in mind that the regime boundaries do not always occur at exactly the same value of KC. They have been described in detail in section

1.5.3 and are generally named as **attached** flow, **symmetric** regime, **asymmetric** regime, **transverse street, diagonal** regime, **three pair** regime. Some of the flow visualisations were also reproduced in the present research for $\beta = 308$.

The behaviour of drag and inertia coefficients for all the four test cases is plotted in figure 3.8.

As the object of this research is to study the behaviour of oscillatory flow at different β numbers, it is important to notice the differences and similarities in the force coefficients as β is varied. In particular, as β decreases the boundary layer thickness increases, as noted in Chapter 1. Also the trend with KC are underlined in the course of this section.

In the range of $KC < 2$ it may be seen that for a given value of KC the drag coefficient drops as the β parameter increases. It is extremely difficult though to measure forces very accurately at small KC values because their magnitude is small. Moreover, the system blower-wave probe was not able to drive small amplitudes below a certain conductivity variation. So there was a limit on the smallest KC that could be reached.

At low KC, below a KC_{cr} of 1 or 2, depending on β , the laminar flow is symmetrical, **attached**, stable and two-dimensional. In this regime the two force coefficients can be computed analytically with a high degree of accuracy via the Stokes-Wang analysis and are found to agree well with the present experimental measurements for sufficiently small KC values, (see also [3], [39]), see figures 3.1, 3.2, 3.3 and 3.8. In this **attached** flow regime the different curves representing the coefficients for different β are all tending towards the appropriate Wang theory line, C_D increasing with decreasing β .

C_D continues to decrease with increasing KC for all β cases but when a certain minimum KC_s is reached it changes trend and starts to increase.

Bearman et al. [3] attributed this increase to the onset of separation and the **symmetric shedding** regime is entered. They noted that this value depends also on the β parameter as the change of trend occurs at different values of KC with different β values. This is evident from the figures presented here too. Separation defined in this way seems to be occurring at higher KC for smaller β , as was found also by Bearman et al. [3] for β between 1665 and 196 at low KC.

Nevertheless to determine the value of KC for the onset of separation is a difficult target to achieve even via flow visualisation techniques. It is not yet clear where it occurs.

Separated flow depends on a number of circumstances. Firstly, it depends on the strength of the shed vortices. As β is decreased increasing the kinematic viscosity of the fluid greater diffusion is expected, which leads to weaker vortices in the formation region due to mixing with opposite signed vorticity induced at the wall and from previous shedding. This may produce a reduction in vortex circulation (due to diffusion) and a decrease in the drag coefficient.

It also depends on the positions of the separation points, which is very difficult to assess.

Moreover, greater diffusion yields thicker boundary layer which may separate more easily and which increase the displacement effect and the drag coefficient.

But the reason for change in the onset of separation is not very clear.

The onset of separation could instead occur at the KC corresponding to the departure of C_D from the Wang theory line. However, the force measurements of the present research could not be taken at KC low enough to gather more insight into the exact values of KC for which this departure occurs.

In the next regime, the **asymmetric** regime for $4 < KC < 8$, the vortices

begin increasingly to dominate. C_D increases with KC and is not so sensitive to β .

The drag coefficient continues to increase and shows a peak in the flow regime defined as the **transverse vortex** regime for $8 < KC < 15$ where, as was noted in Chapter 1, the vortex shedding activity is more intense and influences the forces experienced by the cylinder. This behaviour is common to all the β values examined. In particular, for $KC \sim 12$, a difference of only 20% is noticeable between test case 1 (β of 308) and test cases 3 and 4 (β of 53 and 35). The latter two behave similarly while a difference of about 9% can be seen between test case 1 and 2 (β of 75). In this region for a fixed KC C_D decreases with decreasing β .

As KC increases further these differences attenuate in the **diagonal, third vortex** and the **quasi-steady** regimes where the drag coefficient tends to a constant value.

The trend is opposite to that showed by Sarpkaya, [36], figure 3.9, for a range of β between 5620 and 497, where it was found that an increasing C_D with decreasing β occurred throughout all the KC range. But Obasaju et al., [33], who investigated the oscillatory flow around a cylinder for β ranging between 1665 and 109 found (without making any comments on this) that the trend reverses for β between 301 and 109, see section 1.5.2 and figure 1.4.

Therefore there may be a suggestion here that in the separated region, once a certain β is reached (around 400) the drag coefficient would not vary a great deal when decreasing β further. This is difficult to explain, but it may due to a combination of the effects of decreasing β on separation mentioned above.

The variation of the inertia coefficient with the β parameter is also shown in figures 3.1, 3.2, 3.3 and 3.8 for the four tests studied. For all values of β tested the inertia coefficient C_M remains constant for KC smaller than 3 and

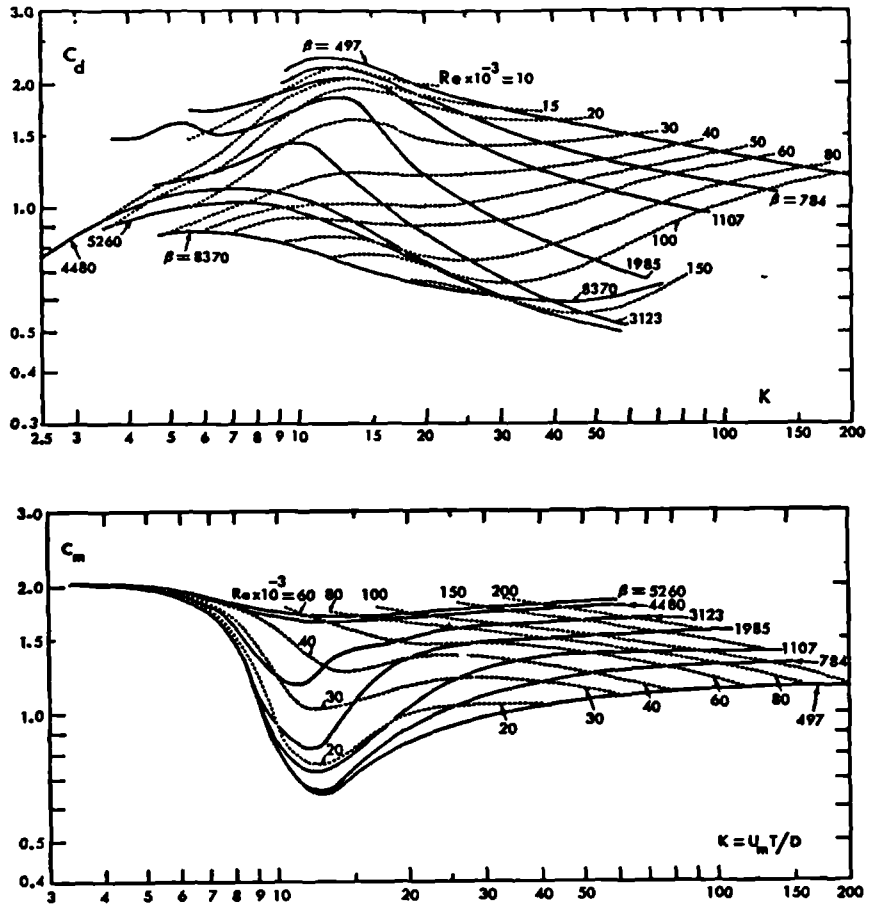


Figure 3.9: Drag and Inertia coefficients versus KC (from Sarpkaya 1976b)

agrees well with Wang's theory: as β increases the value of C_M tends to the potential value of 2 for inviscid flow, as expected.

When KC increases beyond this region C_M starts to decrease to a minimum value reached in the transverse vortex regime. The inertia coefficients for the test cases 2, 3 and 4 show no differences at all in value, while the curve representing case 1 presents lower values for all KCs. This difference reaches 30% starting from the transverse vortex regime.

Also in this case the trend is opposite to that found by Sarpkaya, [36], for β between 5620 and 497.

A possible explanation for the higher value of the inertia coefficient at the low β cases tested in this study must take account of the fact that C_M is proportional to the effective volume 'occupied' by the body. Now, as the boundary layer thickens the effective volume of the cylinder plus the displacement thickness enlarges and therefore this is expected to result in a higher value of the inertia term.

It is interesting to note that the maximum difference in the drag coefficient for different β occurs in the transverse regime where the highest difference in value in the C_{lrms} coefficient takes place, see figure 3.10. This suggests in fact that in this regime the vortex shedding activity may be weaker for lower β values, but it is in any case a region where its influence is remarkable on the flow.

3.3.4 Transverse-force coefficients

Figure 3.10 shows that the peaks in the r.m.s. transverse coefficient occur at approximately the same values of KC in both the cases studied, that is for $\beta = 308$ and $\beta = 70$. They have similar values apart from the first peak of C_{Lrms}, that exhibits values about 60% smaller for the smaller β .

Very interestingly, the peaks and the troughs in the C_{Lrms} correspond to those which are exhibited by the correlation factor (see section 3.2), and this is evident in both cases.

The drop in correlation may be due to a switch in the mode of vortex shedding that does not occur simultaneously over the cylinder span, but an end of the cylinder may still be experiencing a mode, say Mode 1, and the other may already be in the following type of shedding, say Mode 2, as schematically drawn in the diagram below, 3.11. So, at values of KC close to regime boundaries this can be seen as a competition of vortex shedding modes before accommodating to the subsequent mode.

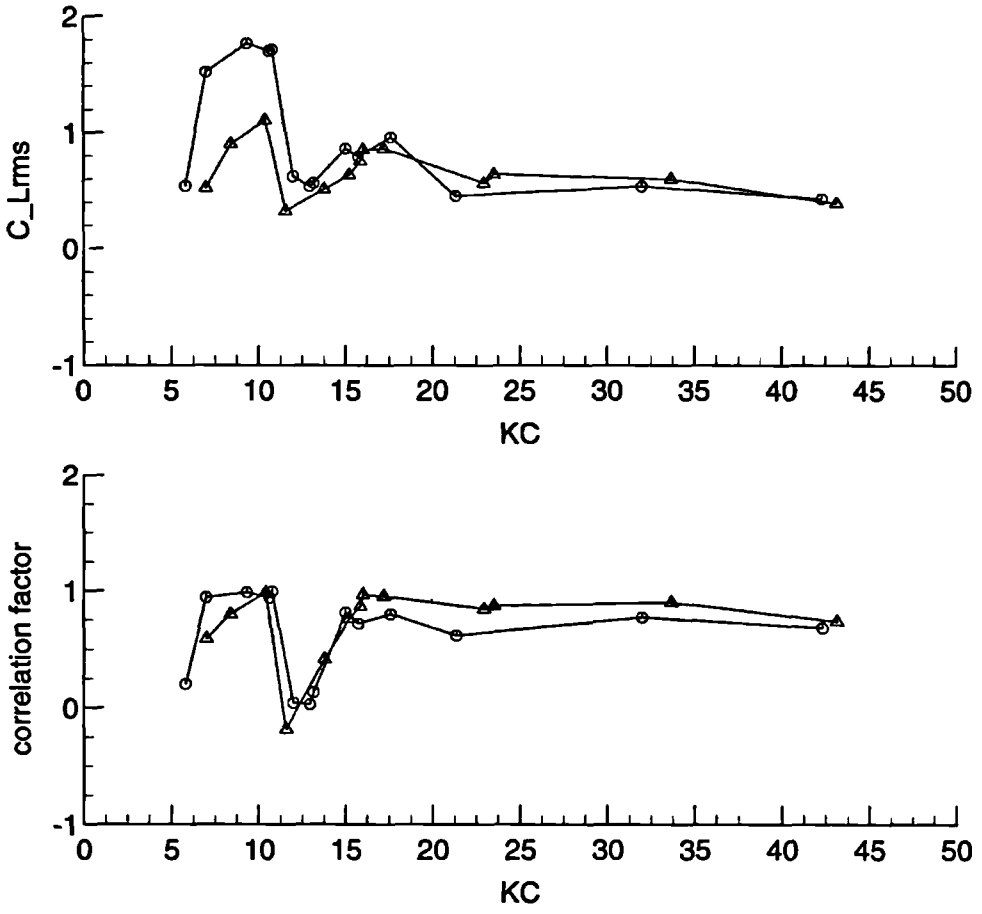


Figure 3.10: $C_{L_{rms}}$ and correlation factor versus KC, o, $\beta = 308$; $\triangle$, $\beta = 70$

A secondary trough can also be seen at KC around 20. So it may be inferred that when looking at a plot presenting C_{Lrms} versus KC, see the curves in figure 3.12, the apparent peak in the region of KC between 5 and 8 is due to passage from a no-shedding or weak-shedding zone for KC smaller than 5, to a 2-D shedding zone. If the shedding remained correlated C_{Lrms} would ideally decrease gradually with KC. However the sudden decrease as KC increases above a value of about 11 which is ascribed to 3-D effects leaves an apparent peak in the C_{Lrms} curve.

As mentioned before (section 3.2) the peaks have been reported by other

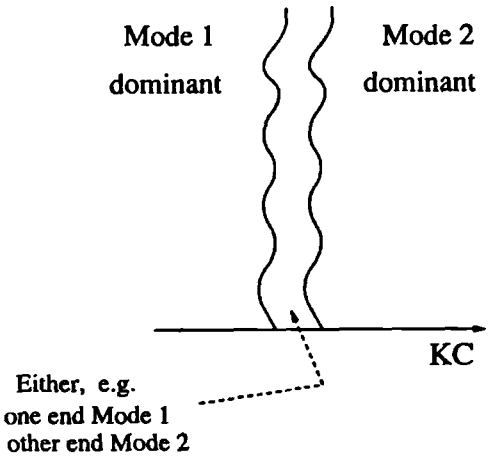


Figure 3.11: Competition of subsequent shedding modes at KC regime boundaries as sketched may result in lack of spanwise correlation between each of the signals from the two cylinder ends

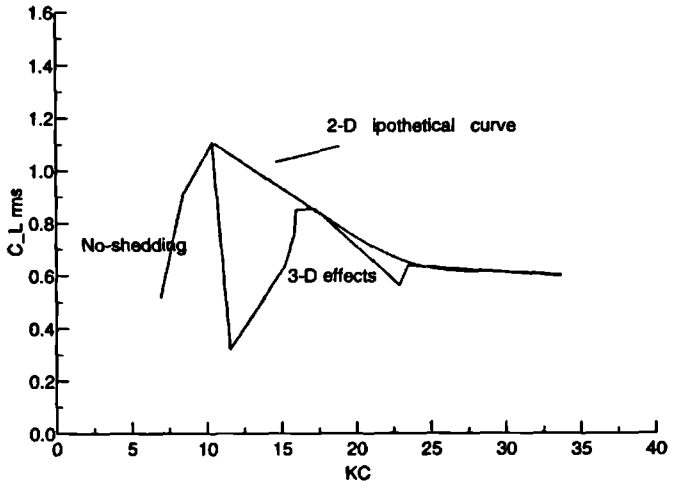


Figure 3.12: $C_{L_{rms}}$ versus KC to outline 3-D effects as evidenced in this research

researchers and confirm the present results. Obasaju et al., [33], referred to the repetitiveness of the vortex shedding, and identified three ranges where this effect is strong, these are at KC = 10, KC = 18, and KC = 26. In these cases they found the vortex shedding highly correlated along the cylinder length, producing stable vortex shedding and a high transverse force. In between these peaks the correlation of the vortex shedding along the cylinder axis was

poor and the vortex shedding weaker, resulting in a reduction of the transverse force.

3.3.5 Morison's equation

As mentioned in Chapter 1 the application of Morison's equation to a complex time dependent flow can be questioned because only the first order terms of a Fourier series of the in-line force are used. Keulegan and Carpenter have shown that the forces on a circular cylinder are concentrated at the fundamental frequency, and significant components occur only at the lower odd harmonics of the fundamental. Several researchers have shown that the agreement between the measured force and Morison's equation would be vastly improved if odd terms up to the fifth harmonic were used, see Keulegan and Carpenter,, [22], Singh, [44], Sortland, [45]. Sarpkaya, [40], suggested a three-term Morison's equation showing that the component of the residue at three times the fundamental frequency is the most important.

Nevertheless the two-term Morison's equation is widely used in the field of off-shore engineering in spite of its known limitations because it works admirably well in all the ranges of KC apart from the transverse regime region.

In the following figures the measured force is compared with that predicted by Morison's equation using the values of C_D and C_M presented in the previous sections for different β, and different KC values. This is done to show how Morison's equation's merits still hold when β is decreased. In particular the in-line force traces referring to test case 1, 2 and 3 are plotted together with the corresponding predicted ones. As expected, the agreement is good at small values of KCs, see for example figures 3.15, 3.19, 3.13, where the flow has just separated and the force is dominated by the inertia term. Morison's equation predicts the force quite accurately both in phase and in magnitude.

In the region of KC between 8 and 20, see for example figures 3.16, 3.17,

3.20, the motion of large vortices results in a poorer prediction and neither the magnitude nor the phase of the force is well estimated.

The agreement improves as KC increases, see for example figures 3.18, 3.14, when a more regular vortex shedding is reached.

3.3.6 Comparison with Numerical Results

Introduction As underlined in Chapter 1, numerical simulation of flows past circular cylinders offers the possibility to study in detail the mechanics of vortex formation and shedding, but attempting to compare computation with experiment has so far given rise to difficulties. These are mainly due to the lack of detailed experimental measurements of forces at low Reynolds number, where the flow is assumed laminar and 2D, and two-dimensional simulations are appropriate and cost effective.

Therefore it is easy to understand that the present work serves as an important step in the research on cylinders in oscillatory flow, because it gives the opportunity to make very detailed comparisons between experiments and computer simulations. The different computations which will be cited in the course of this section were carried out by other researchers in the light of these experiments, in order to compare results at the same values of β, for different KC.

Experimental and Numerical Results Figure 3.21 shows the results for the drag and inertia coefficients obtained by Iliadis [19] who carried out a Finite Element 2D numerical simulation for $\beta = 34$ and $\beta = 53$ in order to make a comparison with the present experimental data at the same β values. The corresponding C_{Frms} coefficients are plotted in figure 3.22.

Figure 3.23 shows the present drag and inertia coefficients for $\beta = 75$, compared with those obtained by the numerical simulation carried out at the

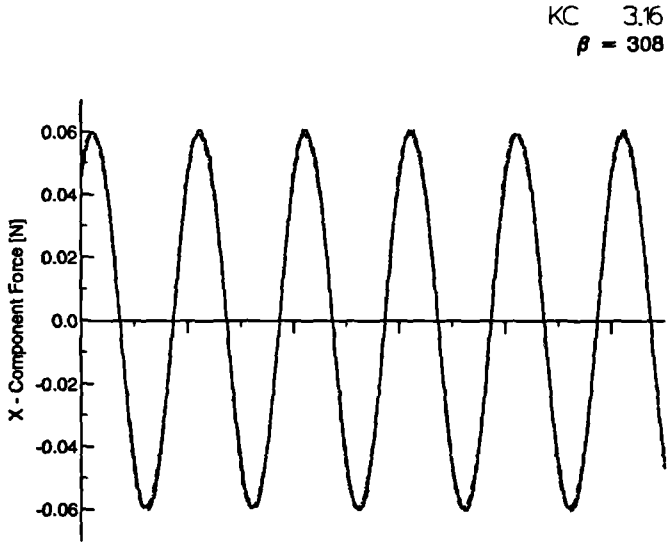


Figure 3.13: Comparison between the measured in-line force time history ——, and the one predicted using Morison's equation — · — · —; KC = 3.16, β =308

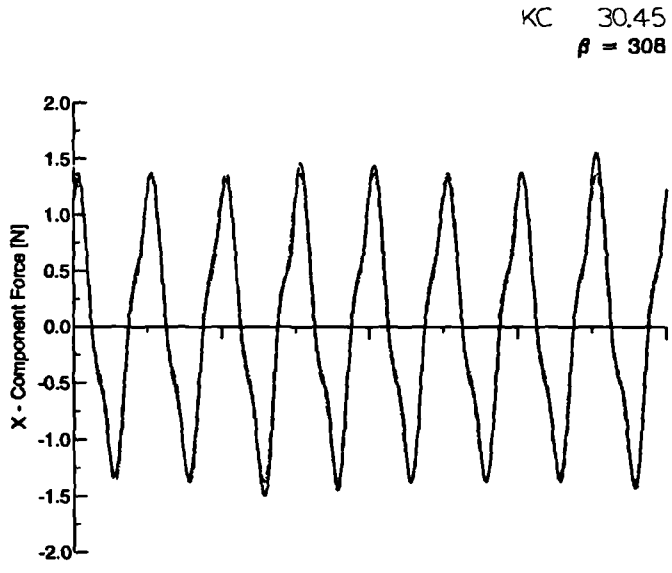


Figure 3.14: Comparison between the measured in-line force time history ——, and the one predicted using Morison's equation — · — · —; KC= 30.45, β =308

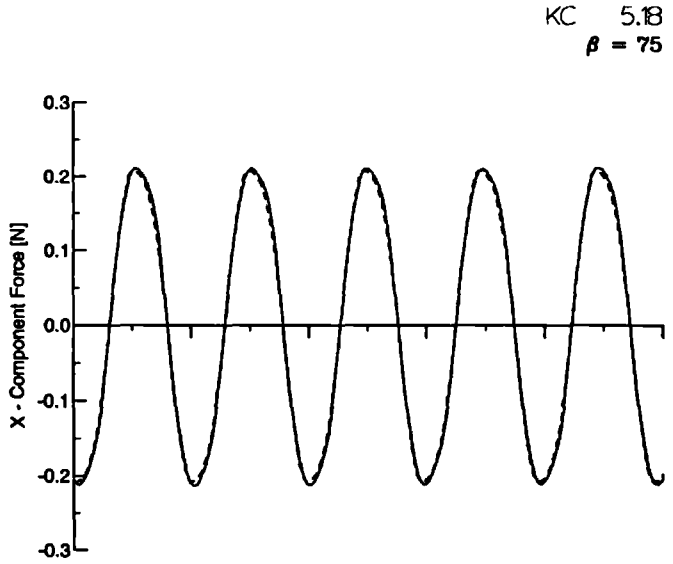


Figure 3.15: Comparison between the measured in-line force time history——, and the one predicted using Morison's equation — · — · —; KC = 5.18, $\beta = 75$

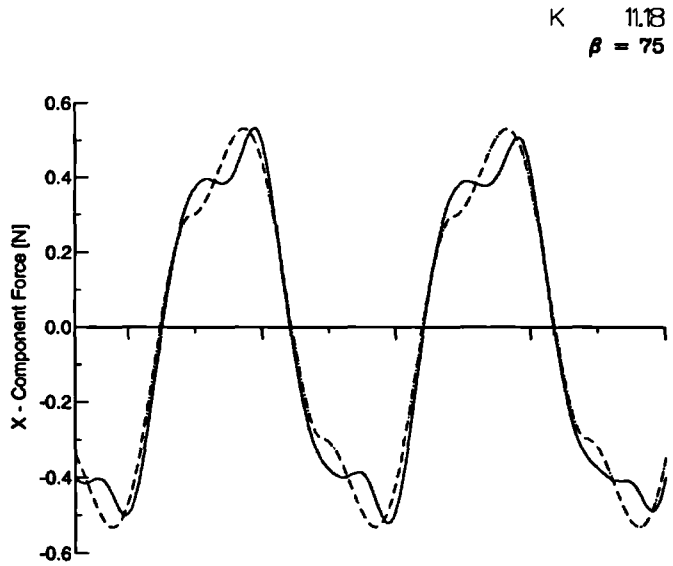


Figure 3.16: Comparison between the measured in-line force time history ——, and the one predicted using Morison's equation — · — · —; KC = 11.18, $\beta = 75$

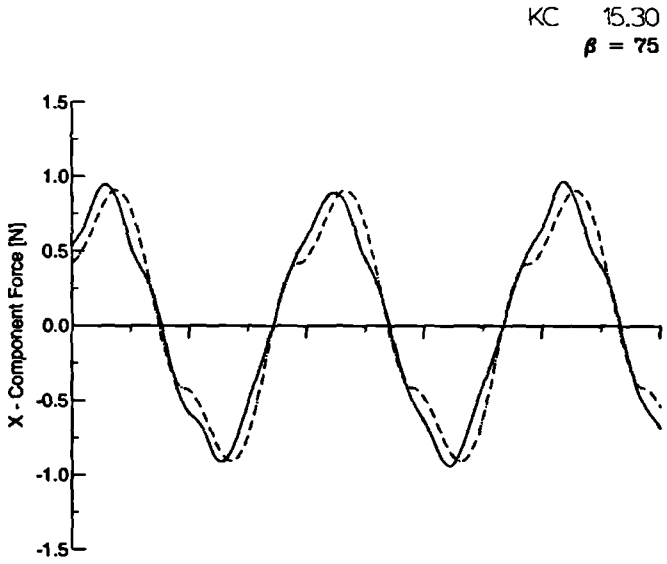


Figure 3.17: Comparison between the measured in-line force time history——, and the one predicted using Morison's equation — · — · —; KC = 15.30, $\beta = 75$

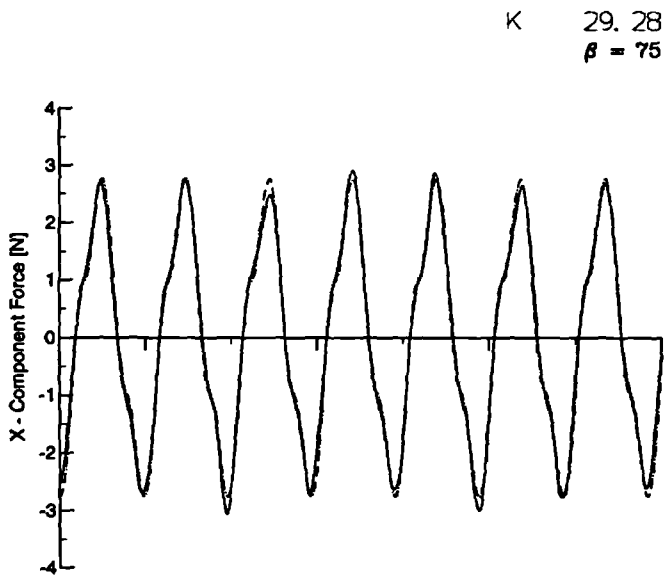


Figure 3.18: Comparison between the measured in-line force time history , and the one predicted using Morison's equation — · — · —; KC = 29.28, $\beta = 75$

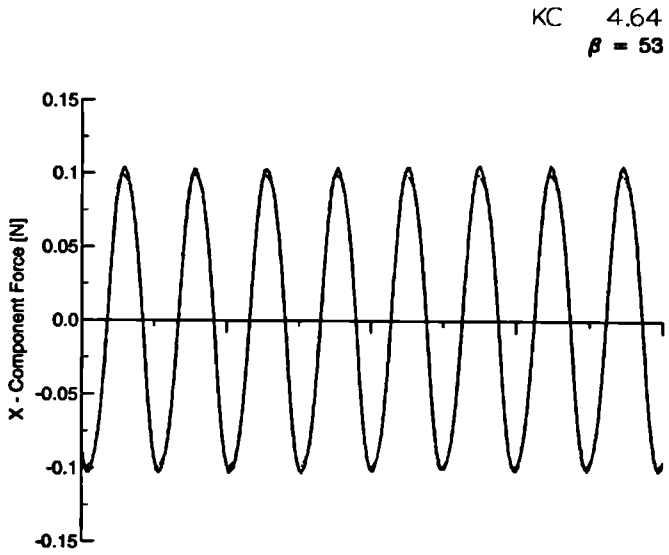


Figure 3.19: Comparison between the measured in-line force time history——, and the one predicted using Morison's equation — · — · —; KC = 4.64, $\beta = 53$

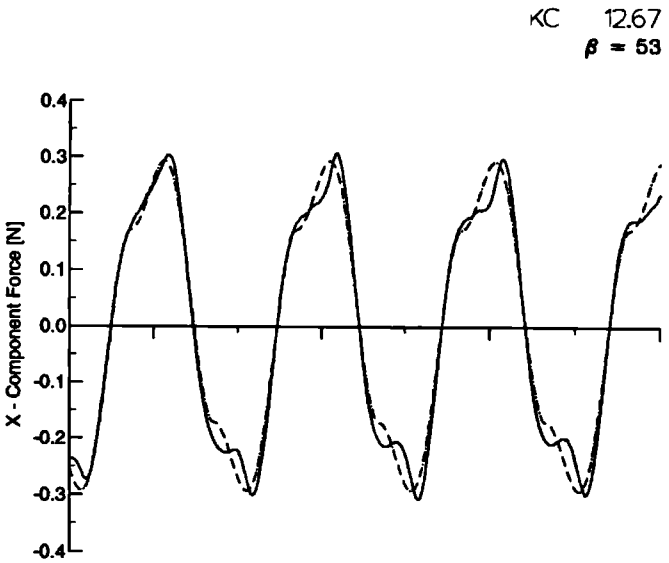


Figure 3.20: Comparison between the measured in-line force time history ——, and the one predicted using Morison's equation — · — · —; KC = 12.67, $\beta = 53$

same β by Sherwin [43], and figure 3.24 shows the comparison at $\beta = 75$ with the results computed by Lin et al., [26]. In the latter case the forces were calculated by using two different methods: a linear momentum method (or Wu's method), and a pressure integration method (integrating along a radial line from the outer boundary of the mesh to the cylinder surface). These results covered a higher range of KC values (up-to 40). The linear momentum method seems to agree better than the pressure integration method with the experimental results.

In addition, in figure 3.25 the C_{Frms} coefficients obtained in the present study and those computed by Lin et al. [26] are plotted.

It may be seen that generally the agreement between experimental and all the numerical results presented (Iliadis, [19], Sherwin, [43], Lin et al., [26]) is always good at low KC. The numerical simulations though do not reproduce the rapid rise of C_D and decrease of C_M at KC around 8, and in particular do not capture the peak in C_D measured at $KC = 10$. At larger KC, from 16 onwards the computed C_D values appear to agree again with those from experiments, figure 3.24. The C_M values computed with the two methods by Lin et al. start to deviate from each other. In the range of KC between 13 and 23 the pressure integration method seems to reproduce better the experimental results, and at higher KC C_M in the computations deviated significantly from each other and from the experimental results. These large variations in the inertia coefficients are nevertheless insignificant in terms of the total loading because the inertia component represents a small proportion of the total force at these KC values and for the same reason is likely to be less accurately predicted at high KC.

The disagreement between numerical and experimental results in the transverse street regime may be due to three-dimensionality in the flow which can-

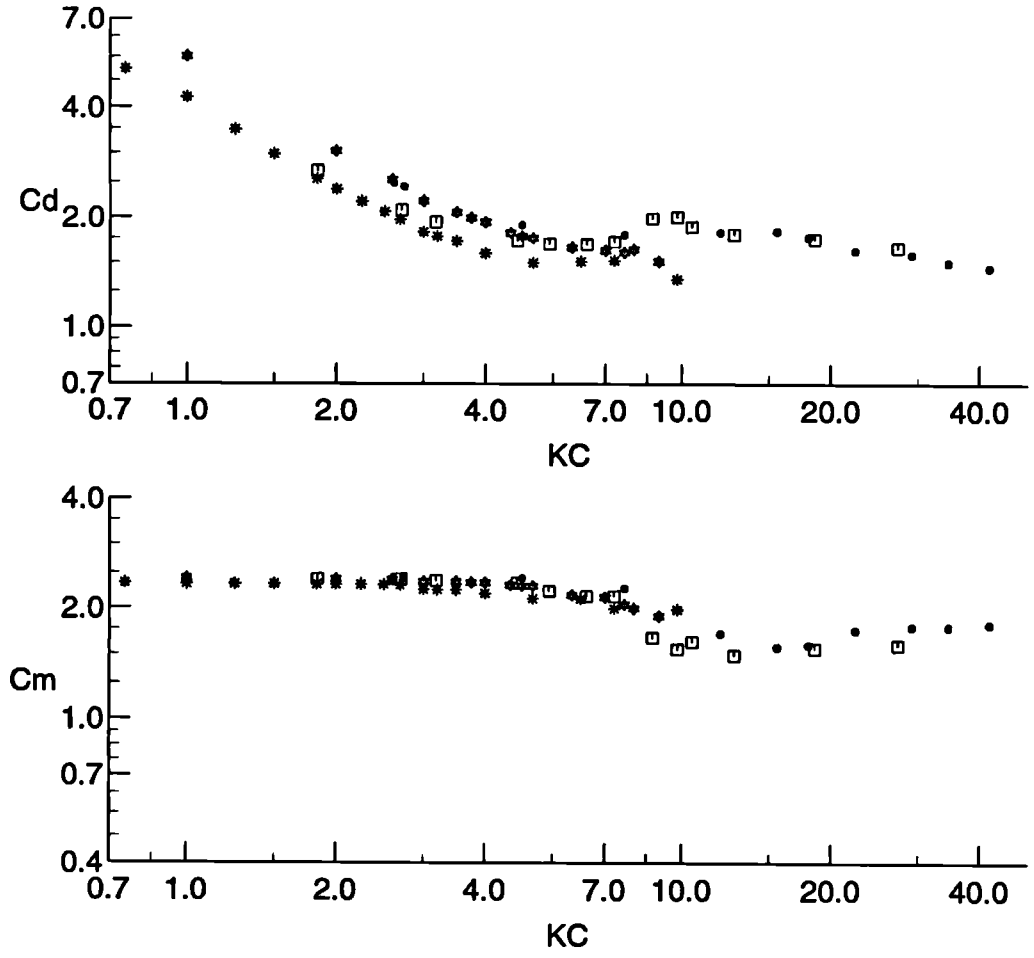


Figure 3.21: Drag coefficient and Inertia coefficient versus KC, Experimental and Numerical results: □, $\beta = 53$, •, $\beta = 35$, present results; Numerical results: ⋆, $\beta = 34$, ∗, $\beta = 53$, Iliadis (1995).

not be reproduced by a 2D simulation, and also to the fact that the Morison's coefficients are rather sensitive to small phase changes in the in-line force maxima and such changes are prevalent especially in the so-called transverse-street regime.

The r.m.s. in-line force coefficients (figures 3.22 and 3.25) are instead relatively insensitive to force-maxima positions in this regime as was demonstrated by Maull and Milliner [28] and in fact the agreement between experimental and

numerical results is extremely good for all the KC values studied. This means that the 2D simulations are all able to predict well the amplitude of the total force but not quite as good to detect the phase difference.

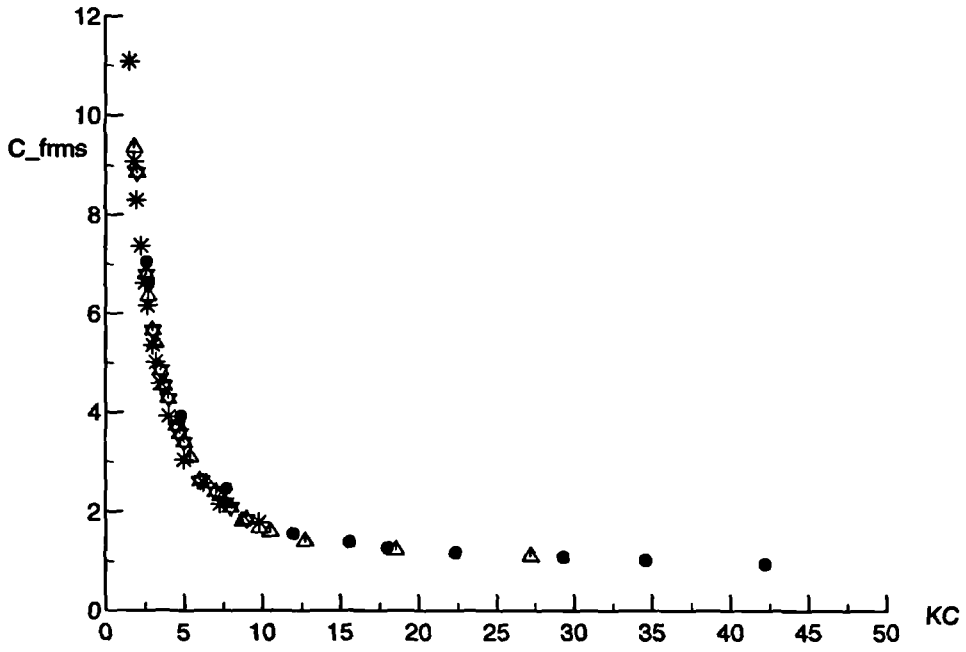


Figure 3.22: Root mean square coefficient for the in-line force versus KC, Experimental and Numerical results: $\triangle$, $\beta = 53$, $\bullet$, $\beta = 35$, present results; Numerical results: $\star$, $\beta = 34$, $*$, $\beta = 53$, Iliadis (1995).

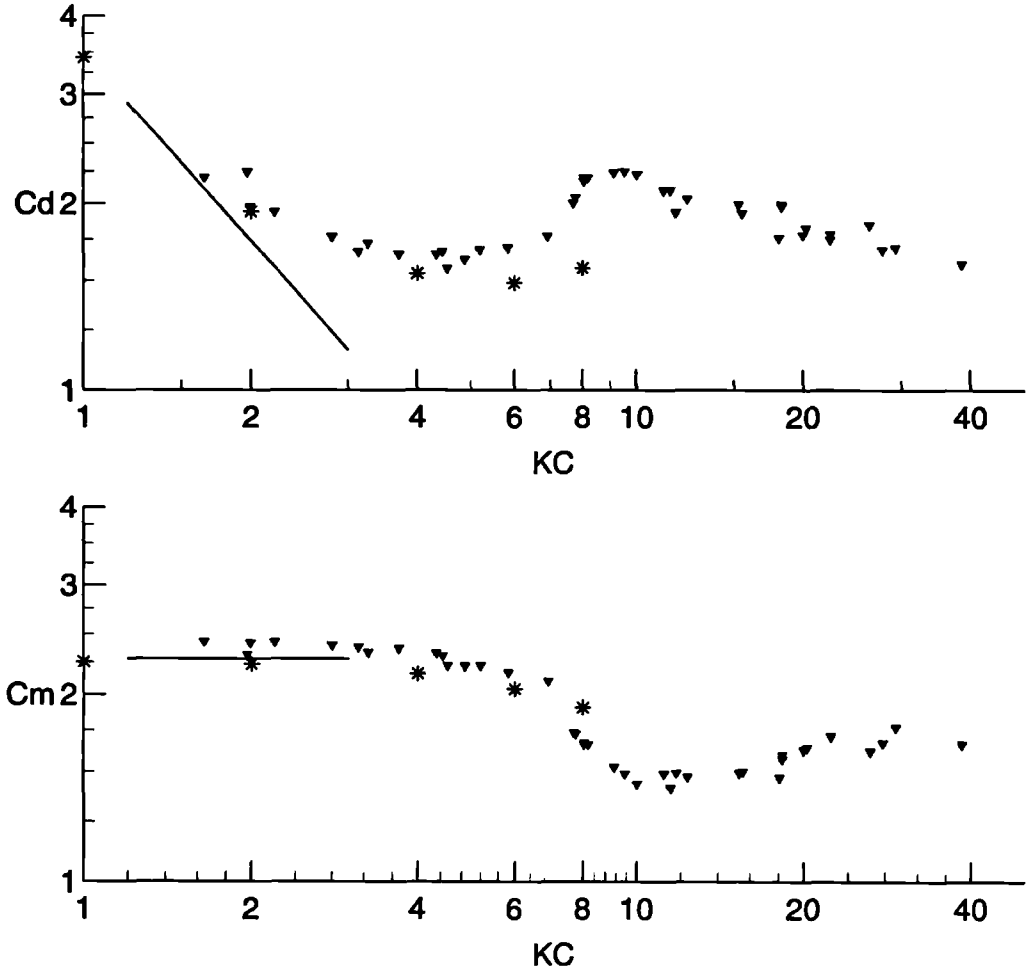


Figure 3.23: Drag coefficient and Inertia coefficient versus KC, Experimental results: ▼, $\beta = 75$, present results; Numerical results: $\beta = 76$: $*$, Sherwin (1995).

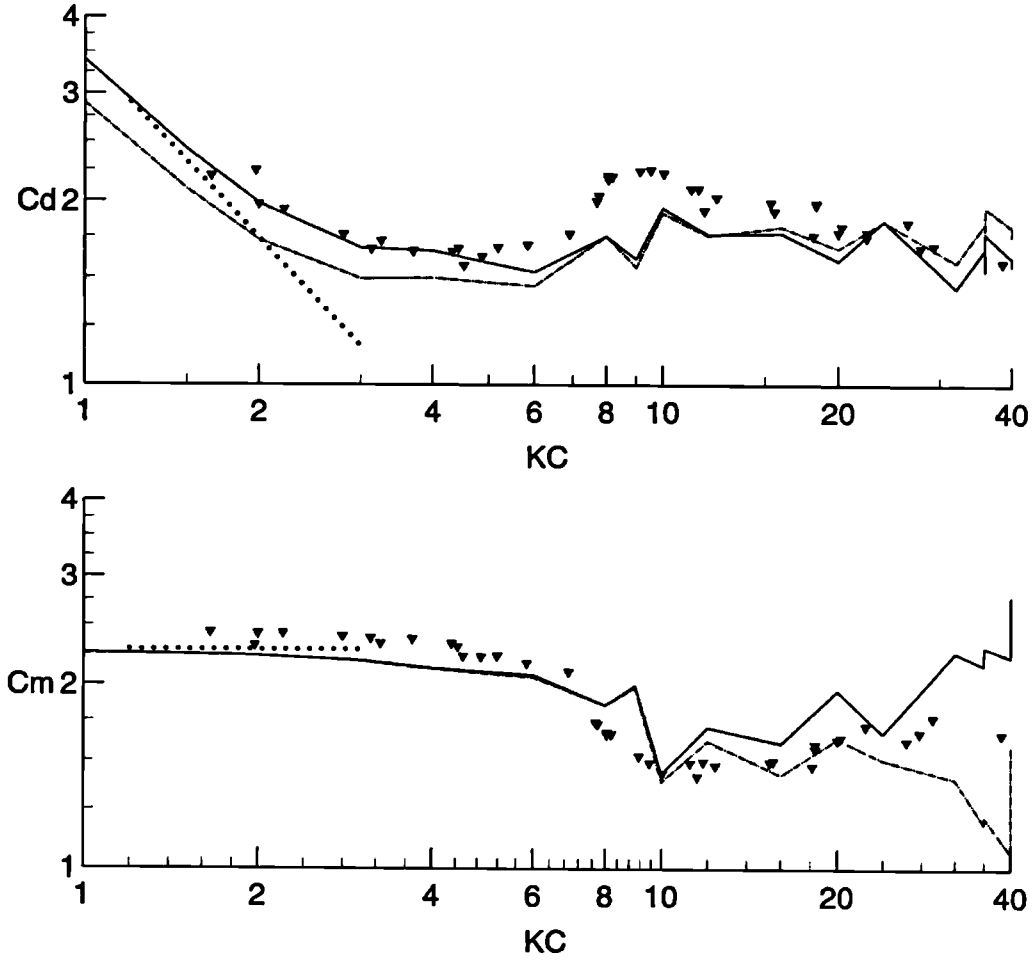


Figure 3.24: Drag coefficient and Inertia coefficient versus KC, Experimental results: ▼, β = 75, present results; Numerical results: β = 76: —, Wu's method, Lin et al.(1996); — · —· - pressure integration method, Lin et al. (1996); dotted line, Wang theory

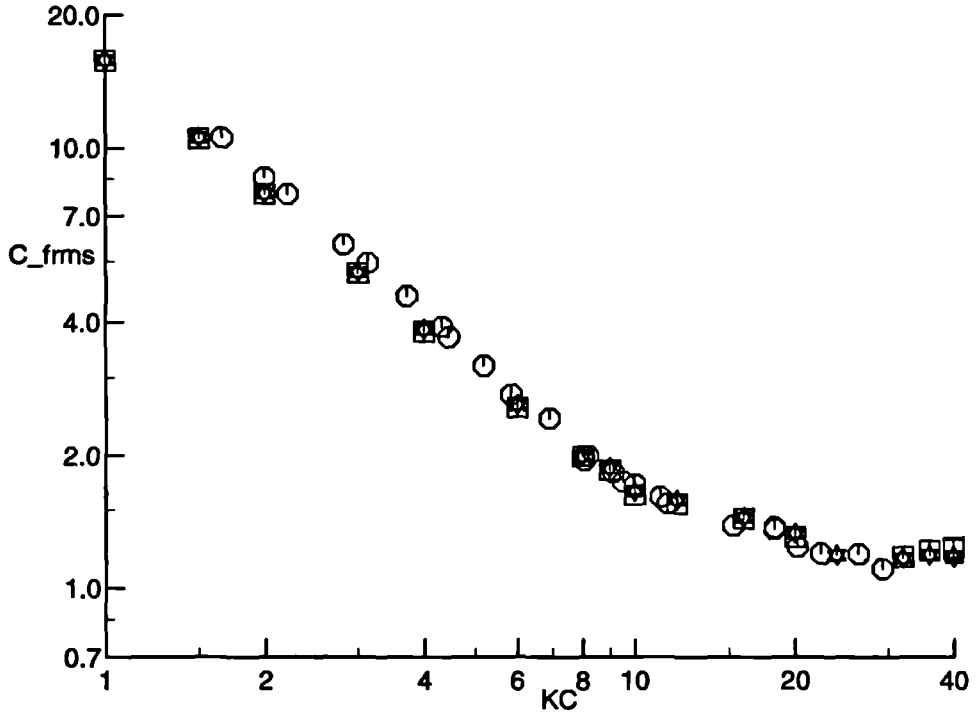


Figure 3.25: Root mean square coefficient for the in-line force versus KC, Experimental and Numerical results: o, $\beta = 75$, present results; Numerical results: $\beta = 76$: $\star$, linear momentum method, Lin et al. (1996), $\square$, pressure integration method, Lin et al.(1996);

Chapter 4

Oscillatory flow past flexibly mounted cylinders

4.1 Introduction

Wave and vortex-induced vibrations present serious problems for the design of small diameter tubular components such as risers. As mentioned in sections 1.1 and 1.6, these elements are particularly prone to resonant excitations hence the in-line and transverse oscillations may be amplified and can lead to dire consequences if not properly estimated and designed.

To date most off-shore design has utilised force coefficients based on rigid cylinder data, but these slender elements should be considered as flexible and the question of what prediction procedure should be used is controversial.

Dynamic behaviour of flexible structures in oscillating flow has received relatively little attention (see Chapter 1), therefore there is need for further research.

If a flexibly mounted cylinder given two degrees of freedom - in-line and transverse with the main flow - is immersed in an oscillatory stream, oscillations may be induced in both directions. In order to study these types of response it is convenient to mount a rigid cylinder on elastic supports and to allow it to respond in one or the other or both degrees of freedom.

Most of the studies conducted so far, for example [9], [30], have concentrated on the transverse response of the cylinder when it is constrained in the in-line direction, which is a direct result of vortex shedding.

Very few studies have investigated instead the in-line response, and recently some unexpected results for $\beta = 750$, [8], have drawn more attention upon this case. If the cylinder motion is restricted to the in-line direction it generally oscillates at the flow frequency and at odd multiples of it due to non-linear drag. In the general case the response is observed to increase smoothly with increasing KC, and is well described by using as a prediction method the relative motion form of the Morison's equation.

But it was found that this is not true for cylinder frequencies close to 3 times the flow frequency. In these cases a resonant peak is observed. This is in the KC range from 8 to 25 and the major component of the response is precisely at three times the flow frequency. The response in resonant conditions is not predicted by Morison's equation (section 1.6 and in particular 5.3.3).

Therefore in order to investigate further the area of in-line vortex-induced oscillations and their resonant behaviour, and to study the influence of lowering β on the cylinder response, the present research was undertaken.

Measurements of the in-line response of an elastically mounted circular cylinder free to move only in-line with the flow performing planar oscillatory motion were made. The tests were conducted at different β values (750, 270 and 60).

4.2 Experimental apparatus and procedure

The U-tube fluid tank described in Chapter 2 was used to generate the oscillatory flow. In this case a support mechanism for the cylinder had to be adopted to render it compliant in the flow. The cylinder was mounted on a pendulum support structure situated above the working section. This structure had already been used for similar experiments, [9], [8], (figures 4.1, 4.2). It is composed of a square flat horizontal plate to which the cylinder is rigidly

mounted with four vertical arms attached to the corners of the plate and to a rigid frame overhead, via thin spring steel strips (flexures). A set of flexures which are of very high stiffness in the transverse direction but quite flexible in-line provide the required degree of freedom. The rigid arms have turnbuckle type adjusters enabling their length and hence the natural frequency, to be varied without the need for completely dismantling the system every time that it is necessary to change the frequency of oscillation. The experiments were performed using both a circular cylinder of 50 mm and one of 30 mm diameter giving, with water as the working fluid, β values of respectively 750 and 270. When the polyethylene glycol 35000 was used in solution with water to produce a working fluid 4.6 times more viscous than water, a diameter of 30 mm was chosen to obtain a β of 60.

For the measurement of the in-line displacement, the use of spring steel flexures had the advantage that the surface strain on them was directly proportional to the cylinder displacement, and therefore the set of flexures used was strain gauged [1] to provide a simple displacement measuring system.

The displacement/strain calibration depended on the length of the suspension arms and was achieved by using accurately machined spacers to displace the cylinder in 1 cm steps over a range of $\pm$ the diameter. This calibration was carried out at the start of each day of experiment. The reliability was checked by repeating it at least twice. Each value was typically within $\pm 0.15\%$ of the mean and was found to be linear for all lengths of the arms. The calibration factor was calculated via a linear regression.

Because the working section is pressurised by virtue of the columns of water in the upright limbs, the pendulum arms were enclosed in an air filled pressurised chamber attached to the top of the working section. The pressure in the

[1] Resistance strain gauges with length 6mm, resistance 120 Ω, GF 2.12, were mounted

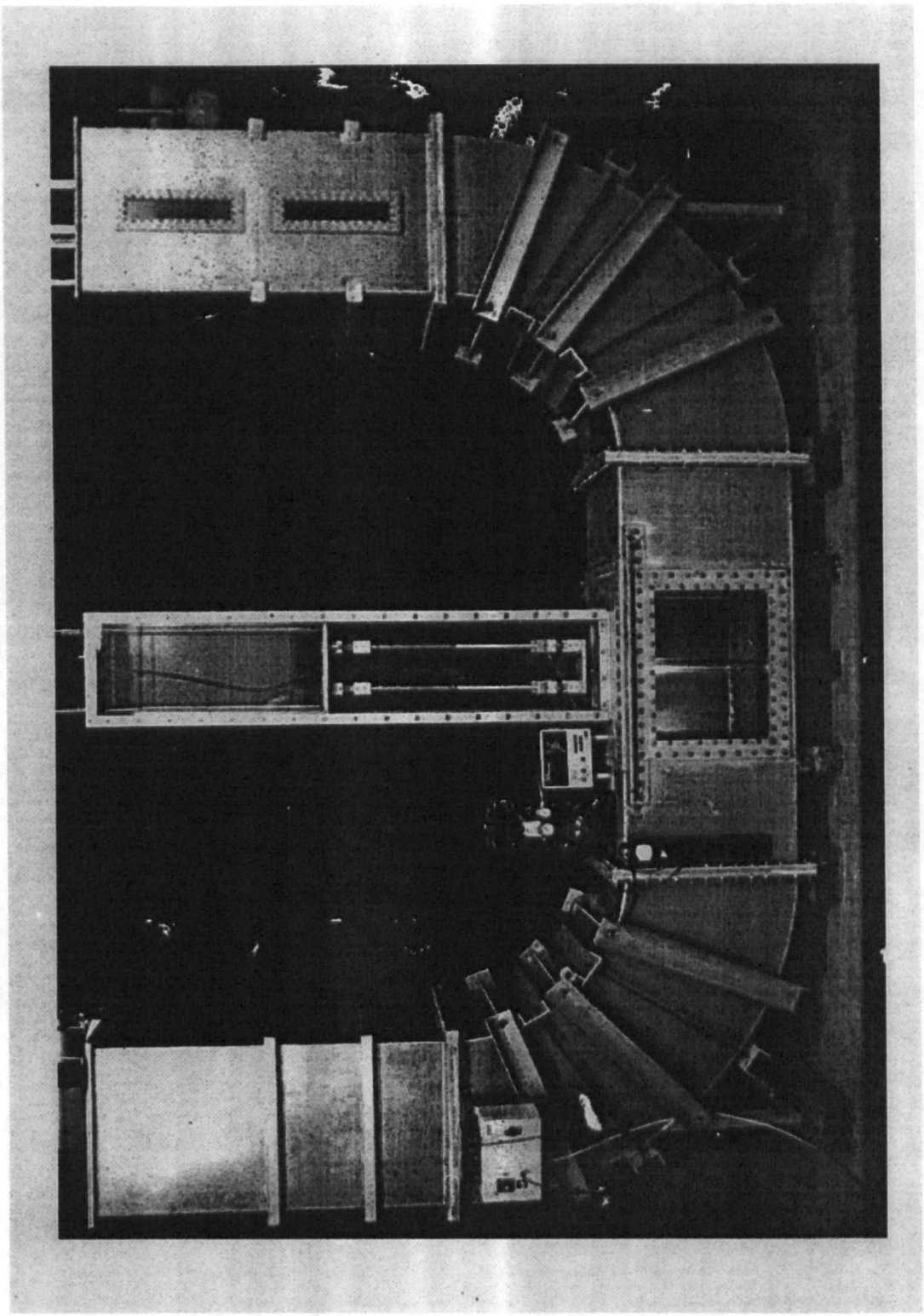


Figure 4.1: U-tube, cylinder and suspension system

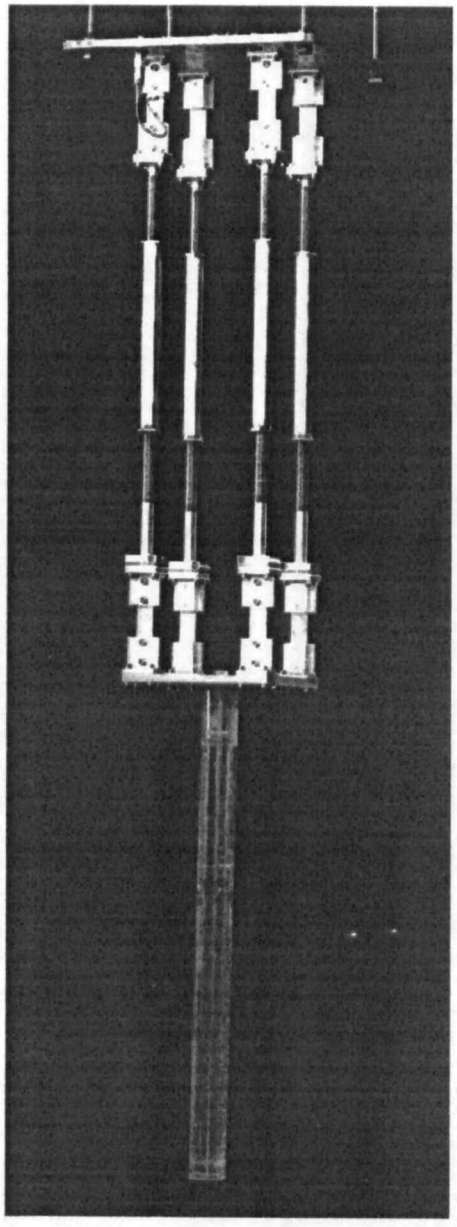


Figure 4.2: View of the cylinder and the pendulum suspension system

chamber was maintained constant using a Druck DPI 500 pressure controller, the source of compressed air being a small electrical compressor. This system enabled the fluid level to be kept precisely at the top of the working section. The controller was also able to combat small leaks, therefore the U-tube could be left unattended even over-night.

Clearance between the tank floor and the lower end of the cylinder was kept as small as possible. However, because this is a pendulum system the cylinder rises slightly as it is displaced laterally. Nevertheless it was found that for a cylinder displacement of about a diameter the cylinder rose by only 1-2 mm, which is an acceptable figure. A diagram of the cylinder motion is presented below, figure 4.3. To minimise wave interference effects at the upper

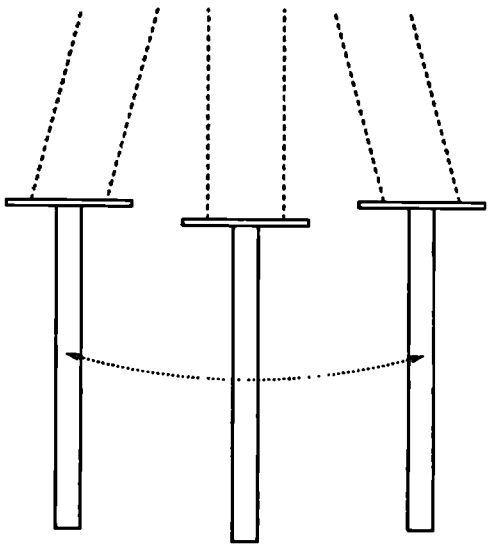


Figure 4.3: Sketch of the cylinder motion

end of the cylinder a perspex plate was positioned in the inside flush with the upper wall of the U-tube. An appropriate hole in the plate gave the cylinder the necessary freedom to move in-line with the fluid oscillations.

4.3 Measurement of the relevant parameters

The relevant parameters have been introduced already in section 1.6. Using the same notation it may be useful to recall that the cylinder displacement x is a function of the following parameters:

$$x/D = f(KC, \beta, m_s/\frac{1}{4}\rho\pi D^2, \zeta_s, f_{ow}/f_w) \tag{4.1}$$

which have been measured as explained below.

KC was calculated as for the fixed cylinder tests, regardless of the relative velocity between fluid and cylinder. The maximum velocity of the incident flow was used in the ratio U_mT/D.

The natural frequency of the system both in air and in water was estimated from the displacement signal of small naturally decaying oscillations. For this so called 'twang test' the system was released from rest at an initial displacement of approximately one diameter. The measurement was taken four times. The natural frequency was calculated from spectral analysis and the average showed that each value differed by less than 0.05% from the mean.

The frequency of oscillation of the cylinder in oscillatory flow, say f_{of}, is neither of the forementioned. It depends on the incident oscillatory flow. The added mass is not the same for a body oscillating at its natural frequency in a fluid otherwise at rest as it is for a body oscillating in a fluid in significant motion. The added mass changes according to different flow conditions, and also to external factors like proximity of other bodies. Nevertheless when the mass ratio is large the added mass becomes less prominent. In fact, the natural frequency of a circular cylinder oscillating in fluid (whether stationary in the far field or not) is:

$$f_{of} = \frac{1}{2\pi}\sqrt{\frac{k_s}{m_s + m_d C_A}} \tag{4.2}$$

where k_s is the structural stiffness, C_A is the added mass coefficient $= C_m - 1$, and depends on the type of motion occurring, m_s is the effective mass and the displaced mass $m_d = \frac{1}{4}\rho D^2 \pi L$. If $C_A = 1$, for a circular cylinder, the response frequency is the same as the one measured for very small oscillations in an inviscid still fluid. If the added mass is neglected ($m_d = 0$), the response frequency equals the one measured in air, neglecting the effect of airflow (strictly it should be measured in vacuo). If the mass ratio $m_r = m_s/m_d$ is large the difference between the two extreme frequencies is small and the value of the added mass coefficient becomes less important.

In this research the frequency ratio used, F_r, is defined as the ratio of the cylinder natural frequency, f_{ow}, to the fluid oscillation frequency f_w, where f_{ow} is the natural cylinder frequency of small amplitude oscillation in still water, because this has been the general definition used in other works too.

The structural damping ζ_s, defined as $\zeta_s = (1/2\pi)\log A_r = \frac{c}{2m\omega_o}$ where A_r is the ratio of the amplitude of successive displacement peaks was also estimated from the twang tests. The damping of the basic system in air was found to be independent of amplitude, varied little with natural frequency and averaged out at very small values according to the different set-ups used.

Having decided upon a particular experimental set-up, the arms of the suspension system were adjusted to obtain the desired cylinder frequency. The stiffness of the system was measured by displacing the mounting plate horizontally by a known amount and evaluating the force necessary to do so via an RS-2Kg load cell which had been previously calibrated. Again the procedure was repeated four times and averaged out to check the reliability (within 0.3% from the mean).

Since the suspension set-up is a compound mass-spring/pendulum system it is not possible to measure the effective system mass directly. The effective

mass in air must therefore be estimated from the measured stiffness and natural frequency in air using the relation: $f_o = \frac{\omega_o}{2\pi} = \frac{1}{2\pi}\sqrt{\frac{k}{m}}$, or by measuring the stiffness and the natural frequency in still water, and subtracting the added mass which for a circular cylinder equals the displaced mass mentioned above, from the resulting effective mass in water.

The wave probe was calibrated as described in section 2.2 before each test was started, and the calibration linearity checked.

The fluid oscillation frequency was calculated via a routine that found the zero crossings of the fluid displacement signal using a linear interpolation between adjacent points on either side of the zero and located therefore the number of cycles actually recorded.

The experiments were carried out at different values of the parameters involved. The values of all the parameters will be listed every time that a given set-up is discussed (see next Chapter).

4.4 The data acquisition system

The water displacement and cylinder response signals from the wave probe and the strain gauges amplifier respectively, in 2 channels, were connected to the Analog-Digital converter, on the laboratory 286 P.C.(see also section 2.7). The U-tube was controlled via a custom designed controller, as described in section 2.2.

Before starting the blower to make the fluid oscillate, zero voltage output for the two channels was read by the computer. Such a zero reading was repeated at the end of each experiment when the blower was switched off and the fluid was set to rest, to make sure that there was no drift in the amplifiers.

A data sampling rate of 20 samples/s was chosen. Sampling times were equal to about 125 U-tube oscillation periods. During a series of runs KC was

never changed by more than an increment of about 1.0 or 2.0 and after every KC change 5 minutes was the time allowed before data collection recommenced.

The series of runs were performed for both increasing and decreasing KC and no hysteresis was noted.

After every run the r.m.s. displacement was calculated for each KC [2] and showed good repeatability over a long period of time (even months).

[2] $X_{rms} = \sqrt{\overline{x_i^2}}$

Chapter 5

Response analysis for flexible cylinders

5.1 Introduction

Previous research on flexibly mounted cylinders has indicated that the fluid-structure interactions of slender members in off-shore structures are extremely sensitive to the ratio of the natural frequency of the structure to the fluid oscillation frequency and to KC values, section 1.6. Almost all of the studies directed towards the understanding of this interaction and the estimate of the forces exerted on circular cylinders are based on the Morison's equation quoted in various parts of this thesis, although it fails to correctly predict the fluid loads in certain circumstances.

For the in-line oscillations of a particular cylinder free to move in-line with the flow motion, Bearman et al., [8], showed that for the particular set-up used, a resonant behaviour occurred when the frequency ratio was close to 2.85, see Chapter 1 and Introduction 4.1. Because this particular case exhibited very interesting features it was decided to repeat these experiments which had been conducted at $\beta = 750$ with the experimental apparatus described in the previous Chapter. Besides, a study of the existing literature on the phenomenon showed that very few studies had been undertaken on in-line responses and it appeared that no considerations had been made on the influence of β on it. Since the main aim informing this thesis is to study any changes in the characteristic behaviour of circular cylinders for the low range of β it was decided

also to measure the in-line response for $\beta = 270$ and 60.

5.2 Test Cases Results

5.2.1 First set-up, non-resonant case, $\beta = 750$

In the first place it was decided to check the system adequacy by trying a case for which the natural frequency of the cylinder was not close to an odd multiple of the fluid frequency. The expected results were that the in-line response would increase monotonically with KC, and that the dominant frequency of oscillation of the cylinder would be the fluid oscillation frequency.

For this set of experiments water was the fluid used. The parameters involved are listed below:

Structural mass of the system or effective mass, $m_s = 3.767$ Kg;

Frequency of oscillation of the system in Air, $f_o = 1.558$ Hz;

Frequency of oscillation of the system in still Water, $f_{ow} = 1.314$ Hz;

Fluid oscillation frequency, $f_w = 0.3003$ Hz;

Cylinder diameter, D = 0.05080 m;

Cylinder length, L = 0.6050 m;

Structural damping , $\zeta_s = 0.001755$;

Mass ratio, $m_r = \frac{m_s}{0.25\rho D^2 \pi L} = 3.074$;

Frequency ratio, $F_r = \frac{f_{ow}}{f_w} = 4.376$.

Measurements of r.m.s. in-line displacements, divided by D, are plotted against KC in figure 5.1, and the power spectrum of the cylinder displacement signal is presented in figure 5.2 for KC = 30.83. The response increases with KC and the dominant frequency of oscillation of the cylinder is the fluid oscillation frequency (i.e. around 0.3 Hz). Moreover, as expected the other peaks above this frequency correspond to all the odd multiples of the fluid frequency.

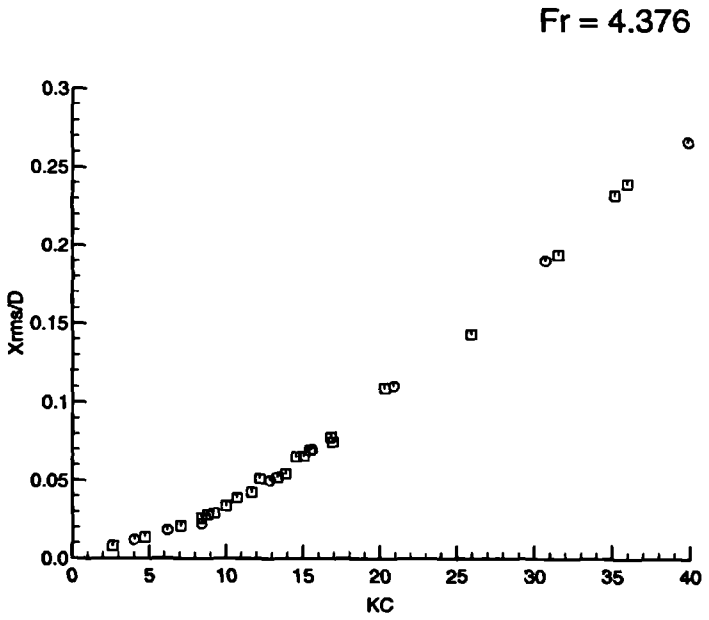


Figure 5.1: In-line measured response (r.m.s./D) versus KC for $F_r = 4.376$ and $\beta = 750$

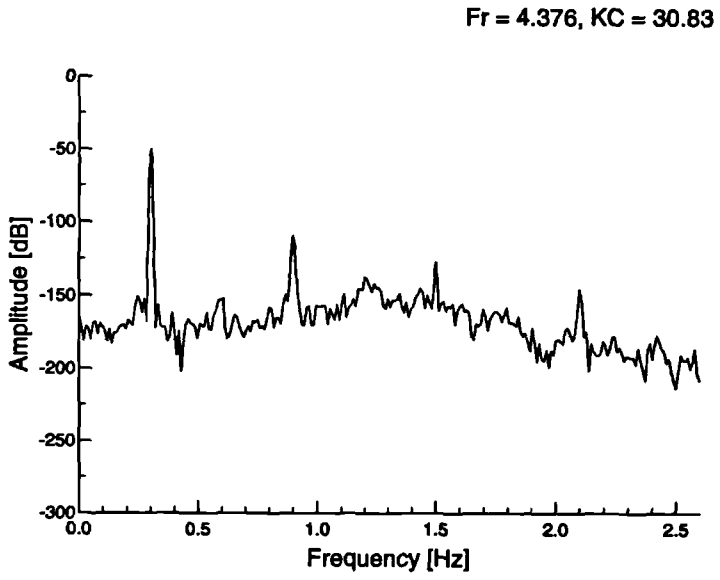


Figure 5.2: Power spectrum of the in-line measured response signal for KC = 30.83, $F_r = 4.376$ and $\beta = 750$

5.2.2 Second set-up, $\beta = 750$

Once confirmed that the system worked well it was then possible to proceed in the research with confidence and to repeat the experiments carried out by Bearman et al., (1992) [8]. In particular the frequency ratios where the response had shown resonant values in the KC range from 8 to 25 were chosen for this second test case. The set-up used in the earlier experiment had to be reproduced. The parameters listed below are the ones that were attained by changing the pendulum arms' length and by adding some masses onto the flat plate to which the cylinder was rigidly mounted, figure 4.2, so that the same conditions could be achieved:

Effective mass, $m_s = 10.750$ Kg;

Frequency of oscillation of the system in Air, $f_o = 0.928$ Hz;

Frequency of oscillation of the system in Water, $f_{ow} = 0.850$ Hz;

Cylinder diameter, D = 0.0508 m;

Cylinder length, L = 0.605 m;

Structural damping, $\zeta_s = 0.001521$;

Mass ratio, $m_r = 8.770$.

The frequency ratio F_r was changed by small increments in the range between 2.808 and 2.960, and a similar response to that obtained in Bearman et al. (1992), [8], was observed. The practical way to vary F_r consisted of changing the fluid frequency a tiny amount each time, by adding a small quantity of water or taking it out of the tank. This practice was preferable to having to empty the tank each time, opening the pressurised chamber and adjusting the pendulum's arms length to change the cylinder frequency. In this way it must be noted that also the β parameter changed slightly (less than 2%), but as the results for the fixed cylinder case would confirm it is most unlikely that these minute variations could influence the results at all. Therefore the tank

oscillation frequency can easily be retraced knowing the frequency ratio and the cylinder frequency of oscillation in water. The maximum response of the resonance peak was reached for a F_r of 2.860 at $KC \sim 14$ very close to that which was noted in [8] (that was F_r of 2.850 at $KC \sim 13$), figure 5.3, figure 1.8. The response was measured, as in [8], for the whole KC range and for F_r over a range from 2.808 to 2.960. The figure shows that the measured peak in the non-dimensional r.m.s. in-line displacement increased from $F_r = 2.808$ to $F_r = 2.860$ and then decreased at F_r around 3.00.

A plot of the power spectrum of the cylinder displacement signal for $F_r = 2.840$ and KC = 12.06 is presented in figure 5.4 to confirm what has been previously stated. The fact that the second harmonic of the fluid frequency is the dominant response frequency is in fact the evident observation that can be drawn. A discussion of the possible reasons for the resonant behaviour is left to section 5.3.

5.2.3 Third set-up, $\beta = 270$

It was then regarded as interesting to investigate the phenomenon, i.e. the resonant response, for different values of β. Leaving the water as the working fluid, a change in the cylinder diameter alone reduced β considerably. Using a 30 mm cylinder diameter resulted in a β value of about 270. This value enabled useful comparisons with the fixed cylinder experiment carried out in this research for $\beta = 308$ (section 5.3.3 and following ones).

As observed in the previous section, because the F_r was varied by changing f_w slightly, β changed accordingly, but its values were within $\pm$ 2% of the nominal value of 270.

As for all the other parameters, where possible it was chosen to keep them close to the ones featured in the experiment named Second Setup. They are: Effective mass, $m_s = 10.41$ Kg;

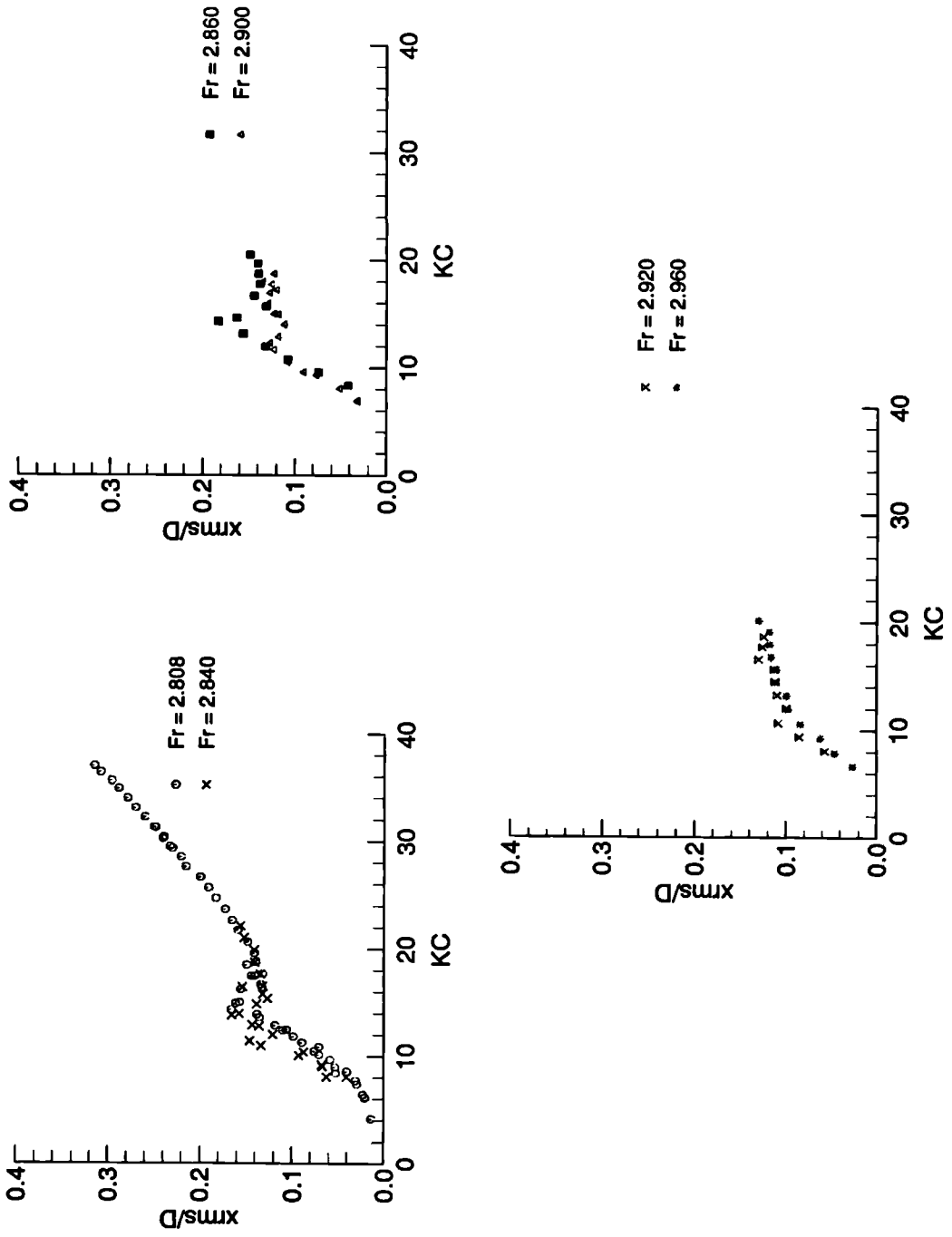


Figure 5.3: In-line measured response (r.m.s./D) versus KC for 6 frequency ratios and $\beta = 750$

Frequency of oscillation of the system in Air, $f_o = 0.928$ Hz;

Frequency of oscillation of the system in Water, $f_{ow} = 0.903$ Hz;

Cylinder diameter, $D = 0.030$ m;

Cylinder length, $L = 0.605$ m;

Structural damping, $\zeta_s = 0.00112$;

Mass ratio, $m_r = 24.34$.

A resonant behaviour was found in this case in the range of F_r between 2.944 and 3.036, and the maximum response was found to occur at KC $\sim$ 10 for $F_r = 2.990$, see figure 5.5

5.2.4 Fourth set-up, $\beta = 60$

In order to decrease β further, polyethylene glycol 35000 in solution with water was used to give a working fluid 4.6 times more viscous than water. The cylinder diameter was kept equal to 30 mm and the resulting β was about 60. In this way when predicting the response via Morison's equation comparisons with the results obtained in this research for $\beta = 75$ and 53 for the fixed cylinder could be made (see section 5.3.3 and 5.3.7).

All the other parameters were the same as those listed for the description of the previous set-up.

The frequency ratio range investigated covered similar values to those studied for $\beta = 270$, that is exactly between 2.917 and 3.007, giving a maximum resonant response at KC $\sim$ 9 for $F_r = 2.961$, figure 5.6.

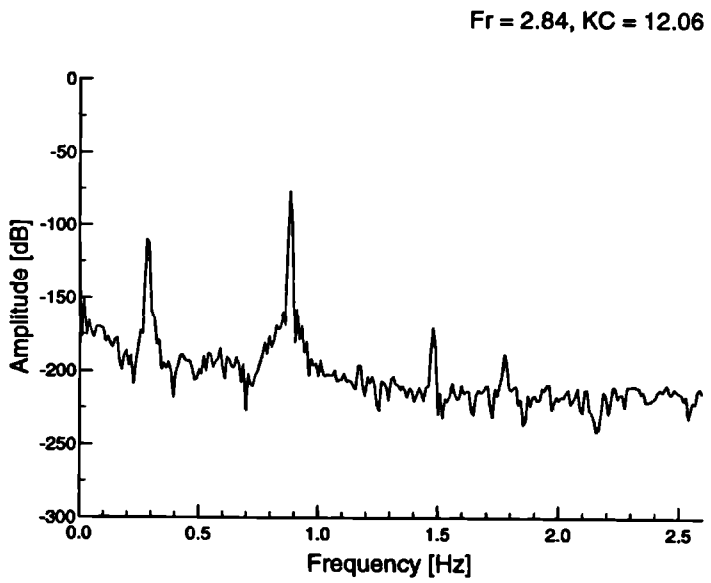


Figure 5.4: Power spectrum of the in-line measured response signal for KC = 12.06, $F_r = 2.840$ and $\beta = 750$

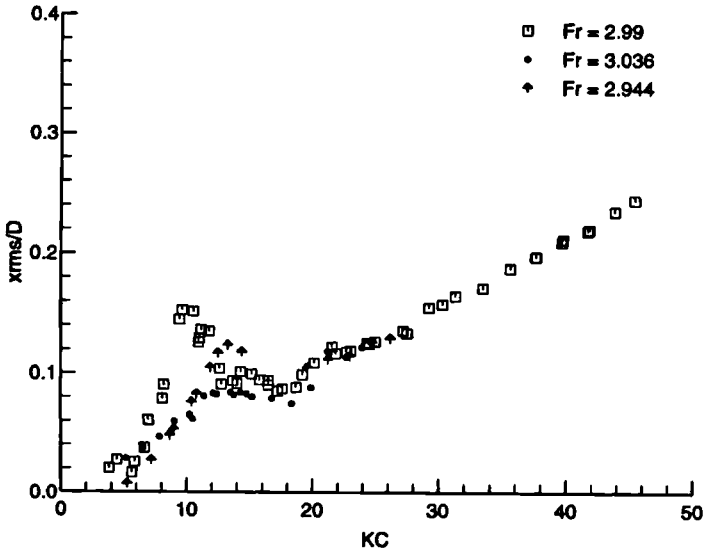


Figure 5.5: In-line measured response (r.m.s./D) versus KC for 3 frequency ratios and $\beta = 270$

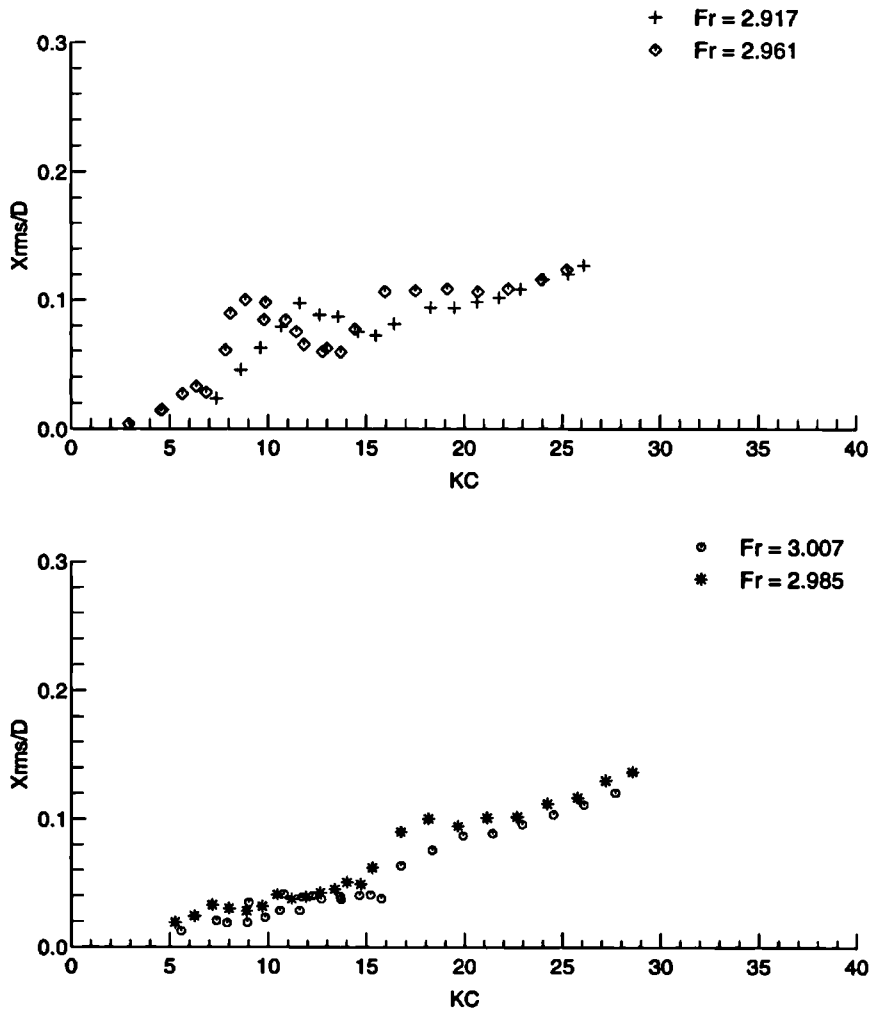


Figure 5.6: In-line measured response (r.m.s./D) versus KC for 4 frequency ratios and $\beta = 60$

5.3 Discussion of the Results

5.3.1 Qualitative Observations

The most interesting aspect of this investigation is the resonant response of the cylinder in the KC range between about 7 to 25 (depending on β) at different values of the frequency ratio.

In order to exclude any doubts that the cause of the resonance in the cylinder response could be connected to the pressure wave input due to the blower, a test to vary the input driving pressure of the U-tube was carried out. The open side of the tank was completely closed and the damping was therefore incremented as seen in section 2.4. In this way the blower was forced to generate a pressure wave much higher than usual. Therefore it was thought that if any unwanted effects were due to the pressure gradient exerted by the blower on the fluid and hence the cylinder these would change when the blower working conditions changed. The experiment was run for the test case named Second Setup at a $F_r = 2.808$. The results repeated nicely the ones presented in figure 5.3 under standard blower conditions.

Therefore the resonance cannot be due to effects caused by the blower.

Looking at the results presented in figures 5.3, 5.5, 5.6, one of the first things that emerges is that, as pointed out in previous studies, the frequency ratio is a parameter which plays a very important role in determining the cylinder response. In fact changing it by very small steps resulted each time in large variations in the cylinder response when the resonant region was approached.

Considering the purpose of this research, that is to study how the physics of the phenomena can change with β , it can be noted at a first glance that the resonant peak appeared in the response in all the cases presented, although it is less prominent as the viscosity is increased, i.e. β is reduced.

When considering the resonant maximum for each case, that is $F_r = 2.860$

for the test case termed Second Setup, $F_r = 2.990$ for the Third Setup and $F_r = 2.961$ for the Fourth Setup is can be noted that they occurred at different KC values. In fact, the KC value corresponding to the maximum response decreases with decreasing β . As for the reason that may be causing these res-

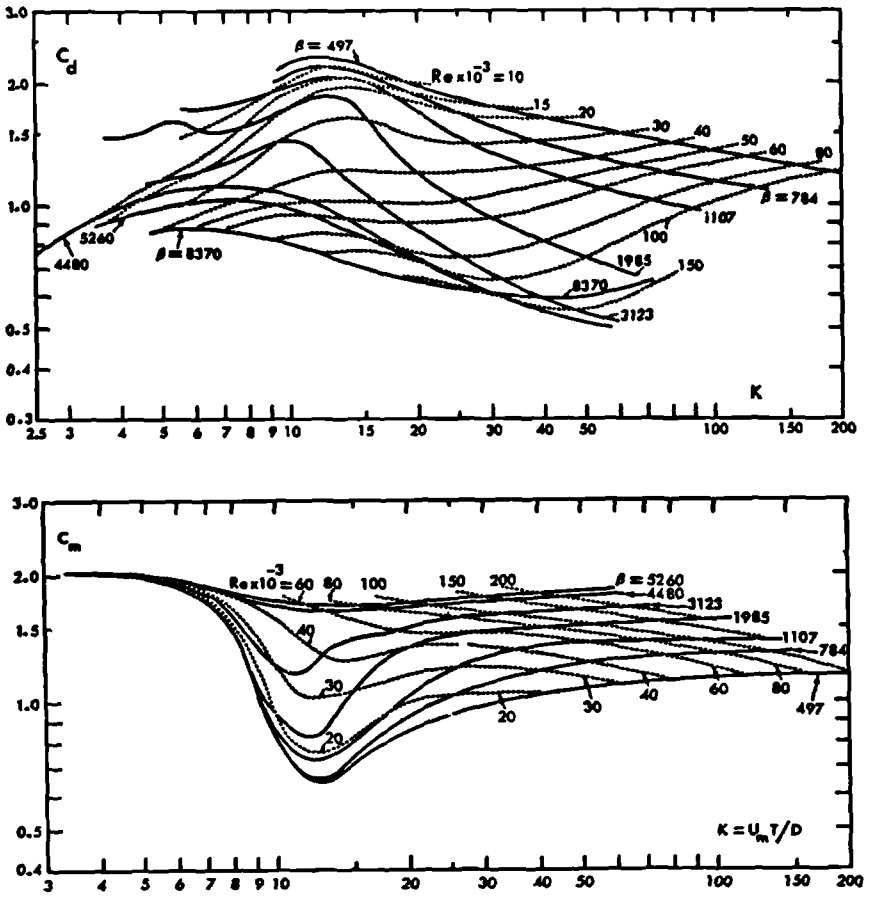


Figure 5.7: Drag and Inertia coefficients versus KC (from Sarpkaya 1976b)

onant peaks some qualitative observations can be made and some conclusions drawn comparing the behaviour of the flexibly mounted cylinder with the fixed cylinder cases. In particular the test case named Third Setup at $\beta = 270$ is thought to be comparable with the Test case 1 for the fixed cylinder, where β was 308, and Fourth Setup at $\beta = 60$ can be studied in comparison with

Test cases 2 and 3 (where β was respectively 75 and 53), see figures in Chapter 3. The Second Setup can be compared with fixed cylinder results taken by Sarpkaya at β 784, see figure 5.7.

Both the peaks in C_D and the troughs in C_M for the fixed cylinder occur at smaller KC values for smaller β suggesting that the region called the transverse street region corresponds to a smaller KC value when β is smaller.

In fact, the resonant peak in the Second Setup corresponds to a KC around 14, at which value Sarpkaya found a maximum in the drag coefficient for $\beta =$ 784, and in the Third Setup occurs at KC $\sim$ 10, where also the higher value of the C_D was observed in figure 3.1. Similarly, C_D for $\beta = 75$ and 53, figures 3.2, 3.3, peak at a lower KC value, around 9, and in the Fourth Setup this is the same KC value at which the maximum occurs for $F_r = 2.961$.

Taking into account the lift coefficient, see figure 3.10, it was noted then that for the cases studied, $\beta = 308$ and $\beta = 70$, a striking three dimensionality appeared to take place at KC around 12.5 for both the cases. This was thought to be due to a change in the vortex shedding mode pattern while the peak between 6 and 11 was ascribed to a stable vortex shedding, highly correlated along the cylinder span.

Now, in the case of the flexibly mounted cylinder, for $\beta = 270$ and 60 the peak in the resonant response occurs mainly between KC = 7 and 13, therefore this might be related to the vortex shedding activity and the way the vortices are shed. A correlated (along the span) vortex shedding at a frequency close to three times the fluid oscillation frequency may in fact be occurring and influencing the cylinder response, which then drops when the vortex shedding becomes weaker.

In this respect it is very interesting to note that for the flexibly mounted cylinder also a secondary peak was present at KC between 18 and 25 for $\beta =$

270 and between 13 and 20 for $\beta = 60$, hence recalling the secondary peaks in the lift coefficient and correlation factor presented for the fixed cylinder. But it is not obvious why a fall in correlation on the rigid cylinder should be connected to a resonant response for the flexible cylinder.

5.3.2 Flow visualisation

Flow visualisation was carried out to investigate any spanwise variations of the vortex shedding in the resonant region. Wool tufts were attached to the cylinder in staggered rows for its whole length (see figure 5.8) and video recordings were taken at a speed of 25 frames per second for KC ranging

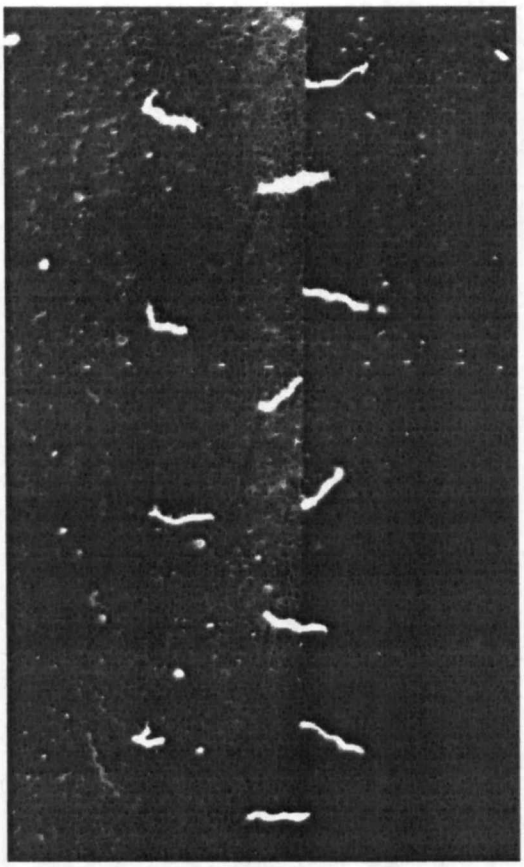


Figure 5.8: Test cylinder with wool tufts during flow visualisation

between 5.04 and 23.88. KC was increased finely in steps of 1 or 2 each time and not less than 5 minutes were allowed for the amplitude to stabilise before passing to the subsequent recording. The set-up reproduced was the one termed Second Setup because pure water allowed a better vision through the perspex windows than the polyethylene glycol solution. A study of the videos showed no evidence of three dimensionality, reinforcing the suggestion of a correlated vortex shedding in the region considered.

5.3.3 Prediction of Forces and cylinder Displacements with Morison's equation

Following the procedure used by Bearman et al. [8] as described in Chapter 1 (section 1.6.2), the possibility of predicting the cylinder response in the in-line direction was investigated both in resonant and non-resonant conditions by using the relative form of Morison's equation [1]:

$$F(t) = \frac{1}{2}\rho D C_D (U - \dot{x}) \mid U - \dot{x} \mid + \frac{1}{4}\pi\rho D^2 C_M (\dot{U} - \ddot{x}) \qquad (5.1)$$

The response of the oscillating cylinder allowed to move only in the in-line direction x, can be described by equation 1.7 reported hereafter:

$$m\ddot{x} + c\dot{x} + kx = F(t) \qquad (5.2)$$

where F(t) is the total fluid force acting on the cylinder.

The general prediction method used in this work consisted of the following steps. Firstly, by substituting the time histories of the measured displacements x(t) and the carefully measured parameters m, c and k in equation 5.2, the in-line force time histories F(t) were obtained. Then this reconstructed F(t) and the measured cylinder displacement x(t) were used in equation 5.1 to

[1] A difference in the form of the equation can be observed when comparing equation 5.1 with that reported in [8], this is simply due to the definition of the mass m in equation 5.2, as already underlined in Chapter 1 footnote 6, page 51

obtain estimates of drag and inertia coefficients for the flexible cylinder. These coefficients are plotted in figures 5.9, 5.15, 5.21 and 5.25 for all the four set-ups against KC. In the same plots drag and inertia coefficients calculated from measurements for the rigid cylinder at similar values of β are presented. The various cases are described in detail in the next sections.

Subsequently, in order to test how well Morison's equation represents the time history of the in-line force acting on a compliant cylinder, the values of the drag and inertia coefficients appropriate for flexible cylinders were put back into equation 5.1, and predicted time histories of the in-line force were computed. Comparisons between predicted and reconstructed time histories are shown.

Finally, the predicted time histories of the fluid force were used in equation 5.2 to generate time histories of cylinder displacement. The r.m.s. coefficients were computed and shown for comparison with the measured ones.

5.3.4 Prediction method applied to the non-resonant case

Firstly the test case defined as First set-up, for $\beta = 750$, (as described in section 5.2.1) was analysed. The force coefficients C_D and C_M for this case are presented in figure 5.9, where also Sarpkaya's values measured for a rigid cylinder at $\beta = 784$ are plotted for comparison. In each case the curves are very similar in shape to those for the fixed cylinder. In particular, the C_D values for the flexible cylinder are somewhat below those for a rigid one and the corresponding C_M values above the fixed cylinder values.

The predicted time histories of the in-line forces and those derived from the measured cylinder displacement for some KC numbers are shown in figures 5.10 and 5.11.

In addition, the measured and the reconstructed cylinder displacement are

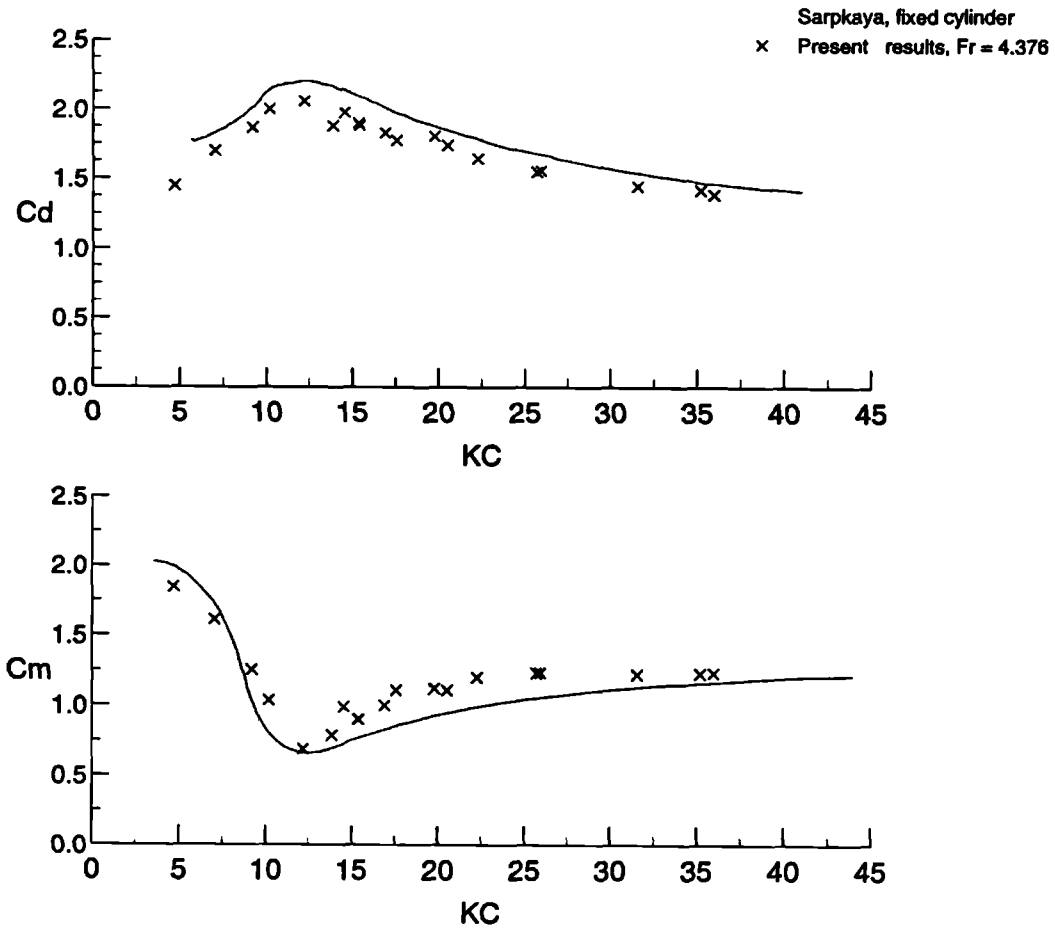


Figure 5.9: Drag coefficient and Inertia coefficient versus KC for the flexible cylinder, First set-up, x, $\beta = 750$, $F_r = 4.376$; and for the fixed cylinder, —, Sarpkaya, $\beta = 784$

plotted in figures 5.12 and 5.13 for the same KC values and the r.m.s. coefficients for KC values between 4 and 35 are presented in figure 5.14. It is possible to note that the r.m.s. values of response increase monotonically with KC both in experiments and in predictions, and the agreement is good for all the KC values investigated. In particular, comparing the time histories cycle by cycle it can be seen that for some flow cycles, the predicted response agrees surprisingly well with experiments in terms of amplitude and phase and this is observed both at low and high KC numbers, and in each case the curves are

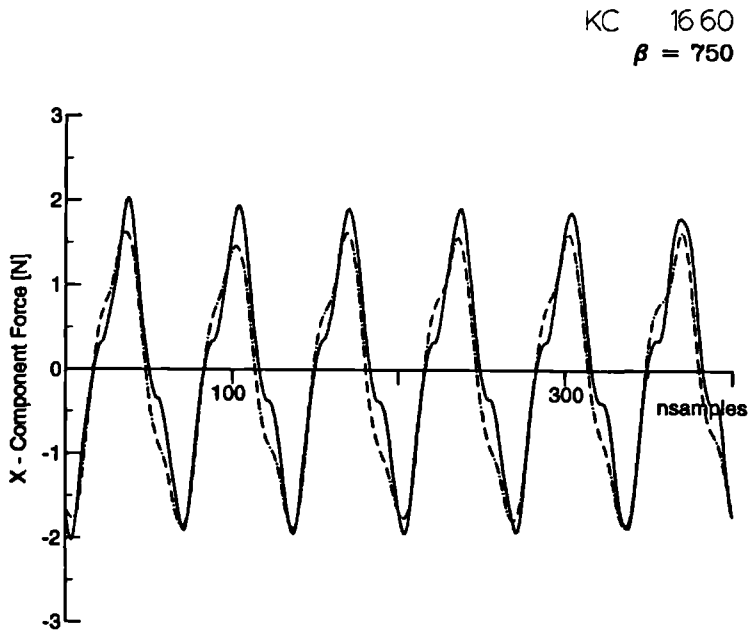


Figure 5.10: Comparison between in-line force trace — from measured cylinder displ. and the predicted one – · – · –; non-resonant case First Set-up, at KC = 16.60

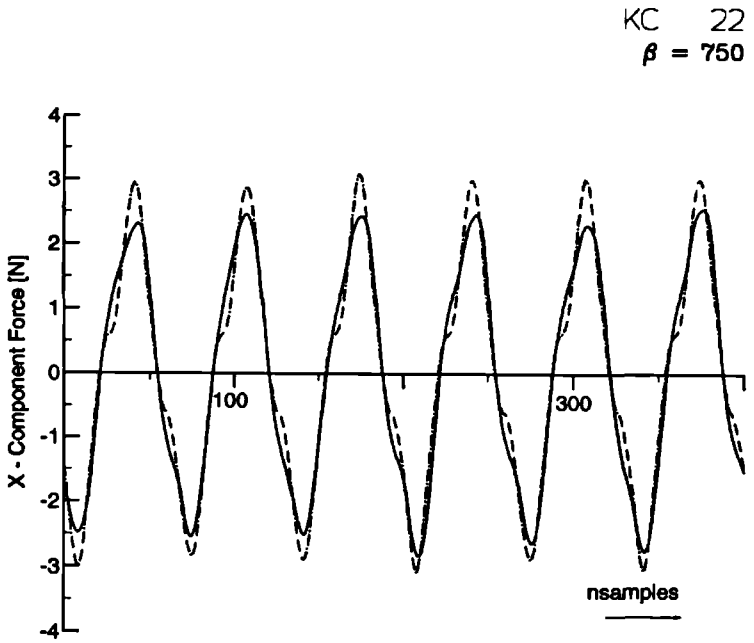


Figure 5.11: Comparison between in-line force trace — from measured cylinder displ. and the predicted one – · – · –; non-resonant case First Set-up, at KC = 22.

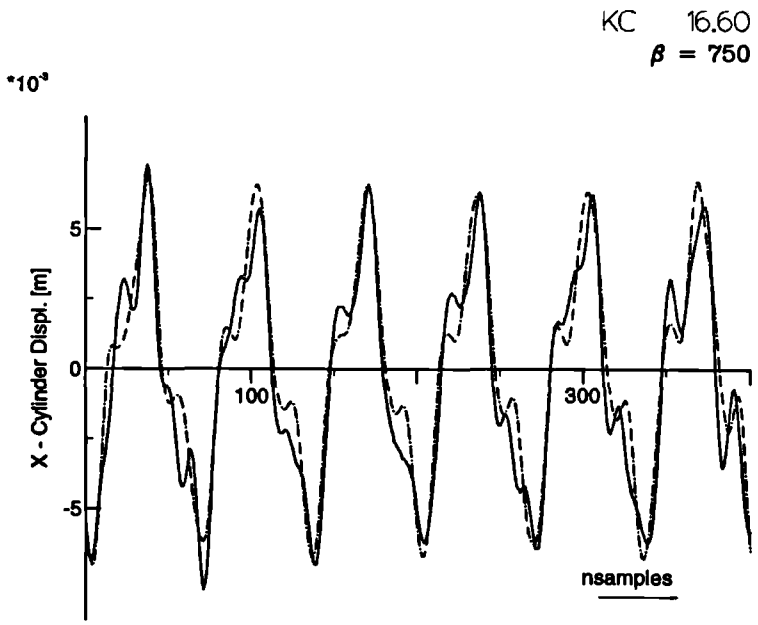


Figure 5.12: Comparison between measured cylinder displ. —, and the reconstructed one — · — · —; non-resonant case First Set-up, at KC = 16.60.

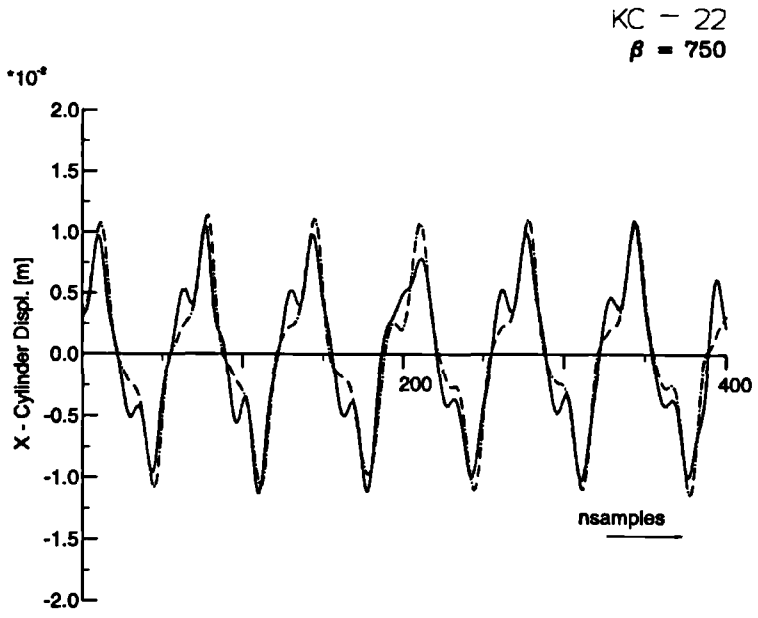


Figure 5.13: Comparison between measured cylinder displ. —, and the reconstructed one — · — · —; non-resonant case First Set-up, at KC = 22.

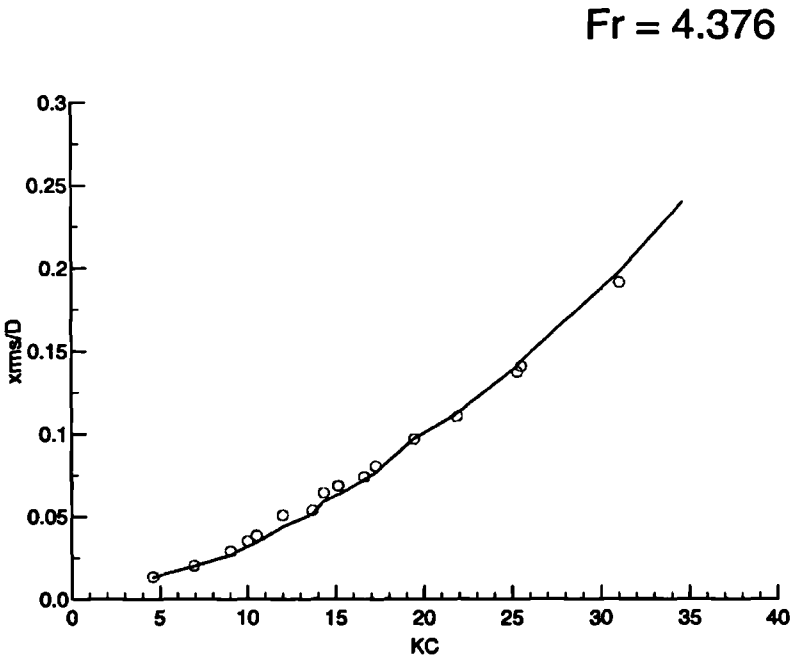


Figure 5.14: In-line response (r.m.s./D) versus KC for the First Set-up case; o measured; — predicted

very similar in shape.

The analysis of these results shows that in a non-resonant case the general form of the response in the in-line direction can be described reasonably well by Morison's equation in relative form, as suggested by Bearman et al. [8].

5.3.5 Prediction method applied to a resonant case at β =750

Referring to test case named Second set-up (section 5.2.2) the resonant case corresponding to the frequency ratio $F_r = 2.808$ has been studied.

Figure 5.15 presents the force coefficients C_D and C_M compared with Sarpkaya's values measured for a rigid cylinder at $\beta = 784$. It shows that the C_D and C_M values for flexible cylinder agree with Sarpkaya's values for KC below 12. For higher KC C_D values remain below those for a rigid one. Firstly they decrease, up-to KC $\sim$ 18 and then they appear to be approaching each other at higher KC. Also C_M exhibits a peculiar jump between KC =12 and 20,

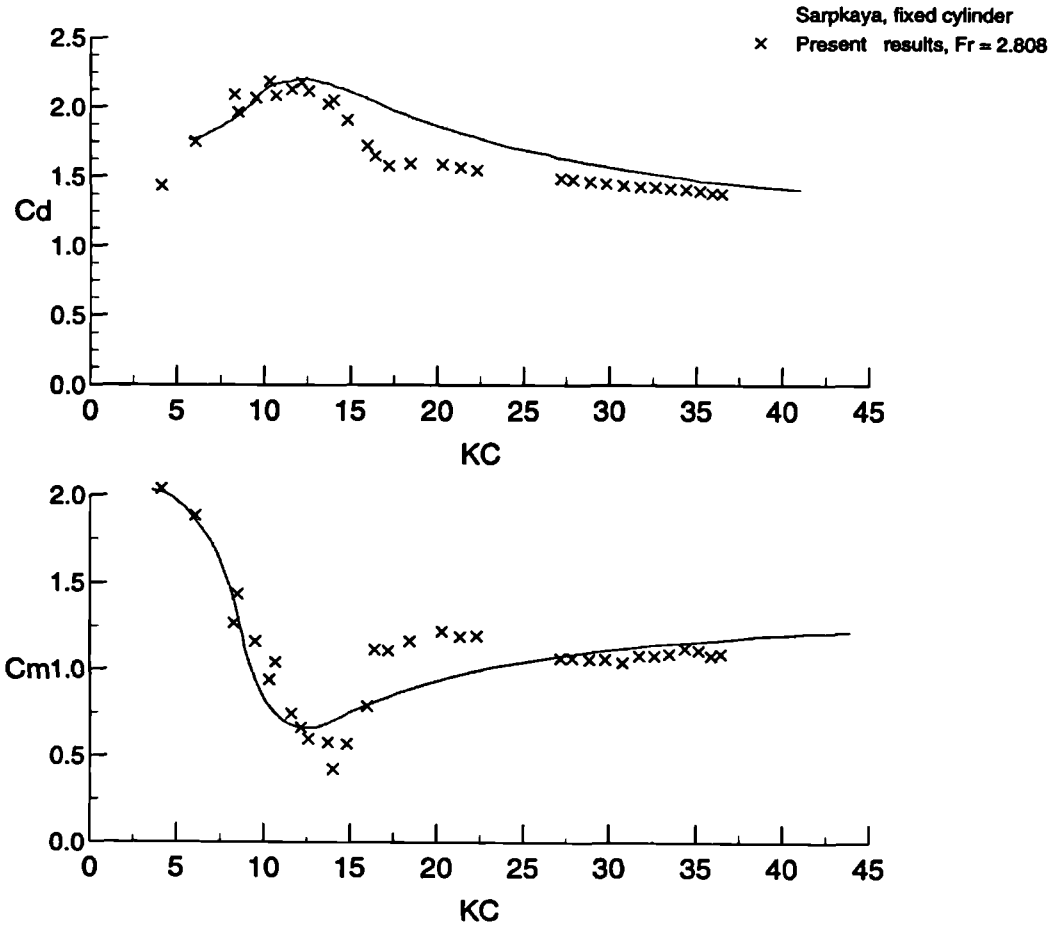


Figure 5.15: Drag coefficient and Inertia coefficient versus KC for the flexible cylinder, Second set-up, x, $\beta = 750$, $F_r = 2.808$; and for the fixed cylinder, —, Sarpkaya, $\beta = 784$

which is the same range of KC where the resonant peak was observed in the r.m.s. coefficient. In this region C_M drops below the rigid cylinder values and increases suddenly to higher values for KC up-to about 22. Above this value C_M stays slightly below the rigid cylinder values. Figures 5.16, 5.17 and 5.18 show the time histories of the predicted and measured responses for KC = 8.50, 14.81 and 29.81. This comparison illustrates the inability of Morison's equation to reproduce the cylinder response both in terms of amplitude and phase. Moreover, this misfit was observed over the whole range of KC, even

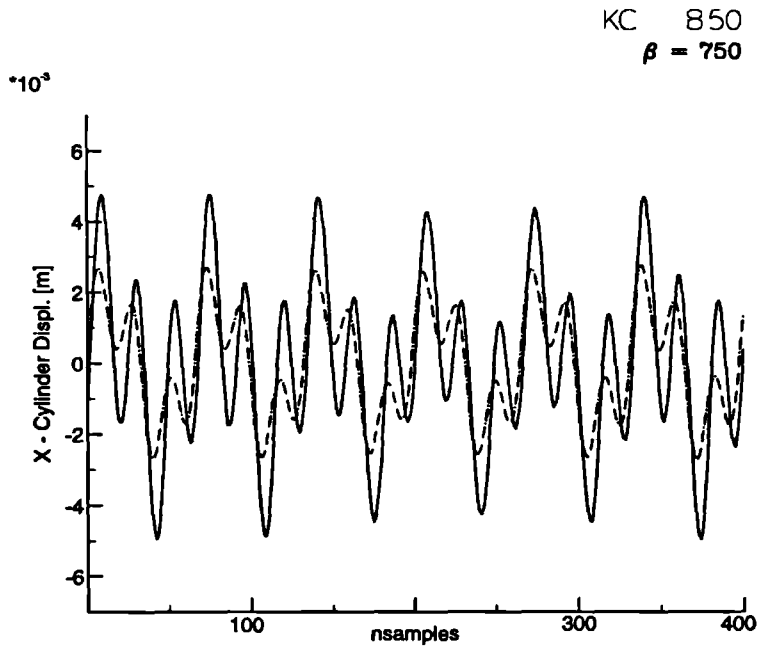


Figure 5.16: Comparison between measured cylinder displ. —, and the reconstructed one — · — · —; resonant case Second Set-up, at KC = 8.50.

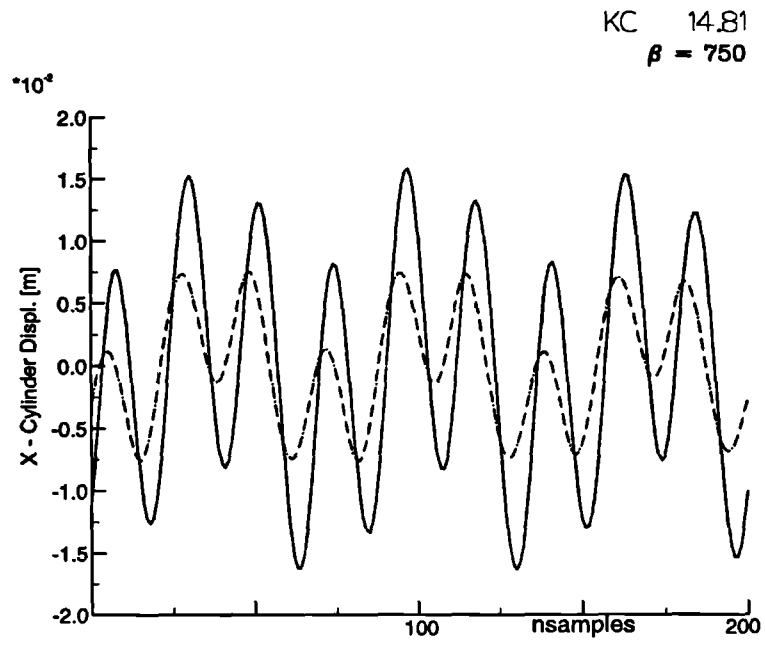


Figure 5.17: Comparison between measured cylinder displ. —, and the reconstructed one — · — · —; resonant case Second Set-up, at KC = 14.81

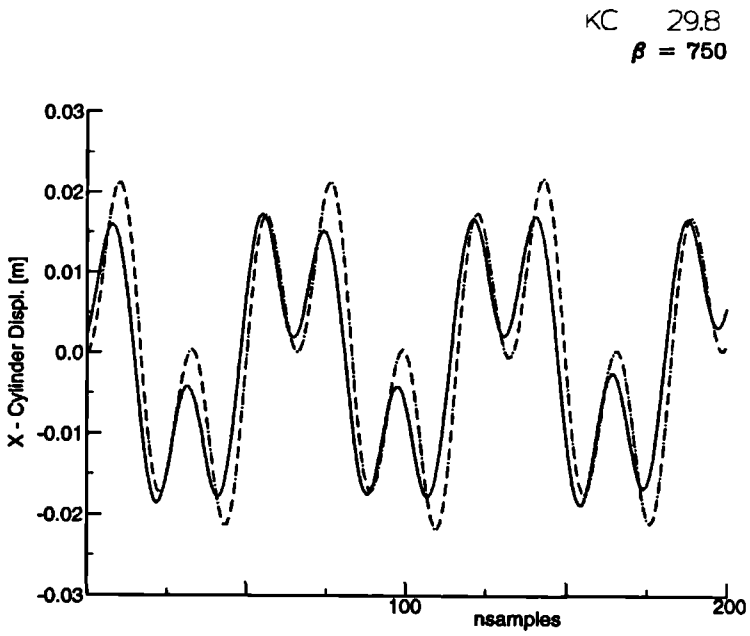


Figure 5.18: Comparison between measured cylinder displ. —, and the reconstructed one — · — · —; resonant case Second Set-up, at KC = 29.81

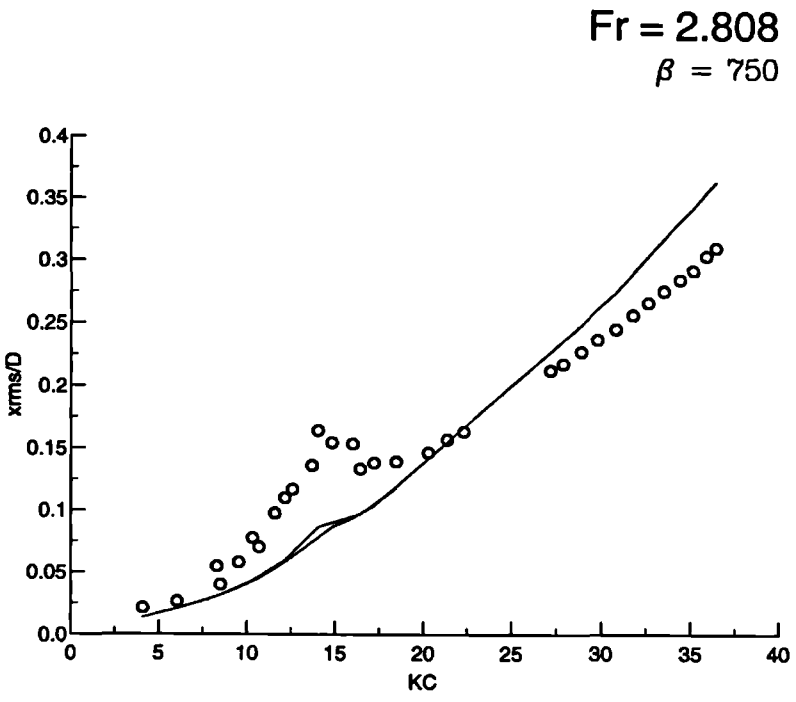


Figure 5.19: In-line response (r.m.s./D) versus KC for the Second Set-up case; o measured; — predicted

outside the resonant peak.

In this respect figure 5.19 clarifies further this argument. The r.m.s. coefficients of the in-line response from both experiments and predictions are plotted against the entire range of KC numbers. An agreement is evident only at small KC values. As KC increases the prediction underestimates significantly the response and misses entirely the resonant behaviour observed in the experiments for KC up to $\sim$ 22. Furthermore, for higher KC the prediction overestimates the measured cylinder response. These findings agree with the numerical prediction attempted by Lin [25], using the Discrete Vortex method. In resonant cases he found very little agreement of the r.m.s. values over the whole range of KC examined. Moreover, figure 5.20 shows the force time history reconstructed with the equation of motion compared with both the predicted one using the flexible cylinder force coefficients, and that obtained using instead Sarpkaya's coefficients appropriate for fixed cylinders. This suggests that (see also section 5.3.7) the agreement cannot be improved using different values of the force coefficients.

5.3.6 Prediction method applied to a resonant case at $\beta = 270$

The same analysis was carried out for the resonant case corresponding to $\beta = 270$ and $F_r = 2.990$ (Third set-up, see section 5.2.3).

Results similar to those described in the previous section were found. Figure 5.21 shows the force coefficients calculated for the flexible cylinder compared with those presented in this thesis for the fixed cylinder at $\beta = 308$.

C_D is smaller and stays below the fixed cylinder values, it drops and rises then between KC 8 and 15 circa. This is the same region of KC where the drop and the subsequent increase in C_M occurs. In particular, this is the region where the resonant peak takes place this time. In this region C_M ap-

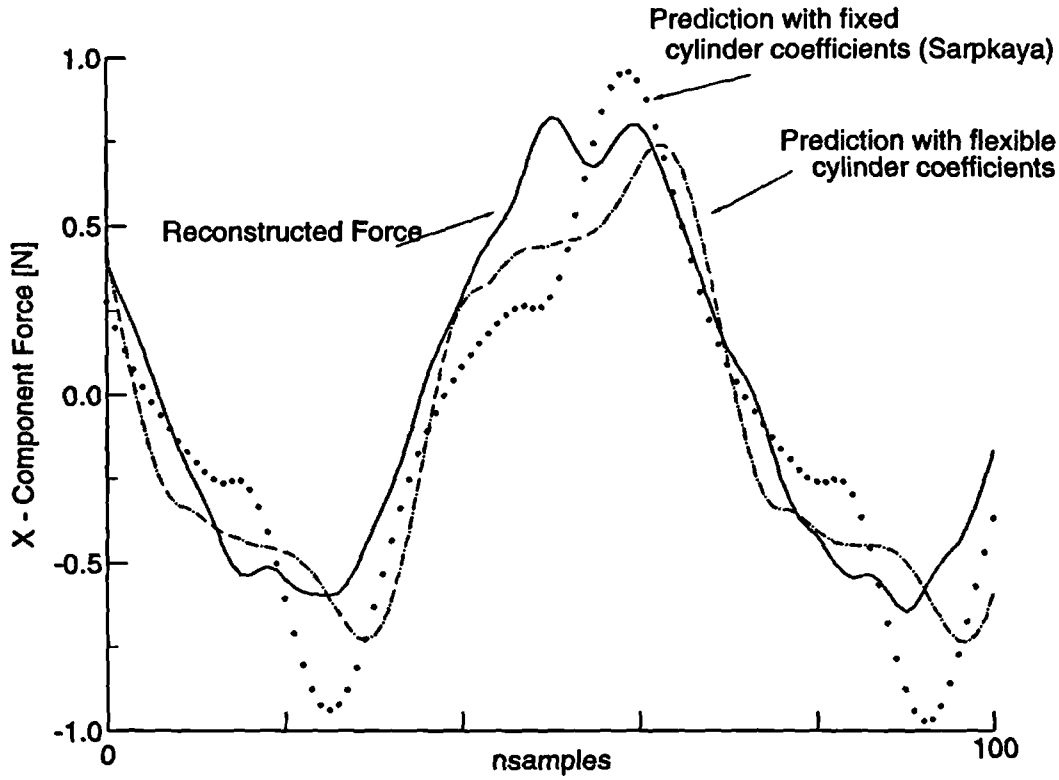


Figure 5.20: Comparison between in-line force trace — from measured cylinder displ. and the predicted one with flexible cylinder coefficients and fixed cylinder ones; resonant case Second Set-up, at KC = 10.0

proaches zero and increases then to values close to the fixed cylinder ones, but never higher than them. As KC increases further C_M remains below the corresponding fixed cylinder values.

Figures 5.22 and 5.23 show the response time histories of the predicted and measured responses for KC = 10.50 and 19.23, and figure 5.24 presents the r.m.s. coefficients. Again it is evident that the prediction based on Morison's equation fails to reproduce the measured displacement. In this smaller β case the r.m.s. coefficients of the predicted in-line response remain below the corresponding measured ones throughout all the KC range, let alone the already stated inability to reproduce the resonant peak.

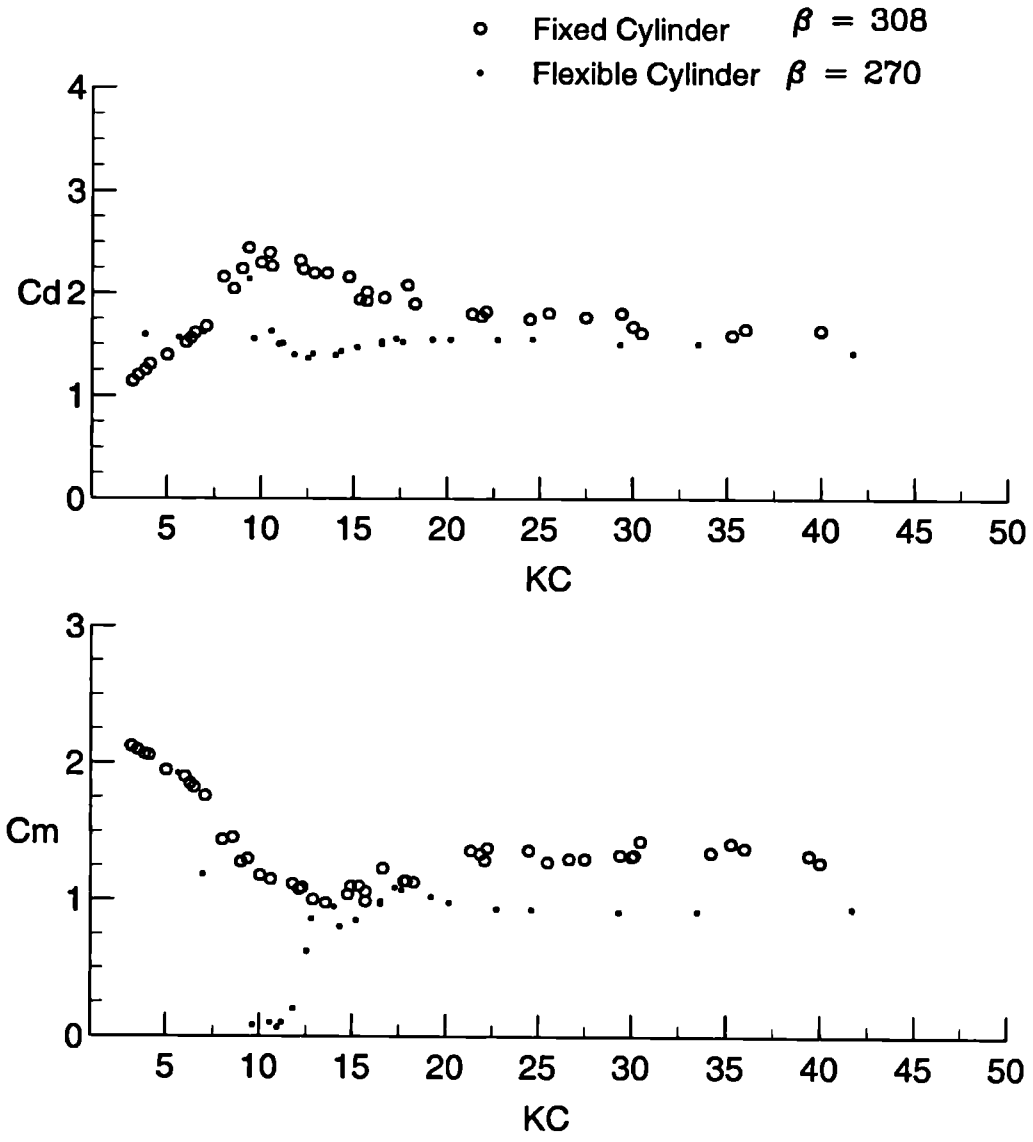


Figure 5.21: Drag coefficient and Inertia coefficient versus KC for the flexible cylinder, Third set-up, o, $\beta = 270$, $F_r = 2.990$; and for the fixed cylinder, • , present research, $\beta = 308$

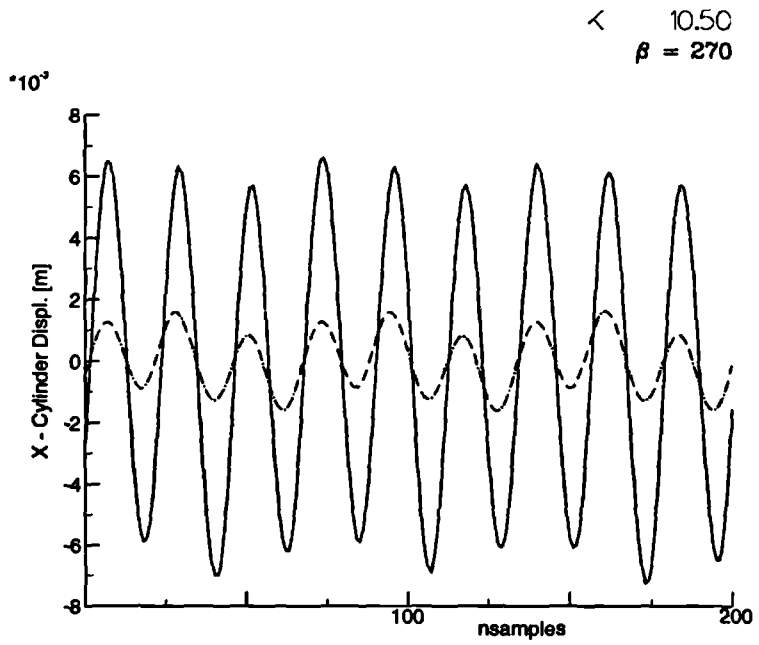


Figure 5.22: Comparison between measured cylinder displ. —, and the reconstructed one — · — · —; resonant case Third Set-up, at KC = 10.50

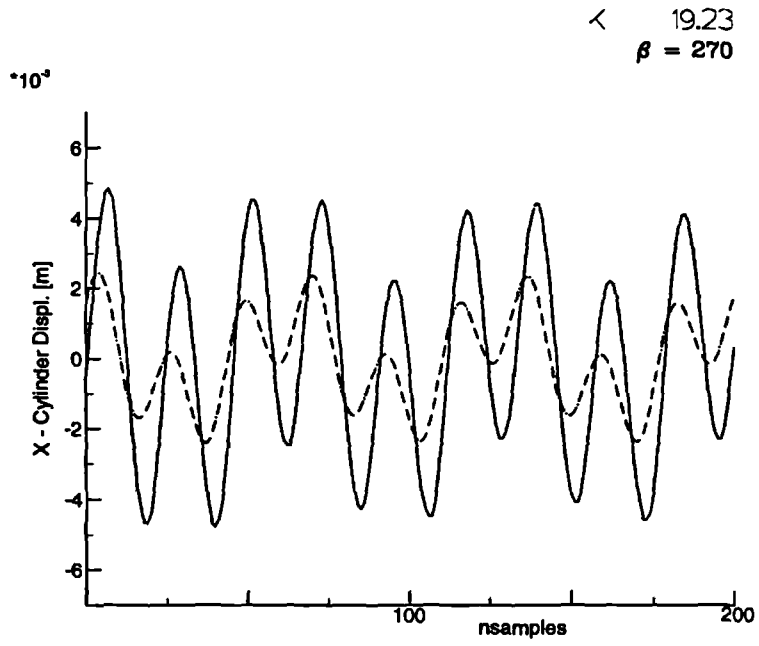


Figure 5.23: Comparison between measured cylinder displ. —, and the reconstructed one — · — · —; resonant case Third Set-up, at KC = 19.23

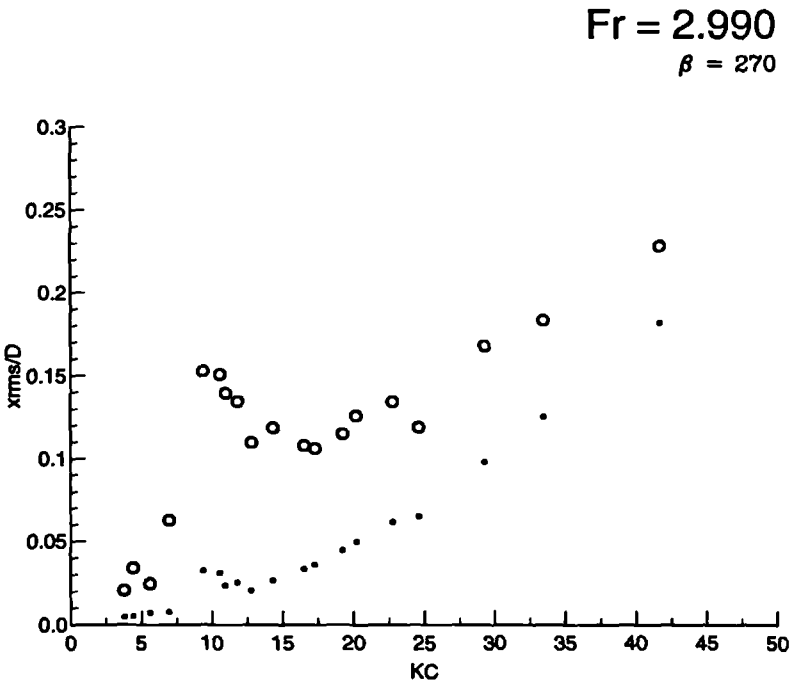


Figure 5.24: In-line response (r.m.s./D) versus KC for the Third Set-up case; o measured; • predicted

5.3.7 Prediction method applied to a resonant case at $\beta = 60$

This resonant case corresponds to $F_r = 2.961$ (Fourth set-up, see section 5.2.4). The observations and the comments made in the previous section apply also to this case. Figure 5.25 is a plot of the force coefficients calculated for the flexible cylinder compared with those presented in the course of this thesis for the fixed cylinder at $\beta = 75$ and 53. The variation in the coefficients occur this time in a lower range of KC, between 7 and 13, again corresponding to the r.m.s. resonant peak range. The r.m.s coefficients of the predicted and measured in-line response are plotted in figure 5.26 where it is very clear that there is underprediction of the response over the whole range of KC.

In addition, as mentioned earlier the cylinder response was also reconstructed using the fixed cylinder coefficients. The resulting r.m.s. coefficient are shown in figure 5.27. It can be noted that such a dramatic change in the

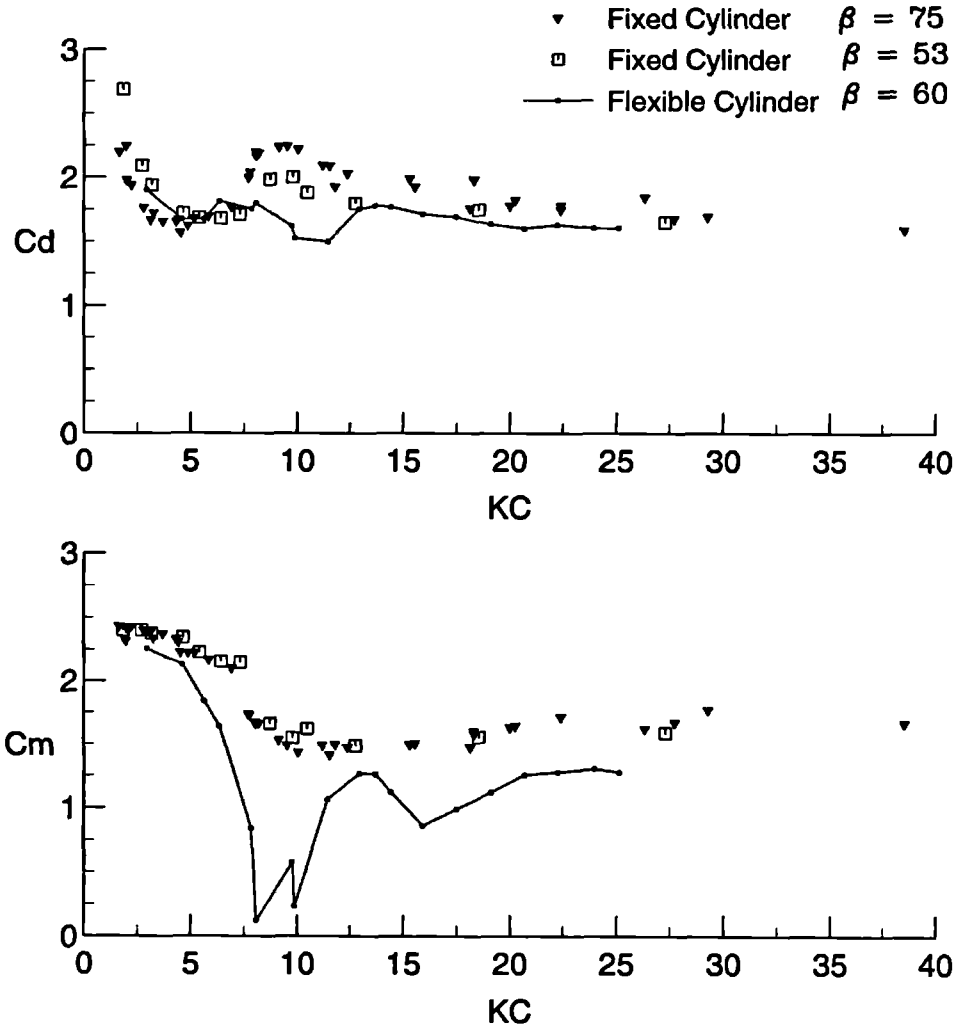


Figure 5.25: Drag coefficient and Inertia coefficient versus KC for the flexible cylinder, Fourth set-up, · $\beta = 270$, $F_r = 2.961$; and for the fixed cylinder, present research, $\beta = 75$ and $\beta = 53$

force coefficients used in equation 5.1 hardly produced any difference in the predicted response.

5.3.8 Remarks on the prediction method

All in all it seems evident that a prediction method based on Morison's equation could be a reliable tool in design only for strictly non-resonant cases.

When a resonance between the cylinder frequency of oscillation and the fluid frequency occurs, not only does the method miss entirely the proper

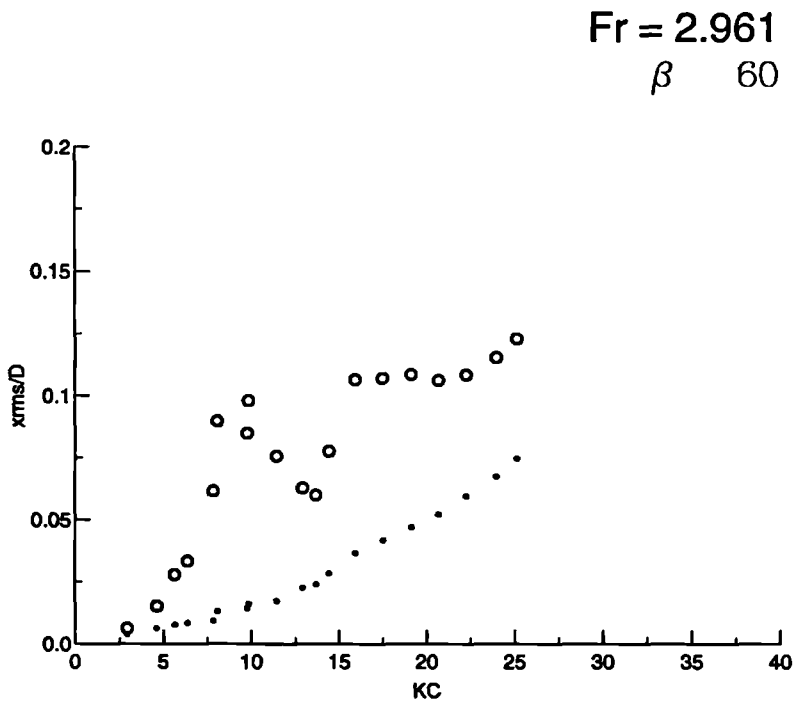


Figure 5.26: In-line response (r.m.s./D) versus KC for the Fourth Set-up case; o measured; • predicted

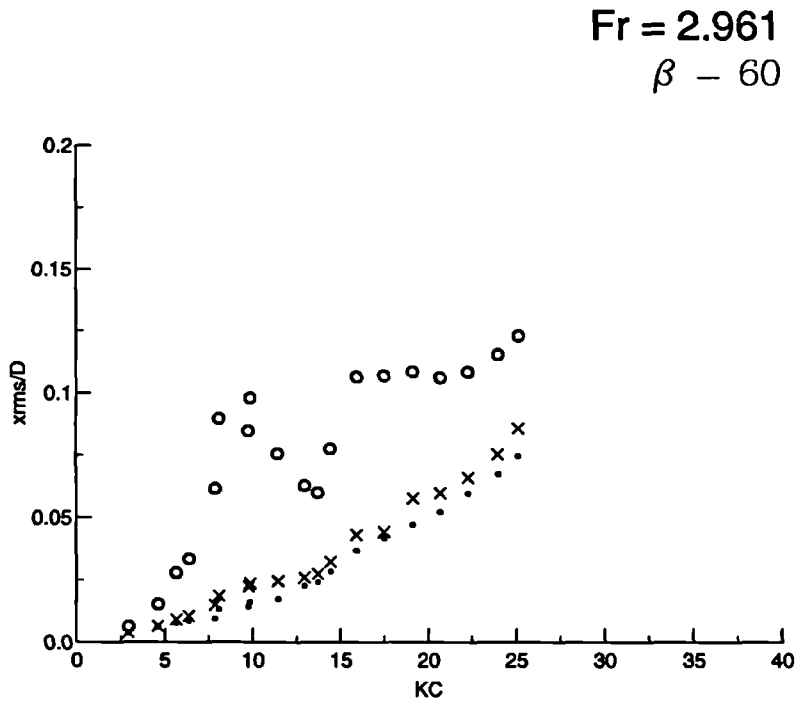


Figure 5.27: In-line response (r.m.s./D) versus KC for the Fourth Set-up case; o, measured; •, predicted with flexible cylinder coefficients; x, predicted with fixed cylinder coefficients

resonant peak in the response, but it also fails to fit the measured response for KC values outside the resonant peak.

Moreover, it was noted that whilst for the resonant case at $\beta = 750$ there was a range of KC (from around 28 onwards) where the prediction overestimated the measured response, this never occurred as β was decreased. For $\beta = 270$ and 60 in fact, the r.m.s. coefficient of the predicted response remained always below the corresponding measured one. So for reasonably high values of β it can be said that although these resonant characteristics are very interesting in that they point out some physical features of the phenomenon they may not be regarded as significant by off-shore engineers (even if they are manifested at full scale β values) because the predicted response at higher KC continues to increase to significantly larger levels than the resonant peak and larger than the corresponding measured one. Therefore the design case is not dictated by the peak amplitude at resonance.The same cannot be said for lower β values.

The inability to predict the resonant peaks via Morison's equation is not difficult to explain. In fact in this relative motion, where the fluid motion combines with the cylinder oscillation, Morison's equation using constant coefficients fails to capture the appropriate frequency components and as for the force coefficients which change according to the type of motion, it is not yet understood how to calculate them in this case. One could be tempted to think that by selecting the "correct" values the prediction might be made to produce more satisfying results.

The present analysis suggests instead that in resonant conditions no matter how much the force coefficients are changed, this prediction fails in any case. The problem is the failure to represent the harmonic content of the force trace which drives the resonance. Therefore a new form of equation would

be required to fit the measured data more accurately over the entire range of KC values investigated.

Chapter 6

Conclusions

Two experimental arrangements, fixed and flexible, were studied. In particular, forces were measured for the fixed cylinder and in-line displacement for the compliant one. The device used to reproduce the oscillatory flow past an immersed cylinder was a U-tube-shaped tank available in the Aeronautics Department at Imperial College (designed by Singh [44], see section 2.2 and 4.2).

6.1 Achievements

A brief summary of the main achievements accomplished in the present research is the object of this section.

- With the aim of measuring forces, at low $\beta(=\frac{D^2}{\nu T})$, an increase of the kinematic viscosity ν was preferred to a decrease in the cylinder diameter D to reduce β so as not to reduce the magnitude of the forces and hence lower their accuracy. The first result of this research, which may prove useful for other researchers, is the fact that a very suitable fluid (non toxic and easy to handle), i.e. polyethylene glycol in solution with water (see section 2.3), has been established.

- Because the force measuring system was required to work at several metres depth under water it was necessary to make the strain gauged load

cells waterproof. Tests were conducted on different sealants and coating materials. These showed that many products which can perform very well in moisture, prove unsuitable when totally immersed in a fluid. A rubber coating material was finally used which overcame these problems (sections 2.5.2 and 2.5.3).

- For the fixed cylinder a first test case with pure water was conducted in order to test the device and make comparisons with other experimental works at the same β (i.e. 308). Once this proved successful the solution water-polyethylene glycol was adopted in different percentages to give β equal to 75, 53 and 35. For each of the four test cases in-line forces were measured and force coefficients C_D, C_M, C_{frms} and C_{ftot} were calculated from the force time histories. In general varying β did not produce large changes in the force coefficients. C_D and C_M in the inertia-regime agreed well with Wang's analytical results and in the other regimes C_D values where found to be slightly smaller than those at β of 308, and C_M values higher.

- Test case named 2, with $\beta = 75$, was repeated by changing the cylinder diameter and the fluid viscosity. This permitted the investigation of whether the results were affected by blockage effects. The blockage ratio ranged between 0.067 to 0.05. The good repeatability of the results showed that blockage effects were negligible.

- A comparison of the present results with numerical ones obtained by several researchers was also undertaken and showed remarkable agreement, particularly for the C_{frms} coefficients that are insensitive to phase changes.

- Transverse forces were measured in the cases $\beta = 308$ and $\beta = 70$ and C_{Lrms} coefficients were calculated. They showed a similar trend over the whole range of KCs examined, and exhibited a smaller value for β =70, in the range of KC between 7 and 11. A correlation factor between the force signals measured at the two ends of the cylinder was calculated. When plotted against KC and compared with C_{Lrms} it showed that the two quantities are clearly related. In particular a sharp drop in both the coefficients could be interpreted as a deviation from 2-dimensional vortex shedding. So even at low β values some three dimensionality effects could play an important role especially in the region of KC termed transverse regime, as also previous researches had evidenced.

- For the compliant cylinder in-line displacements were measured in specific frequency ratio ranges. Three β values have been studied, i.e. β equal to 750, 270 and 60. $\beta = 750$ (with mass ratio ~ 8.9) was an exact repetition of experiments carried out by other researchers, [8], and the results obtained herein confirmed what was observed then. The measured root mean square in-line displacement showed a resonant peak which occurred in a critical region of KC, between 8 and 20. This was not predicted by applying Morison's equation in relative form, which proved inadequate over the entire range of KC investigated, although it could still work in strictly non-resonant conditions. The peak was found also when studying the other β cases, and because the viscosity is higher the response decreased as β is lowered. Qualitative remarks considering also comparisons with the fixed cylinder results suggest that the resonant peaks might be related to the vortex shedding activity, but the complexity of the phenomenon does not allow us to consider the problem completely solved. Currently some numerical simulations are

being carried out by other researchers, but so far they are still unable to demonstrate the resonant peaks.

- Flow visualisations were carried out to gather more information about the flow field and possible three-dimensionalities of vortex shedding but, as expected, there is no evidence that the peaks should be due to 3-D effects. In fact it would be unlikely that a lack of spanwise correlation in the shedding could increase the cylinder response.

Bibliography

[1] R.I. Basu. Aerodymanic forces on structures of circular cross section. part 1. Model-scale data obtained under two-dimensional conditions in low-turbulence streams. *Journal of Wind Engineering*, 21:273–294, 1985.

[2] G.K. Batchelor. *An introduction to fluid dynamics.* Cambridge University Press, 1967.

[3] P.W. Bearman, M.J. Downie, J.M.R. Graham, and E.D. Obasaju. Forces on cylinders in viscous oscillatory flow at low KC numbers. *J. Fluid Mech.*, 154:337–356, 1985.

[4] P.W. Bearman and J.M.R. Graham. Hydrodynamic forces on cylindrical bodies in oscillatory flow. *Second International Conference on Behaviour of Off-shore structures, Imperial College, London UK*, pages 309 321, 1979.

[5] P.W. Bearman, J.M.R. Graham, P. Naylor, and E.D. Obasaju. The role of vortices in oscillatory flow about bluff cylinders. *Proc. Intl Symp. on Hydrodynamics in Ocean Engng, Trondheim, Norway, August, Norwegian Hydrodynamic Laboratories, Trondheim, Norway*, pages 621–635, 1981.

[6] P.W. Bearman, J.M.R. Graham, and E.D. Obasaju. A model equation for the transverse forces on cylinders in oscillatory flow. *Appl. Ocean Research*, 6:166 172, 1984.

[7] P.W. Bearman, J.M.R. Graham, Lin X.W., and Meneghini J.R. Numerical simulation of flow induced vibration of a circular cylinder in uniform and oscillatory flow. *Proceedings sixth International Conference on Flow-Induced vibration, London, UK*, pages 231–240, 1995.

[8] P.W. Bearman, X.W. Lin, and P.R. Mackwood. Measurement and prediction of response of circular cylinders in oscillating flow. *Proc. of the 6th Int. Boss conf., London, UK, 7-10 July*, 1992.

[9] P.W. Bearman and P.R. Mackwood. Non-linear vibration characteristics of a cylinder in an oscillating water flow. *IMechE Int. Conf., Flow induced Vibrations, Brighton*, 1991.

[10] J.R. Bishop. A new coefficient for total wave force. Technical Report NMI R77 (OT-R-8017), National Maritime Institute, 1980.

[11] G. Bugliarello. The resistance to accelerated motion of spheres in water. *La Ricerca Scientifica*, 26(2):437–442, 1956.

[12] L.E. Coates. Unpublished. 1984.

[13] C.J. Garrison. Drag and inertia forces on a cylinder in harmonic flow. *J. of Waterway, Port, Coastal and Ocean Engin. ASCE*, 103(WW2):169–190, 1990.

[14] J.H. Gerrard. The mechanics of the formation region of vortices behind bluff bodies. *J. Fluid Mech.*, 25, 1966.

[15] J.M.R. Graham. Forces on cylindrical bodies in oscillatory flow at low Keulegan-Carpenter numbers. *Symposium on Mech. of wave-induced forces on cylinders, Bristol UK-Paper B1*, 1, 1978.

[16] J.M.R. Graham. The forces on sharp-edged cylinders in oscillatory flow at low Keulegan-Carpenter number. *J. Fluid Mech.*, 97:331 346, 1980.

[17] P. Hall. On the stability of the unsteady boundary layer on a cylinder oscillating transversely in a viscous fluid. *J. Fluid Mech.*, 146:347 367, 1984.

[18] H. Honji. Streaked flow around an oscillating circular cylinder. *J. Fluid Mech.*, 107:509–520, 1981.

[19] G. Iliadis. Private comunication. 1995.

[20] B.L. Iversen and R. Balent. A correlating modulus for the fluid resistance in accelerated motion. *Journal of Applied Physics*, 22(3):324–328, 1951.

[21] S.R. Keim. Fluid resistance to cyliners in accelerated motion. *Journal of the Hydraulics Division - ASCE*, 83(6), 1956.

[22] G.H. Keulegan and L.H. Carpenter. Forces on cylinders and plates in oscillating fluid. *Journal of Research, National Bureau of Standards*, 60:423 440, 1958.

[23] S. Kuhtz, P.W. Bearman, and J.M.R. Graham. Problems encountered in measuring forces over immersed bodies. *Experimental Techniques, SEM*, accepted for publication in 1996.

[24] A.D.K. Laird. Water forces on flexible oscillating cylinders. *Journal of the Waterways and Harbors Division, ASCE*, 3:125 137, 1962.

[25] X.W. Lin. Prediction of in-line response of flexible cylinders in oscillatory flow. Technical report, Department of Aeronautics, Imperial College of Science, Technology and Medicine, London, UK, Unpublished report, 1995.

[26] X.W. Lin, P.W. Bearman, and J.M.R. Graham. A numerical study of oscillatory flow about a circular cylinder for low values of β parameter. *Journal of Fluids and Structures*, accepted for publication 1996.

[27] D.J. Maull and D. Kaye. Oscillations of a flexible cylinder in waves. *Proceedings International Conference on Behaviour of Off-shore structures*, 2:535–547, 1988.

[28] D.J. Maull and M.G. Milliner. Sinusoidal flow past a circular cylinder. *Coastal Engineering*, 2:149–168, 1978.

[29] K.G. McConnell and Q. Jiao. The in-line forces acting on an elastically mounted cylinder oscillating in still water. *Experimental Mechanics*, 26:66–70, 1986.

[30] K.G. McConnell and Y.S. Park. The frequency components of fluid-lift forces acting on a cylinder oscillating in still water. *Experimental Mechanics*, 22(6):216–222, 1982.

[31] K.G. McConnell and Y.S. Park. The response and the lift-force analysis on an elastically mounted cylinder oscillating in still water. *Proceedings International Conference on Behaviour of Off-shore structures*, pages 671 680, 1982.

[32] J.R. Morison, M.P. O'Brien, J.W. Johnson, and S.A. Schaaf. The force exerted by surface waves on piles. *Petroleum Translations AIME*, 189:149–154, 1950.

[33] E.D. Obasaju, P.W. Bearman, and J.M.R. Graham. A study of forces, circulation and vortex patterns around a circular cylinder in oscillating flow. *J. Fluid Mech.*, 196:467–494, 1988.

[34] A. Roshko. Experiments on the flow past a circular cylinder at very high Reynolds number. *J. Fluid Mech.*, 10:345–356, 1961.

[35] T. Sarpkaya. Lift, drag and added mass coefficients for a circular cylinder immersed in a time dependent flow. *J. Appl. Mech., ASME*, 30:13–15, 1963.

[36] T. Sarpkaya. In line and transverse forces on smooth and sand-roughened cylinders in oscillatory flow at high Reynolds numbers. Technical Report NPS-69SL-76062, Naval Postgraduate school, Monterey, Calif., 1976.

[37] T. Sarpkaya. Vortex shedding resistance in harmonic flow about smooth and rough circular cylinders at high Reynolds number. Technical Report 2 Feb., Naval Postgraduate school, Monterey, Calif., 1976b.

[38] T. Sarpkaya. Force on a circular cylinder in viscous oscillatory flow at low Keulegan-Carpenter numbers. *J. Fluid Mech.*, 165:61–71, 1986.

[39] T. Sarpkaya. In line and transverse forces on smooth and rough cylinders in oscillatory flow at high Reynolds numbers. Technical Report NPS69-86-003, Naval Postgraduate school, Monterey, Calif., 1986.

[40] T. Sarpkaya and M. Isaacson. *Mechanics of wave forces on offshore structures.* Van Nostrand Reinhold Company Inc., 1981.

[41] T. Sawaragi, T. Nakamura, and H. Kita. Characteristics of lift forces on circular pile in waves. *Coastal Engineering in Japan*, 19:59 71, 1976.

[42] H. Schlichting. *Boundary layer theory.* Pergamon Press, London, 1955.

[43] S. Sherwin. Private comunication. 1995.

[44] S. Singh. *Forces on bodies in an oscillatory flow.* PhD thesis, Dept of Aeronautics, Imperial College, London, 1979.

[45] B. Sortland. Flow measurements in oscillating flow on ship sections and circular cylinders in a U-tube water tank. Technical Report UR-86-52, Department of Marine Technology, Trondheim, Norway., 1986.

[46] G.G. Stokes. On the effect of internal friction of fluids on the motion of pendulums. *Trans.Camb.Phil.Sec.9*, 1851.

[47] T. Tatsuno and P.W. Bearman. A visual study of the flow around an oscillating circular cylinder at low Keulegan-Carpenter numbers and low stokes numbers. *J. Fluid Mech.*, 211:157–182, 1990.

[48] P. Walker. *The forces on a circular cylinder in oscillatory flow plus a current.* PhD thesis, Dept of Aeronautics, Imperial College, London, 1990.

[49] C.Y. Wang. On high frequency oscillatory viscous flows. *J. Fluid Mech.*, 32:55–68, 1968.

[50] C.H.K. Williamson. Sinusoidal flow relative to circular cylinders. *J. Fluid Mech.*, 155:432–449, 1985.

[51] C.H.K. Williamson. 2-D and 3-D aspects of the wake of a cylinder, and their relation to wake computations. *Vortex Dynamics and Vortex Method - Lectures in Applied Mathematics*, pages 719–751, 1991.